

1 **LHCb RICH upgrade -**
2 **Engineering Design Report**
3 **for the Elementary Cell**
4 **of the Photo-Detector***



6 Issue: 2
7 Revision: 1

8 Reference: LHCb-xyz-2015
9 Created: January 12, 2015
10 Last modified: January 12, 2015

11 **Prepared by:** TBD, Edited by Alessandro Petrolini^a,
12 ^aLHCb/RICH, CERN, Switzerland
13

*Report prepared for the LHCb RICH upgrade EC EDR.

DRAFT

Abstract

2 LHCb RICH upgrade: documentation for the EDR of the Elementary Cell of the Photon-Detector.

Document Status Sheet

1. Document Title: LHCb RICH upgrade - Engineering Design Report for the Elementary Cell of the Photo-Detector			
2. Document Reference Number: LHCb-xyz-2015			
3. Issue	4. Revision	5. Date	6. Reason for change
1	4	January 12, 2015	DRAFT - First version.
2	1	January 12, 2015	Second version, post-review, including answers to the report of the referees.

- 5 • Approved by: Massimo Benettoni, Angelo Cotta Ramusino, Flavio Fontanelli, Christoph Frei,
6 Gianluigi Pessina, Trevor Sadvige, Steve Wotton.
- 7 • Approved by:
- 8 • Approved by: Carmelo D'Ambrosio, Antonis Papanestis.

Contents

10	1 Introduction and assumptions	5
11	1.1 Conventions and acronyms	7
12	2 Requirements	7
13	3 Design	9
14	3.1 MaPMT	13
15	3.2 Base-Board	13
16	3.2.1 High Voltage for the MaPMT	13
17	3.2.2 PCB design	15
18	3.2.3 The measurement of the temperature of the BaseB	20
19	3.3 FEB	20
20	3.4 BackB	20
21	3.5 Mechanical case	22
22	3.6 Local Magnetic Shielding	24
23	3.6.1 Design	24
24	3.6.2 Integration of the MS into the EC	27
25	3.7 Optical adapter system	27
26	3.8 Drawings	27
27	3.9 Critical design issues	27

1	4 On-detector electronics overview	27
2	4.1 DB	35
3	4.2 Grounding and Shielding of the EC	35
4	4.2.1 Base-Board	35
5	4.2.2 The Magnetic Shield	35
6	5 Overview of the Photo-Detector Assembly	36
7	5.1 Layout of RICH2	38
8	5.2 Layout of RICH1	38
9	6 EC Interface to the super-structure	38
10	6.1 Mechanical interface	38
11	6.2 Thermal interface	39
12	6.3 Electrical interface	40
13	6.4 High Voltage distribution	40
14	6.4.1 Power supplies	40
15	7 EC assembly and disassembly	41
16	8 Budgets	41
17	8.1 Geometry	41
18	8.2 Mass	41
19	8.3 Power	41
20	9 Possible Radiation issues	41
21	9.1 Expected Radiation Levels	45
22	10 Prototyping	45
23	10.1 Mockup	45
24	10.2 Mechanical measurements on the BaseB	45
25	10.3 Electrical measurements on the BaseB	48
26	10.4 Thermal measurements on the BaseB	48
27	10.5 Stress tests on the BaseB	50
28	11 Quality Assurance	50
29	12 Repair and Maintenance	51
30	13 Project schedule	52
31	14 Project validation via test-beam	52
32	15 Inventory and bookkeeping during production and operations	52
33	16 The EC-H for the new R12699-M64 Flat Panel MaPMT	54

1	17 The LHCb environment	54
2	17.1 Expected occupancy	54
3	18 References	57
4	A The R11265-M64 MaPMT	58
5	A.1 Data-sheet	59
6	A.2 Total Photo-Detection efficiency	59
7	A.2.1 Comparison of the SBA with UV/borosilicate spectral responses	59
8	A.3 Dark current	62
9	B The R11265-M64 MaPMT in the RICH of LHCb	62
10	B.1 Operating voltage, gain and ageing	62
11	B.2 Biasing of the MaPMT	63
12	B.3 Prototyping	64
13	B.4 Ageing	64
14	C The new R12699-M64 Flat Panel MaPMT	66
15	D The new R12699-M64 Flat Panel MaPMT in the RICH of LHCb	67
16	E Data Sheets	67
17	F Referee's report	79

List of Figures

19	1 TEST	5
20	2 EC break-down scheme.	6
21	3 Specifications of the CLARO front-end chip.	8
22	4 Concept scheme of the EC [15] (not an engineering drawing).	9
23	5 Picture of one EC/PDM developed for the LHCb RICH upgrade (for use with the MAROC chip).	10
24	6 Concept scheme of the EC and PDM design (not to scale, not an engineering drawing).	11
26	7 Overall view of the EC design with no magnetic shield (engineering drawing). Legend: gold: MaPMT; grey: Aluminium structure; yellow: FEB; red: connectors; green: BaseB and BackB; yellowish-green: sockets for the MaPMT.	12
27		
28		
29	8 Electrical scheme of the HV voltage divider for the MaPMT, with three power supplies.	14
30	9 Engineering drawing of the custom socket for the MaPMT.	16
31	10 Top view of the BaseB (facing the MaPMT).	17
32	11 Stackup of the BaseB PCB.	17
33	12 SAMTEC-HSEC8-120	18
34	13 Bottom Layer of the BaseB (away from the MaPMT).	18
35	14 Electrical scheme of 1/2 BaseB.	19
36	15 View of the bottom layer of the BaseB with the two temperature sensors.	20

1	16	Construction details of the FEB and the BackB inside the EC assembly.	21
2	17	FEB overview.	21
3	18	BkBd artwork.	23
4	19	View of the front-side of the BackB.	23
5	20	View of the BackB and EC assembly from the back-side.	24
6	21	Mechanical design of the EC: sides.	25
7	22	Mechanical design of the EC: bases.	26
8	23	Details of the MaPMT mounting.	28
9	24	Scheme of the DB	35
10	25	36
11	26	View of the EC array.	37
12	27	Top view of the EC array.	37
13	28	Routing of the HV cable.	41
14	29	EC sizes: top view (longitudinal sizes to be checked/confirmed).	42
15	30	EC sizes: side view, detail of the MaPMT housing (longitudinal sizes to be	
16		checked/confirmed).	42
17	31	EC sizes (longitudinal sizes to be checked/confirmed).	43
18	32	EC sizes (longitudinal sizes to be checked/confirmed).	43
19	33	FEB sizes (longitudinal sizes to be checked/confirmed).	44
20	34	Mockup of the EC.	46
21	35	Various mockups, front-side.	47
22	36	Various mockups, back-side.	47
23	37	Top and bottom layers of the BaseB in steady-state. The BaseB is mounted on the case	
24		of the EC.	48
25	38	Left: view of the middle of the PCB. The resistors of the voltage divider are clearly	
26		visible as the hottest components while the socket temperature is colder. Right: view	
27		of the side of the BaseB showing how the PCB stabilizes at a rather uniform average	
28		temperature.	49
29	39	Top (left) and bottom (right) layers of the PCB. The BaseB is not mounted on the case	
30		of the EC.	49
31	40	QA flow chart for the EC	50
32	41	Exploded view of the EC.	51
33	42	Test-Beam Setup (1).	52
34	43	Test-Beam Setup (2).	53
35	44	Test-Beam Setup (3).	53
36	45	The EC-H concept design.	55
37	46	View of the connectors on the back of the BaseB.	56
38	47	FEB for the EC-H.	57
39	48	Spectral response of the R7600 MaPMT for the different photo-cathodes and entrance	
40		windows available from Hamamatsu.	60
41	49	borosilicate (left) and UV (right) spectral response used to compare the yields and the	
42		resolutions.	60
43	50	Window transmittance degradation due to the radiation damage.	62

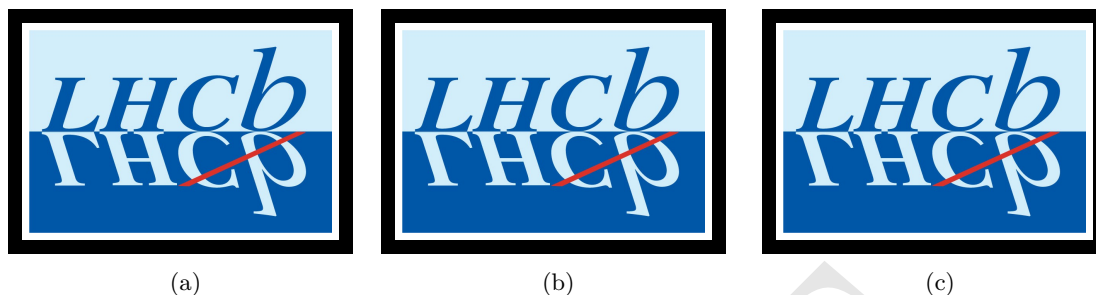


Figure 1: TEST

1	51	Nominal gain versus supply voltage with the standard voltage divider (from Hamamatsu).	65
2			
3	52	Relative anode current as a function of the MaPMT operating time.	66
4	53	Spectral transmittance of the window of R8900 (equal to R11265-M64 according to Hamamatsu) and of the H10966 (equal to the R12699-M64 according to Hamamatsu) for both UV glass and borosilicate glass window. The -03 suffix indicates the UV glass curve.	68
5			
6			
7			
8	54	Spectral response of the R12699-M64 for UV glass (left) and borosilicate glass (right) entrance window (in green) compared with the spectral response of the R11265-M64 (dashed).	68
9			
10			

List of Tables

12	1	Mass budget for one EC	42
13	2	Power budget for one EC	43
14	3	The spectral response efficiency for borosilicate and UV glass window.	61
15	4	Total anode current for different occupancies at nominal gain and with a safety factor 2.	63
16	5	Gain linearity for different occupancies	64
17	6	MaPMT expected lifetime for different occupancy for the average curve and for the -1σ curve. The last column indicates the number of MaPMT in RICH in percentage which are subject to that occupancy.	67
18			
19			

1 Introduction and assumptions

21 The upgrade of the LHCb RICH is described in [12, 5].

22 MaPMT are being used as photo-sensors. At present, two types of MaPMT are foreseen:

- 23 • Hamamatsu R11265-M64 (currently available with bialkali/SBA/UBA photo-cathodes and
24 borosilicate/UV-glass windows);
- 25 • Hamamatsu R12699-M64 (biakali photo-cathode and borosilicate window only, so far).

26 These MaPMT are housed by the so-called *Elementary Cell* (EC), which allows operation and readout
27 of the MaPMT. RICH1 will only use the R11265-M64 MaPMT (good for high-occupancy regions);
28 RICH2 will use the R11265-M64 MaPMT in its central part (high-occupancy regions), while R12699-
29 M64 (with twice the pixel size) will be used in the upper and lower parts of the focal plane, where the
30 occupancy is lower.

31 This EDR will present the full design of the EC for four close-packed R11265-M64 (EC-R).

1 Introduction and assumptions

- 1 The EC-R is common to both RICH1 and RICH2. The design of the EC for one single R12699-M64 (EC-
- 2 H), which was staged due to the later availability of the R12699-M64 with respect to the R11265-M64,
- 3 will be outlined in section 16. The R12699-M64 has a square size about equivalent to four close-packed
- 4 R11265-M64 and about twice the pixel size. Therefore the sizes of the EC-R and EC-H are about the
- 5 same.
- 6 A schematic break-down of the EC is shown in figure 2.

EC break-down				
RICH Photo-Detector Assembly	Photo-Detector Module (PDM)	Elementary Cell (EC)	MAPMT	4 R11265 MAPMT or 1 R11699 MaPMT
			BaseBoard (BB)	Base-Board for the Elementary Cell <i>Thermo-structural PCB, voltage divider, sockets for the MAPMT, connectors to f/e electronics, HV connections, temperature sensors, integrated passive thermal components, holes/screws/spacers/...</i>
			Magnetic Shield (MS)	Magnetic Shield <i>Suitably shaped material, HV insulation between MS and MAPMT, grounding.</i> MS integration mechanics If any.
			Front-End Boards (FEB)	f/e electronics CLARO boards <i>PCB, connections to FEB, connections to DEB, passive thermal system, anything else</i> CLARO-chips
			BackBoard (BkBd)	Back-Board for the Elementary Cell <i>Thermo-structural PCB, connectors to FEB, connectors to DEB, HV connections, temperature sensors, integrated passive thermal components, holes/screws/spacers/...</i>
			EC case	mechanical structure of the EC <i>Machined Alu plates, holes/screws/spacers...</i> passive thermal components of the EC <i>thermal pads, bridges, tapes...</i>
				HV cables / connectors
				LV cables / connectors
				EC integration
				DCS

Figure 2: EC break-down scheme.

7 The front-end electronics had its own dedicated EDR [22], to which the reader is referred for all the
8 read-out aspects.

9 The design proposed for the housing of the MaPMT for the RICH upgrade has its roots in the R&D
10 work done for the current LHCb RICH (MaPMT option) before the choice of the HPD [7, 8, 9, 10].

11 As the final layout of the Photo-Detector Assembly (PDA) is still under optimization, as of today, the
12 following baseline figures will be assumed in this report:

- 13 • RICH1: two PDA made of 10 rows × 24 columns EC-R, that is, 480 EC, and 1920 R11265-M64;
- 14 • RICH2: two PDA made of 24 rows × 12 columns EC, that is, 576 EC, with:
 - 15 – 192 EC-R, that is 768 R11265-M64 (the 8 central rows);
 - 16 – 384 EC-H, that is 384 R12699-M64 (the upper and lower rows).

17 This makes a total of:

- 18 • 672 EC-R;
- 19 • 384 EC-H;
- 20 • for a total of 1056 EC.

- 1 A contingency for spares of $\approx 20\%$ will be assumed (that is a total of ≈ 1267 EC is targeted for
- 2 production).
- 3 The two focal planes and MaPMT planes of RICH2 are vertical. The two focal planes and MaPMT
- 4 planes of RICH1 are not: they lay one above and the other one below the beam-pipe; they inclined
- 5 with respect to the horizontal plane (see [5]).
- 6 An operating lifetime in the LHCb environment of 15 years is assumed.

1.1 Conventions and acronyms

8 Main acronyms:

- 9
 - EC := Elementary Cell:
 - 10 – EC-R: housing 2×2 R11265-M64 MaPMT;
 - 11 – EC-H: housing 1 R12699-M64 MaPMT.
 - 12 • PDM := Photo-Detector Module, made of a suitable number of EC;
 - 13 • BaseB:= Base-Board;
 - 14 • BackB:= BackB;
 - 15 • FEB := Front-End Electronics Board (a.k.a. CLARO board, housing the CLARO front-end
 - 16 chips [22]);
 - 17 • DB := Digital (electronics) Board;
 - 18 • MS := Magnetic Shielding for the MaPMT;
 - 19 • PDA := Photo-Detector Assembly.

20 In this report a local system of coordinates with the z axis perpendicular to the MaPMT plane and

21 with the x and y axes on the MaPMT plane, along the MaPMT sides is used. The x axis is horizontal,

22 for both RICH1 and RICH2.

2 Requirements

24 The photo-sensor is required to be sensitive to single-photons from the near-UV to visible wavelength

25 range; fast enough (faster than the 25 ns of the LHC BCO); with pixel size of about 3 mm, in the high-

26 occupancy regions, (as determined by the optics and requirements on the Cherenkov angle resolution),

27 but a larger pixel size of about 6 mm may be tolerated in the low-occupancy regions of RICH2; capable

28 to instrument a large area of the order of one square meter with a large geometrical acceptance; with

29 dark-counts one order of magnitude lower of the expected signal occupancy; capable to survive for 15

30 years operation in the LHCb environment.

31 The focal length of the main optics is as large as a few meters, and the spread of the local incidence

32 angles on the PDA plane is small; moreover, the pixel size is about 3 mm or more. Therefore the optics

33 has a depth of focus as large as a few cm, such that the precision of positioning of the MaPMT on the

34 focal plane along the z axis has a tolerance of a few cm and it is not therefore a critical issue.

35 Different functionalities are combined together into the so-called EC of the PDA of the RICH, housing

36 and operating the MaPMT. A totally modular solution, based on fully autonomous functional units,

37 is preferred, for ease of construction, reliability, maintenance and repair.

38 The housing of the MaPMT is a complex task, due to the large number of MaPMT and the many

39 requirements, including: close-packing on a large surface, ease of access for repair and maintenance,

40 constraints of volume, mass and power, structural stability, thermal control, electrical insulation and

41 magnetic shielding as well as general EMC issues; all these aspects require safe design margins.

2 Requirements

1 In order to save on the required resources and simplify the design, different functions are integrated
2 together into the EC, such as: mechanical supporting structure, HV and voltage divider for the MaPMT,
3 electrical connections from/to the MaPMT, thermal dissipation functionalities for heat transfer to
4 the cooling system, optical (lenses and/or optical filter, if any), electromagnetic (including electrical
5 insulation and magnetic shielding), shielding from external background light, Detector Control System
6 (DCS), possible components for calibration. Each EC is thus a fully autonomous device, housing,
7 operating and securing in place the MaPMT, the front-end boards as well as any other ancillary
8 system.

9 A suitable optical system might be required in order to build a uniform optical collection surface in
10 front of the photo-sensors, recovering dead regions and reducing losses of photons *.

11 Close-packing of the MaPMT inside one EC as well as close-packing of different EC inside the PDA
12 is required, in order to have a large geometrical acceptance, as uniform as possible, while reducing
13 dead-areas. Moreover, the EC is required to be a robust, light and compact one. Both the MaPMT and
14 the front-end electronics dissipate heat which must be efficiently removed by the close-packed array.
15 Heat transfer to the cooling system can be effectively helped by designing the mechanical supporting
16 structure to act also as a low thermal impedance path for heat conduction to the cooling system. DCS
17 components must be foreseen, in particular a few temperature sensors, located near hot-spots and/or
18 in thermal contact with the mechanical supporting structure. Monitoring of the gain of the MaPMT
19 would be an essential tool to correct for ageing, by changing the gain of the f/e pre-amplifiers as well
20 as to equalize the different channels.

21 The MaPMT will be readout by the CLARO front-end chip [22] (CLARO chip, in short), a dedicated
22 front-end chip developed for this experiment, whose specifications are summarized in figure 3.

	Required
Power consumption (idle)	< 1 mW / channel
Max input capacitance	≈ 20 pF (up to ≈200 pF out of specs)
Max output capacitance	≈ 50 pF (up to ≈200 pF out of specs)
Amp gain settings	1, 1/4, 1/7, 1/10 (2 bits)
Amp leading edge	< 5 ns
Amp trailing edge	< 15 ns
Amp dynamic range at gain 1 [1/10]	> 5 Me- [50 Me-]
Amp recovery from saturation	< 50 ns for signals up to 20x dynamic range*
Amp input impedance	< 200 ohm
Amp noise	< 10 ke- RMS
Comp delay	< 5 ns
Threshold settings at gain 1 [1/10]	64 steps x 30 ke- [300 ke-] (6 bits)
Threshold range at gain 1 [1/10]	0 ÷ 2 Me- [0 ÷ 20 Me-]

Figure 3: Specifications of the CLARO front-end chip.

*In the current baseline, the inclusion of an optical system is not foreseen; in fact the enormous engineering complications required to implement the optical adapter do not seem to be compensated by an appealing enough increase of the performance.

3 Design

2 In this section EC will mean EC-R, unless specified otherwise. The preliminary EC-H design is presented
3 in section 16.

4 The Photo-Detector Assembly, housing the MaPMT and their readout electronics and ancillary systems,
5 is conceived as a totally modular assembly, easily adaptable/scalable to different geometries of the PDA
6 and based on fully autonomous atomic functional units: the Elementary Cell (EC); the Photo-Detector
7 Module (PDM) is made of a suitable number of EC; a super-structure groups a suitable number of
8 PDM into rows/columns with ease of access (see section 5).

9 The concept scheme of the EC is shown in figure 4.

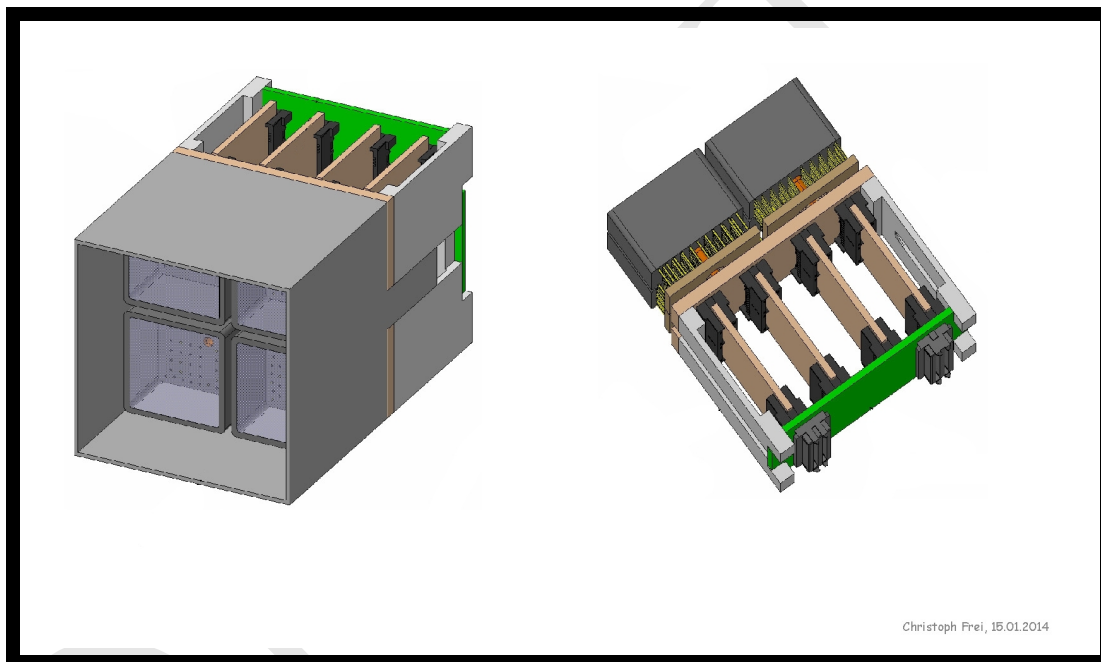


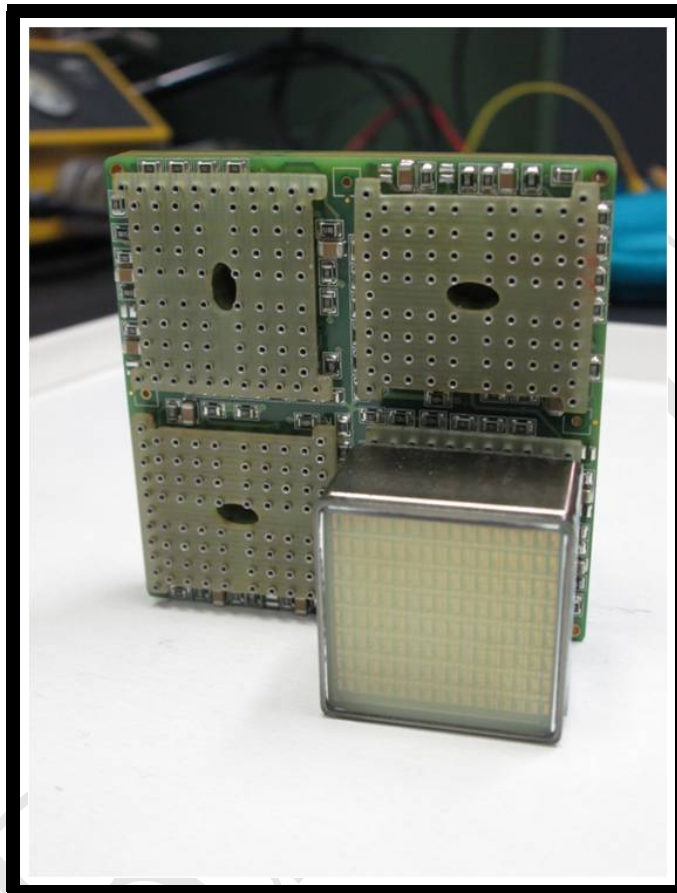
Figure 4: Concept scheme of the EC [15] (not an engineering drawing).

10 The EC is built around a thick PCB (the BaseB), with custom SMD sockets to house the MaPMT
11 as well as the voltage dividers and temperature sensors for the DCS. Thick copper layers inside the
12 BaseB are used to take out the heat produced by the voltage dividers, via thermal conduction along
13 the metallic parts. On the back-side of the BaseB eight connectors interface to the four FEB, each one
14 housing eight 8-channels CLARO chips. The HV cable starts from the center of the BaseB. Suitable
15 holes for screws are foreseen to secure the BaseB to the Aluminium case of the EC and the MS to
16 the BaseB and/or Aluminium case. The CLARO chip is mounted on the FEB as close as possible to
17 the MaPMT, in a compact structure, minimizing the input capacitance to the FEB. Four FEB per
18 EC are sandwiched between the BaseB and a BackB. The BackB interfaces the output of the FEB to
19 the DB, each one serving one line of eight contiguous MaPMT. All the components are kept together
20 by a light Aluminium structure (the case), serving both as mechanical supporting structure and for
21 thermal transfer by conduction; moreover it provides a safety ground for the EC and some shielding
22 of the FEB. The case is fastened to the supporting super-structure and in thermal contact with the
23 cooling system.

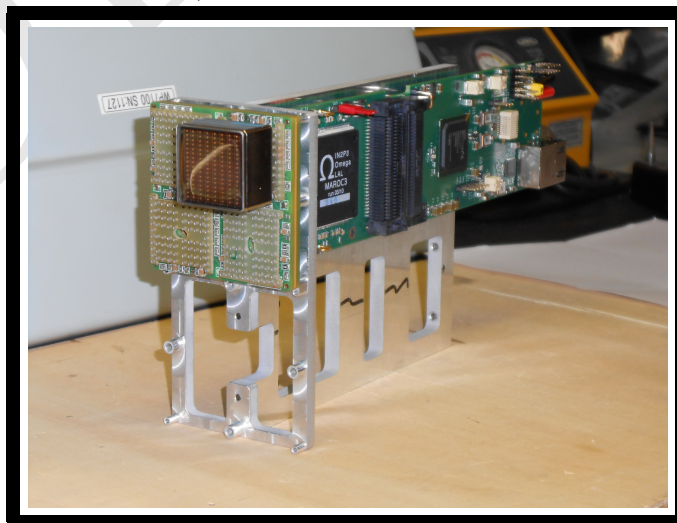
24 It must be emphasized that some design choices (for instance some sizes) are critical and are waiting
25 from final confirmation after executive design (done), prototyping (done), testing on a test-beam (done
26 in October and November) and final tests in laboratory (in progress).

27 A picture of an obsolete prototype BaseB (for use with the MAROC chip) with one MaPMT installed
28 is shown in figure 5a. A picture of an obsolete prototype PDM for laboratory tests (for use with the
29 MAROC chip) is shown in figure 5b. This system will be used as a part of the Quality Assurance
30 (see section 11), for analogue measurements and characterization of the MaPMT and the EC in the
31 production phase.

- 1 Newer prototypes corresponding to the current baseline are presented in section 10.



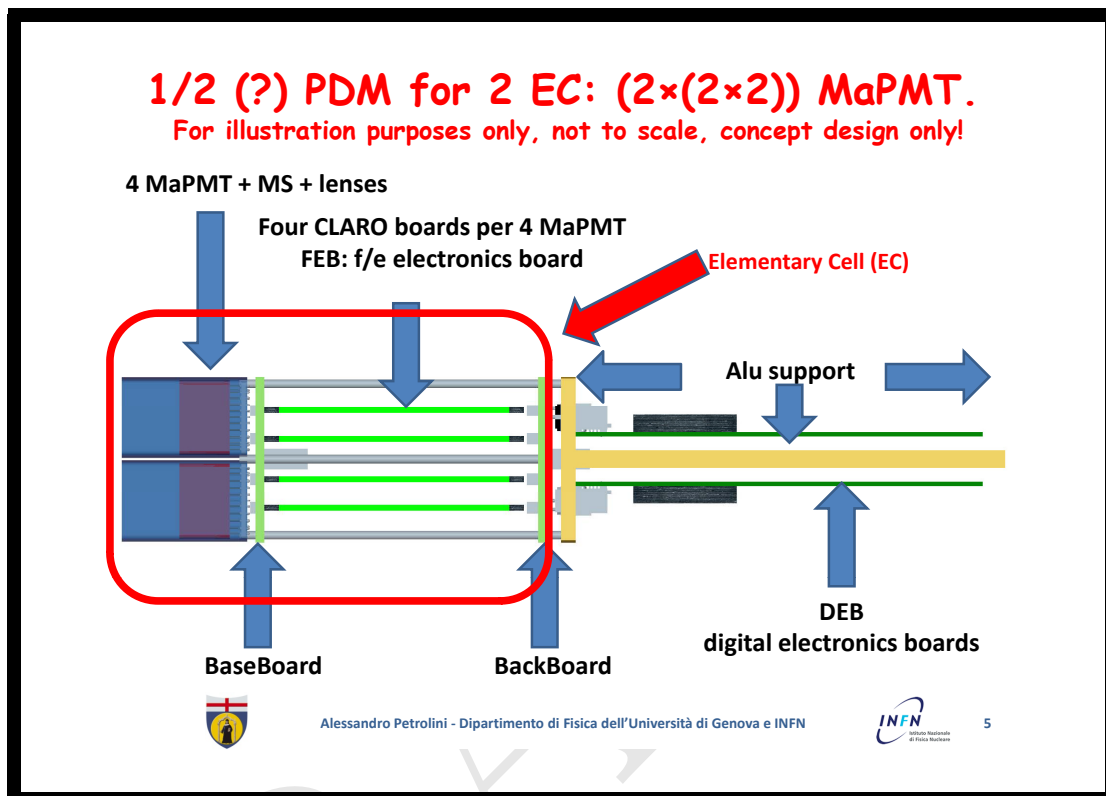
(a) Picture of one R11265-M64 MaPMT installed on its BaseB (for 4 MaPMT) developed for the LHCb RICH upgrade (for use with the MAROC chip).



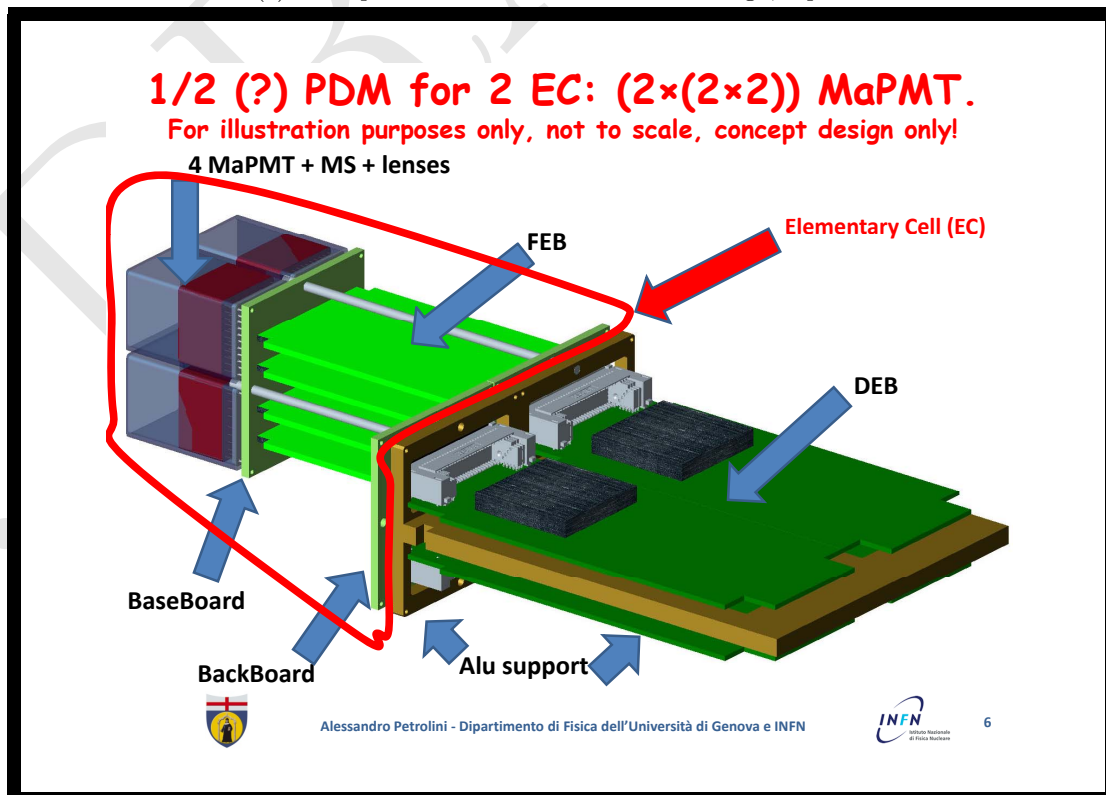
(b) Picture of one PDM developed for the LHCb RICH upgrade (for use with the MAROC chip).

Figure 5: Picture of one EC/PDM developed for the LHCb RICH upgrade (for use with the MAROC chip).

- 2 The concept scheme of the MaPMT housing design is shown in figure 6.
- 3 The overall view of the EC, from the front-side and from the back-side, is shown in figure 7.

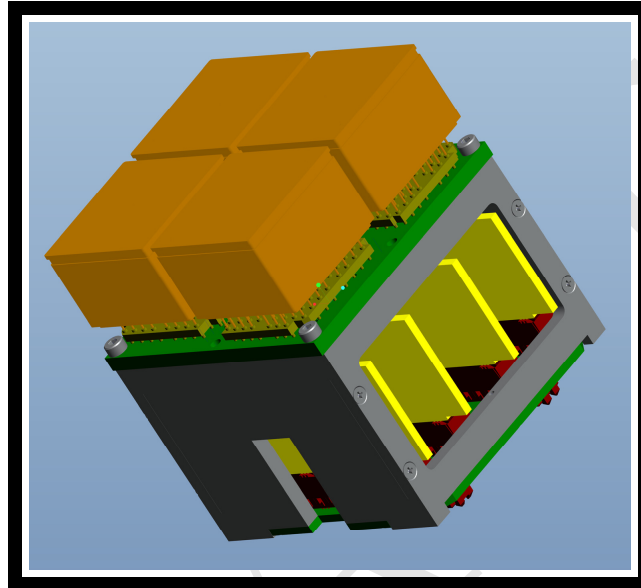


(a) Concept scheme of the EC and PDM design, top view.

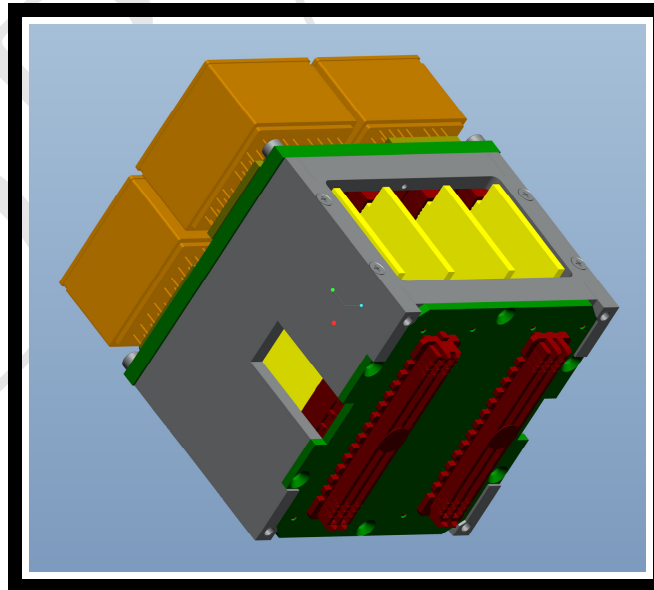


(b) Concept scheme of the EC and PDM design.

Figure 6: Concept scheme of the EC and PDM design (not to scale, not an engineering drawing).



(a) Overall view of the EC design, from the front-side (no magnetic shield).



(b) Overall view of the EC design, from the back-side (no magnetic shield).

Figure 7: Overall view of the EC design with no magnetic shield (engineering drawing). Legend: gold: MaPMT; grey: Aluminium structure; yellow: FEB; red: connectors; green: BaseB and BackB; yellowish-green: sockets for the MaPMT.

- 1 The architecture of the EC was driven by the requirement to keep as short as possible the connections
- 2 from the MaPMT anode to the input of the front-end chip for improved signal immunity.

3.1 MaPMT

- 4 The selected MaPMT are described in detail sections [A](#) and [C](#); their data sheets are shown in ap-
- 5 pendixes [E](#).
- 6 A careful system design is required, as the overall sensitivity of MaPMT is known to vary: with operating
- 7 time, while maintaining constant illumination, applied voltage and ambient conditions (ageing); on
- 8 switching the output current, after removing and re-applying either the light input or overall voltage
- 9 (hysteresis); as a consequence of changes in the ambient temperature and/or external electromagnetic
- 10 fields.
- 11 Gain control will be provided both by tuning the HV values (see sections [6.4](#), [3.2.1](#), [B.1](#)) and by
- 12 gain/threshold control of the CLARO chips (see section [\[22\]](#)).
- 13 Gain monitoring can be accomplished by dedicated threshold scans and/or from real data (TBC).
- 14 The MaPMT will be operated with anode grounding and negative HV applied to the photo-cathode;
- 15 this scheme eliminates the potential voltage difference between the anode and the external readout
- 16 circuit.
- 17 However, the metal (KOVAR) housing case of the MaPMT is connected to the PK potential. Therefore,
- 18 when operating the MaPMT under negative high voltage, the metal housing also becomes negative high
- 19 voltage. This requires a careful design for safety and insulation (see section [4.2](#)).

3.2 Base-Board

- 21 The BaseB version presented here fits the EC-R.
- 22 The BaseB, a thick PCB, is the skeleton of the EC. It is equipped with four SMD custom sockets
- 23 through which the R11265-M64 receive the bias voltages and deliver the anode signals. The opposite
- 24 side of the BaseB is equipped with eight connectors through which the anode signals are routed to
- 25 the four FEB. In addition to that, the BaseB hosts sensors for measuring the temperature of the
- 26 BaseB itself, located close to the FEB in order to be sensitive to the temperature of the FEB too (see
- 27 section [3.2.3](#)).
- 28 The design of the PCB aimed at obtaining a product with good performances but also to follow
- 29 industrial standards in order to improve the reliability and to save on the production costs.
- 30 In the current baseline design the pitch between two neighbouring MaPMT inside the EC is 28.0 mm.
- 31 After full validation of the current conservative and safe design, a possible further small reduction of
- 32 the pitch will be investigated, as this would improve the geometrical acceptance. A further reduction
- 33 of the pitch, if at all possible, has implications on the design and reliability of all the components of
- 34 the EC: routing of the electrical traces, minimal insulation spacing between components under HV,
- 35 design of the case and design of the mechanical fasteners in the reduced space, size of the connectors
- 36 and design of the PCB of the BaseB, FEB and BackB. The trade-off between the better performance
- 37 of the RICH versus manpower, risk and reliability will be evaluated.
- 38 In the current design of the BaseB, it was avoided to use any additional space along the edges, in order
- 39 to allow close packing of different EC and keep the pitch of two neighbouring MaPMT belonging to
- 40 two neighbouring EC as close as possible to the pitch of the MaPMT inside the EC.
- 41 It should be noted that the mechanical precision quoted by Hamamatsu for the MaPMT is rather poor:
- 42 $\pm(0.2 \div 0.5)$ mm.

43 *3.2.1 High Voltage for the MaPMT*

- 44 The electrical scheme of the on-board voltage divider is shown in figure [8](#). See section [B.1](#) for more
- 45 details.

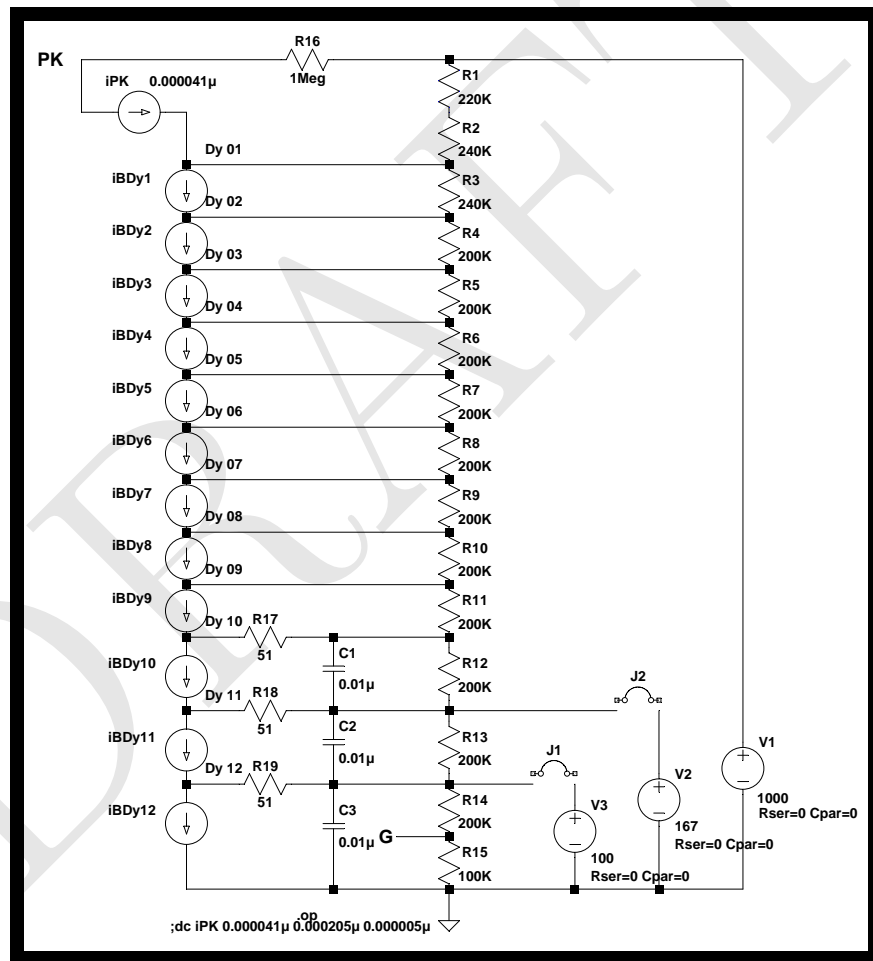


Figure 8: Electrical scheme of the HV voltage divider for the MaPMT, with three power supplies.

1 In order to cope with the average gain variation between different R11265-M64, up to 1:3 from spec-
2 ifications, the MaPMT will be grouped for similar gain and one single PDM will be populated with
3 MaPMT with similar gain. In this way, the gain of different PDM will be equalized by suitably setting
4 the HV (see section 6.4). In order to cope also with the gain variations between different pixels of the
5 same R11265-M64, up to 1:3 from specifications, the CLARO chip allows setting the gain and threshold
6 on a channel-by-channel basis (see figure 3 and [22]). Moreover this feature of the CLARO chip gives
7 one more option to equalize the average gain of different MaPMT, without changing the HV. Tests
8 are on-going to confirm that the gain changes with ageing is similar for MaPMT/pixels with the same
9 gain; nevertheless the capability of the CLARO to set the gain and threshold on a channel-by-channel
10 basis, would allow a time-dependent equalization of gain.

11 3.2.2 PCB design

12 A baseline was defined; main specifications:

- 13 • pitch between the 4 MaPMT inside the EC: 28.0 mm (individual 0.5 mm thick MS are possible
14 as well as one single MS per four MaPMT is possible);
- 15 • size of the EC: square 55.4 mm side (that is, size of the BaseB PCB);
- 16 • pitch between the two pairs of FEB: 12.6 mm, centred on the MaPMT;
- 17 • pitch between the two connectors to the DB: 28.0 mm;
- 18 • pitch between any two EC: $\approx 55.4 \text{ mm} + 0.6(1.0) \text{ mm} = 56.0(56.4) \text{ mm}$ (TBC); it depends on the
19 MS, if any; it also depends on the direction, whether along or perpendicular to the row/column.

20 At each corner and at the center of each side (TBC) a 2.0 mm hole is located (for M2.0 screws); the
21 center of every hole is at 2.0 mm from the edge of the BaseB.

22 The PCB is made of 4 essentially identical quadrants each one carrying a custom socket [†] for the
23 MaPMT (see figure 9) and its voltage divider. It was preferred to improve the reliability adopting one
24 voltage divider per MaPMT in order to avoid to loose the full EC in case of fault of one single MaPMT.

25 The components, resistors and capacitors, of the voltage dividers were placed on the top layer (see
26 figure 10), as close as possible to the corresponding dynode: the routing was carried on as far as
27 possible on the top layer; whenever impossible the inner layer was used. Resistors of the voltage divider
28 have the 0306 case [‡]. Capacitors of the voltage divider have the 1206 case [§] (10 nF). The voltage rating
29 of the components is 150 V and the power rating is 0.2 W (TBC).

30 The temperature coefficient of the resistors must be checked (see Hamamatsu) (TBC).

31 The HV arrives at the center of the BaseB. Each MaPMT is rotated by 90 degrees with respect to its
32 neighbours so that all photo-cathode pins are at the center of the BaseB. Moreover this rotation allows
33 a better usage of the limited available space because the dynode pins of the MaPMT are only present
34 along two opposite sides of the MaPMT.

35 Three independent HV lines are present, with nominal values: $VH1 = 1000 \text{ Vcc}$, $VH2 = 167 \text{ Vcc}$,
36 $VH3 = 100 \text{ Vcc}$. The three HV wires plus ground were directly soldered on the back of the BaseB. Note
37 that, based on the current expectation, VH2 and VH3 may be only required in about one hundred
38 MaPMT at the center of RICH1 (VH1 only is sufficient elsewhere). Thin HV cables will be soldered
39 on the BaseB.

40 The proposed cable is the (not-shielded) AlphaWire 39X2205, capable to withstand 5kV, with a di-
41 ameter 1.8 mm; it is insulated with silicone rubber and readily available. These cables will arrive to
42 a patch panel to connect to cables coming from the power supplies. Tests will be carried on (both in
43 laboratory and test-beam) to check whether a shielded HV cable provides better immunity from noise.

44 The option of using a connector was abandoned due to lack of space.

[†]DSMI electronics SA

[‡]PANASONIC Anti-Surge Thick Film Chip Resistors, 0603, Type ERJP03.

[§]TDK C3216-X7R-2J-103K - 630V.

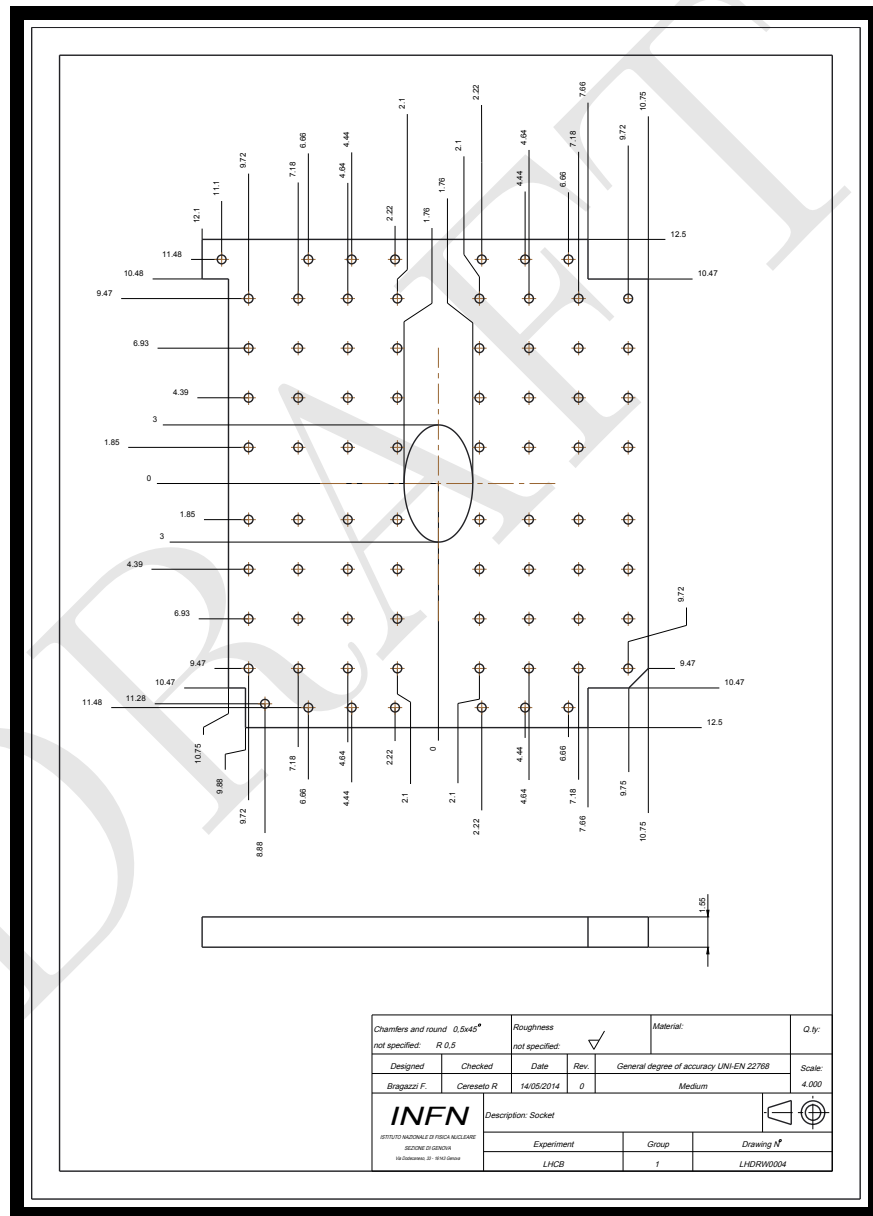
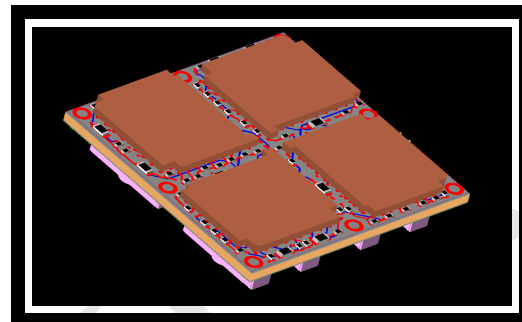
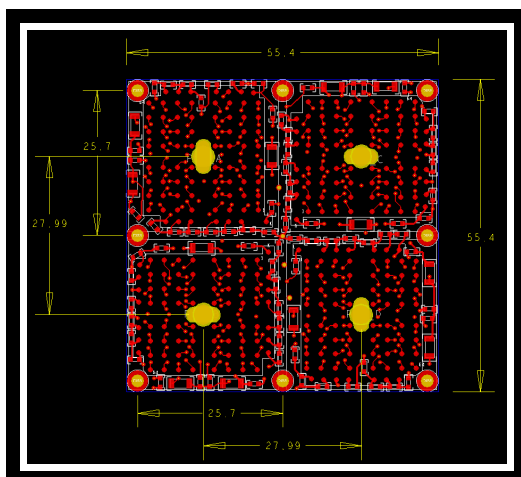


Figure 9: Engineering drawing of the custom socket for the MaPMT.



(b) 3D top view of the BaseB.

(a) Top Layer of the BaseB.

Figure 10: Top view of the BaseB (facing the MaPMT).

- 1 The temperature of all the EC, and in particular of the MaPMT and CLARO, must be kept well under
- 2 control in order to allow a proper functioning of the MaPMT (lower dark counts) and stability of the
- 3 parameters of both the MaPMT and CLARO. Therefore, in order to help with heat dissipation, the
- 4 PCB has been designed to drive the heat through copper layers within the PCB, to the aluminium
- 5 case of the EC. Six heat-sink internal copper planes, each one 0.105 mm thick, have been introduced.
- 6 The BaseB PCB has a total of 12 layers (see the stackup in figure 11) and a thickness $t \approx 3.1$ mm
- 7 (maximum thickness compatible with 0.3 mm diameter vias).

Subclass Name	Type	Material	Thickness (MIL)	Conductivity (mho/cm)	Dielectric Constant	Loss Tangent	Negative Artwork	Shield	Width (MIL)
1	SURFACE	AIR			1	0			
2	TOP CONDUCTOR	COPPER	1.37	595900	5.2	0			16.0
3	DIELECTRIC	FR-4	8	0	4.5	0.035			
4	INNER_1 CONDUCTOR	COPPER	1.37	595900	4.5	0.035			16.0
5	DIELECTRIC	FR-4	8	0	4.5	0.035			
6	GND_T PLANE	COPPER	1.37	595900	4.5	0.035			
7	DIELECTRIC	FR-4	8	0	4.5	0.035			
8	DISS_1 PLANE	COPPER	4.13	595900	4.5	0.035			
9	DIELECTRIC	FR-4	8	0	4.5	0.035			
10	DISS_2 PLANE	COPPER	4.13	595900	4.5	0.035			
11	DIELECTRIC	FR-4	8	0	4.5	0.035			
12	DISS_3 PLANE	COPPER	4.13	595900	4.5	0.035			
13	DIELECTRIC	FR-4	8	0	4.5	0.035			
14	DISS_4 PLANE	COPPER	4.13	595900	5.2	0.035			
15	DIELECTRIC	FR-4	8	0	4.5	0.035			
16	DISS_5 PLANE	COPPER	4.13	595900	4.5	0.035			
17	DIELECTRIC	FR-4	8	0	4.5	0.035			
18	DISS_6 PLANE	COPPER	4.13	595900	4.5	0.035			
19	DIELECTRIC	FR-4	8	0	4.5	0.035			
20	GND_B PLANE	COPPER	1.37	595900	5.2	0.035			
21	DIELECTRIC	FR-4	8	0	4.5	0.035			
22	INNER_2 CONDUCTOR	COPPER	1.37	595900	4.5	0.035			8.0
23	DIELECTRIC	FR-4	8	0	4.5	0.035			
24	BOTTOM CONDUCTOR	COPPER	1.37	595900	5.2	0			16.0
25	SURFACE	AIR			1	0			

Figure 11: Stackup of the BaseB PCB.

- 8 The anodes of the MaPMT are routed to eight SAMTEC HSEC8-120-01-L-DV-A-K connectors (see
- 9 figure 12), placed on the backside of the BaseB (see figure 13). Signal traces are as short as possible,
- 10 to minimize parasitic capacitances.
- 11 The electrical scheme of 1/2 BaseB is shown in figure 14.

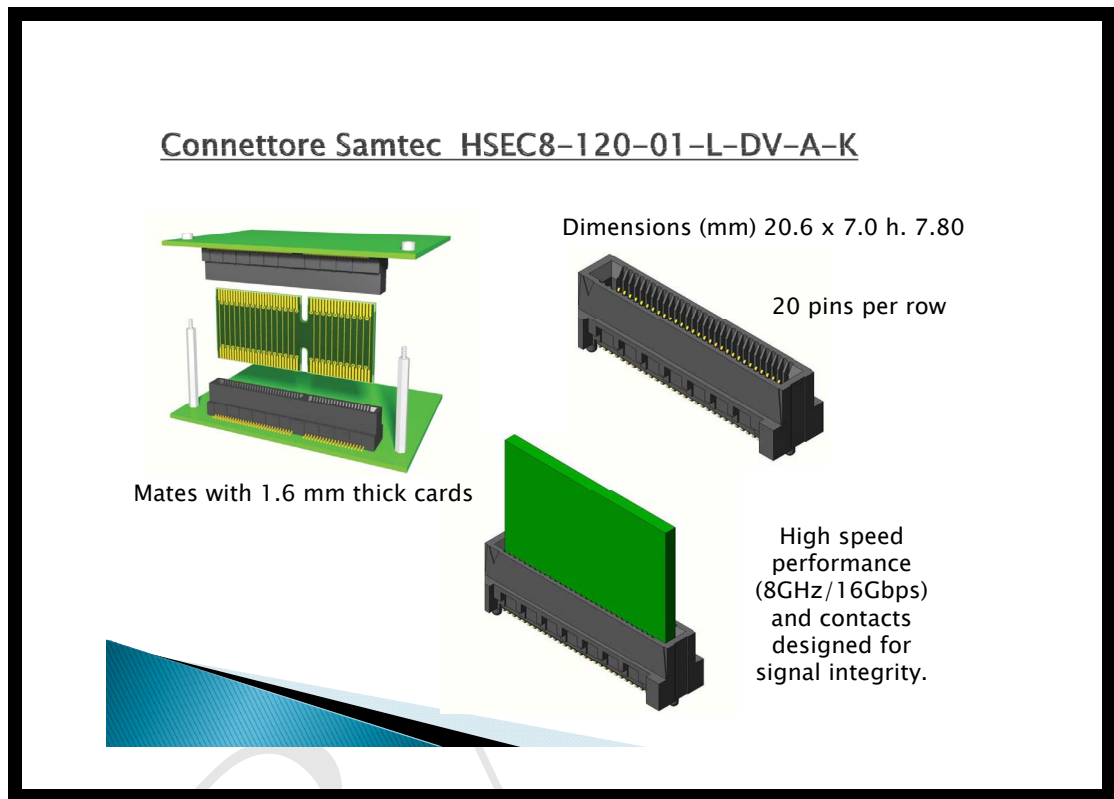
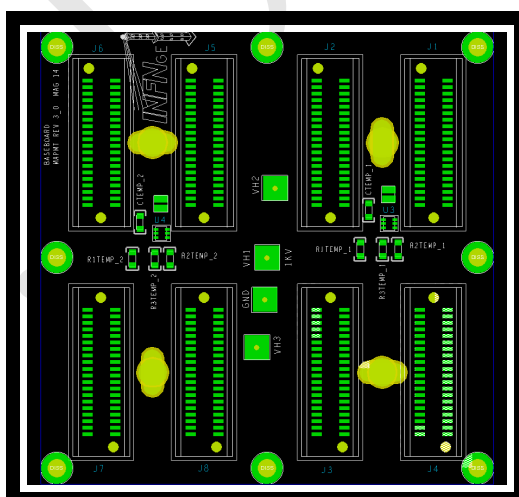
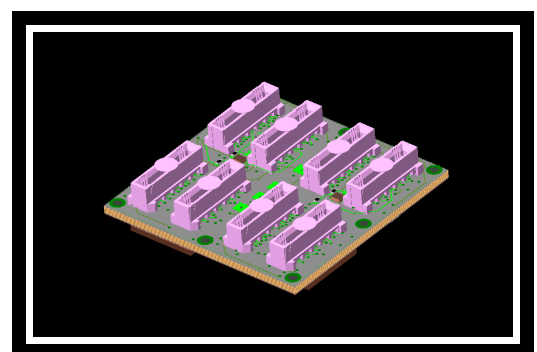


Figure 12: SAMTEC-HSEC8-120



(a) Bottom Layer of the BaseB.



(b) 3D bottom Layer of the BaseB.

Figure 13: Bottom Layer of the BaseB (away from the MaPMT).

1 3.2.3 The measurement of the temperature of the BaseB

2 The BaseB also houses two temperature sensors, for redundant monitoring of the temperature of the
3 BaseB.

4 The temperature sensors used in the prototypes are the active temperature sensors TMP102[¶], biased
5 and read-out by the DB through the FEB connectors and the FEB, which reserve a few traces to this
6 purpose.

7 A view of the bottom layer of the BaseB with the two temperature sensors is shown in figure 15.

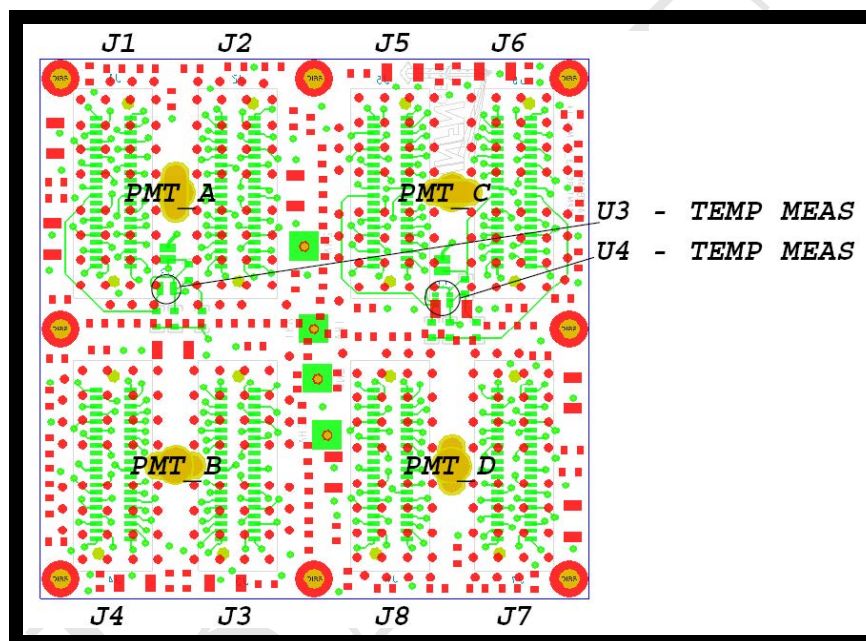


Figure 15: View of the bottom layer of the BaseB with the two temperature sensors.

8 For the final production version it was decided to use two SMD PT100 sensors, readout, through the
9 FEB, by the GBT-SCA present on the DB. In fact, the GBT-SCA ASIC [4] on the DB has an ADC
10 that can digitise up to 32 multiplexed analogue channels.

3.3 FEB

12 The FEB is described in all details in the documents produced for the CLARO/FEB EDR [24]. The
13 FEB version presented here fits the EC-R.

14 The CLARO FEB is a PCB designed to support the CLARO8 ASIC exploited inside the EC. In this
15 report CLARO chip will always imply the CLARO8 (8-channels) chip.

16 Figure 16 shows some construction details of the FEB and the BackB inside the EC assembly.

17 An overview of the design of the FEB is shown in figure 17.

3.4 BackB

19 The BackB is described in all details in the documents produced for the CLARO/FEB EDR [24]. The
20 BackB version presented here fits the EC-R.

21 The BackB is the interface between the FEB and the DB, routing the signals from the FEB to the DB,
22 via connectors:

- 23 • front of the BackB, from the FEB: HSEC8-150-01-L-DV-A-K (4 per BackB);

[¶]Texas Instrument TMP102

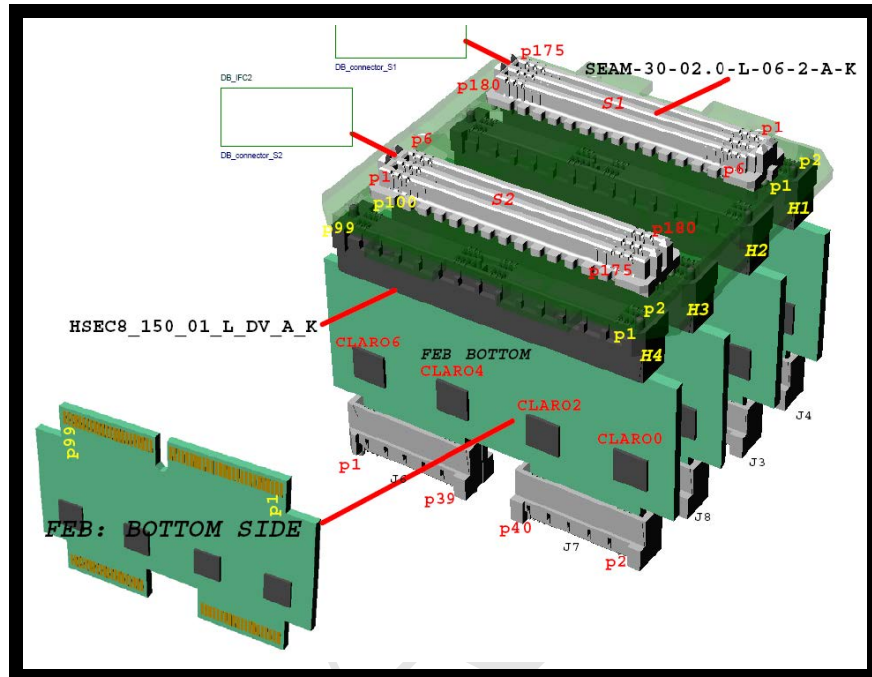


Figure 16: Construction details of the FEB and the BackB inside the EC assembly.

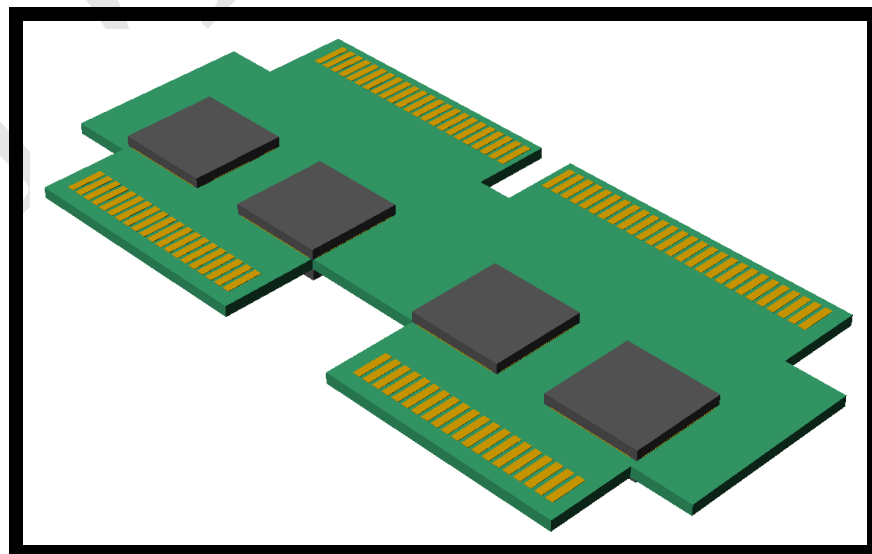


Figure 17: FEB overview.

1 • back of the BackB: SEAM-30-02.0-L-06-2-A-K (2 per BackB) (mating SEAF-30-01-L-06-2-RA
2 on the DB).

3 The two connectors to the DB are rotated, one with respect to the other, by 180° in the plane of the
4 BackB so that two identical DB, after mounting, will have their components facing the center of the
5 row/column.

6 Moreover a few ancillary components are present.

7 • A 10-bit DAC with I2C interface, followed by an analogue fanout/level adapter, to drive the
8 *TEST_level* line. This is routed (through the edge connectors) to the *TEST_analog_voltage_level*
9 of the connected CLARO chip to determine the amount of charge injected by each diagnostic
10 test pulse into the input of the enabled CLARO chip channels.

11 • A PCA9555 I/O expander with I2C interface, which provides the FEB with the individual CLARO
12 *chain_enable* signals. The output of the I/O expander are static and are only significant during
13 the SPI transactions scheduled by the DB for the configuration of the CLARO on the connected
14 FEB. The I2C expander is not required to store any long term information.

15 • Some additional digital buffer and level adapters.

16 The I2C bus (I2C.SDA, I2C.SCL) controlling the on-board DAC and I/O expander could also control
17 the TMP102 temperature sensors with I2C interface. It is also possible, by rearranging some resistors,
18 to connect the TMP102 to a separate I2C bus (AUX.SDA, AUX.SCL) connected to the DB.

19 All devices on board may be operated at a (2.5 ÷ 3.3) V power supply voltage. The total power
20 dissipation on the BackB is about 4 mW.

21 The development of the BackB artwork could be finalized only after the dimensional constraints,
22 determined by the design of the super-structure and cooling system, were settled. The same dimensional
23 constraints made also the routing of the PCB more difficult.

24 The artwork of the BackB is shown in figure 18.

25 A view of the front-side of the BackB is shown in figure 19.

26 A view of the BackB assembled into the EC, seen from the back-side is shown in figure 20. The figure
27 shows that the BackB also serves as structural element of the EC, by keeping in place the FEB.

3.5 Mechanical case

29 The version of the case of the EC presented here fits the EC-R.

30 The metal mechanical supporting structure of the EC also serves to take out the heat produced inside
31 the EC to the refrigerating fluid via thermal conduction. and as detector safety ground at the EC.

32 It is made by anticorodal Aluminium plates, 3 mm thick, properly machined and made black, if neces-
33 sary (TBC), either by painting or anodising, in order to absorb stray-light. Good thermal contact will
34 be ensured by a suitable thermal grease and/or glue (TBC) (and/or thermal pads/tapes).

35 The mechanical structure will be assembled by four machined plates: two identical sides (see figure 21)
36 plus two identical top/bottom bases (see figure 22) assembled via M1.6 stainless steel screws.

37 The BaseB will be mounted onto the mechanical super-structure via M2.0 stainless steel screws. The
38 BackB will be mounted onto the mechanical structure via M1.6 stainless steel screws (2/4/6-TBD).
39 BaseB and BackB will sandwich the four FEB.

40 The exact length of the Aluminium case, that is the length along the *z* direction, will be tuned after
41 tests and measurements on prototypes to the best value, taking into account soldering, connectors,
42 possible thermal pads (TBD).

43 The mechanical structure of the EC will be mounted on the row/column super-structure via four
44 M2.0(M2.5?) (TBC) stainless steel screws. In the first prototypes M2.5 stainless steel screws have been
45 used; this required to make a small part of the two side-plates 4 mm thick, instead of 4 mm. As this
46 make the construction much more complex than using a flat 3 mm thick plate, it is foreseen in the final

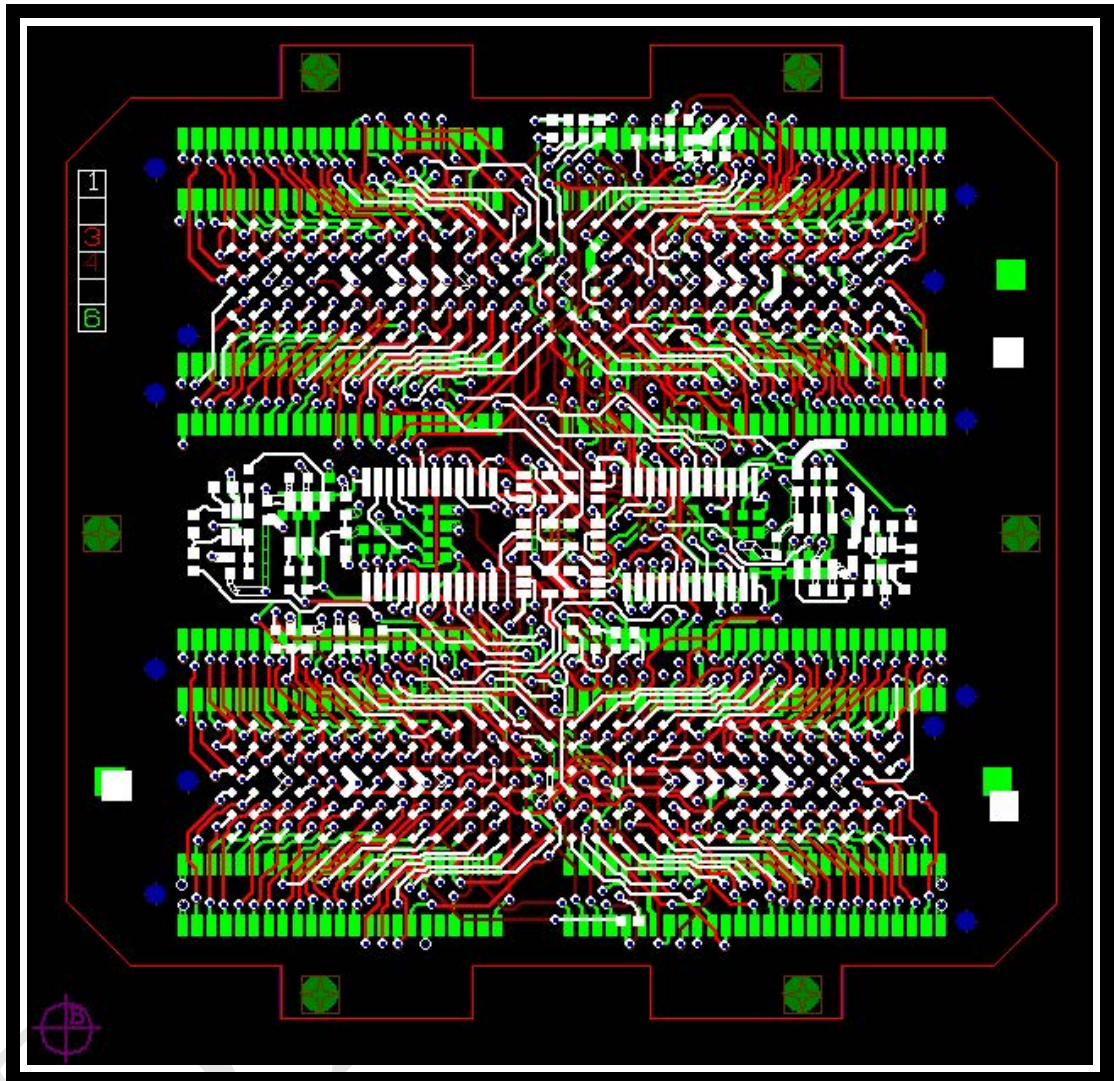


Figure 18: BkBd artwork.

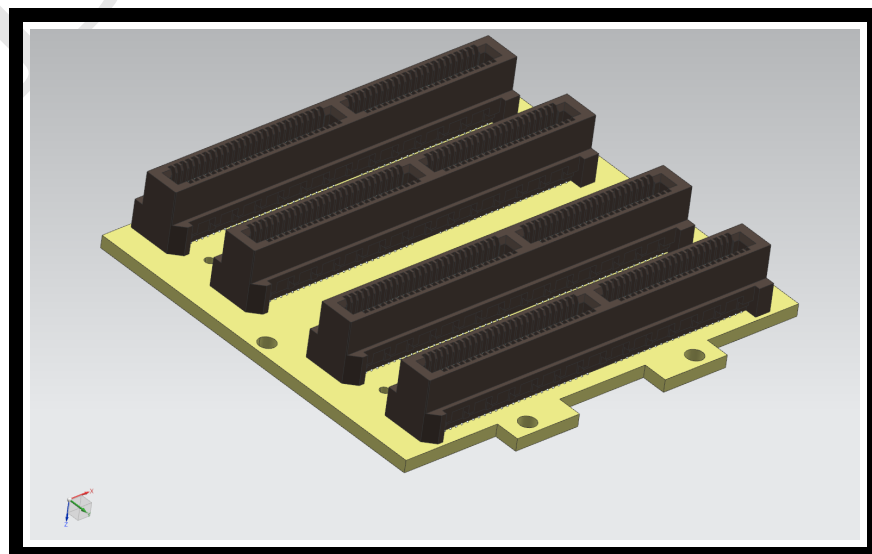


Figure 19: View of the front-side of the BackB.

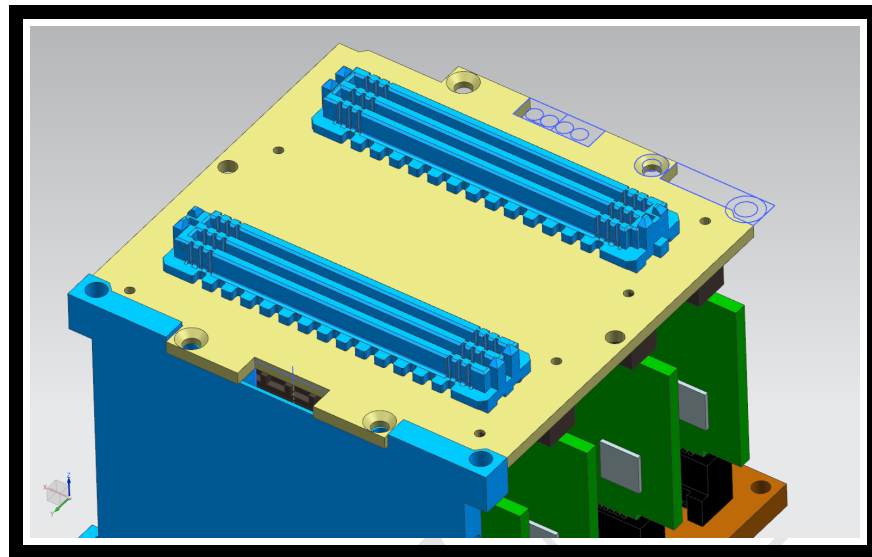


Figure 20: View of the BackB and EC assembly from the back-side.

1 version to use M2.0 stainless steel screws on the flat 3 mm thick plate. In fact, preliminary tests on the
2 prototype confirm that the structure is robust enough from the mechanical point of view (TBC).

3 An array of EC will be installed column-wise/row-wise in a fixed position; all EC will be aligned along
4 the direction of the plane of the FEB; rows/columns of EC must be able to slide one near the other, for
5 mounting and dismounting (see section 5). Therefore the size of the mechanical case has been reduced
6 by 1 mm with respect to the size of the BaseB in the direction perpendicular to the EC array, in order
7 to have a larger clearance, wherever possible, between to arrays of EC.

3.6 Local Magnetic Shielding

9 See [22] for the behaviour of R11265-M64 in magnetic fields.

10 The magnetic shields surrounding the PDA reduce the fringe magnetic field to a maximum value of
11 ≈ 2.5 mT in RICH1 and ≈ 0.5 mT in RICH2 [6].

12 However, in order to obtain a further reduction, additional local shields have been foreseen. It is
13 expected that the shields will protrude by up to approximately ≈ 10 mm beyond the surface of the
14 photo-cathode window. Therefore a careful design will be required in order for the MS not to introduce
15 shadowing of Cherenkov photons.

- 16 • Most likely a MS is not needed in the central (EC-R) part of RICH2;
- 17 • Most likely a MS is needed in all RICH1 (all EC-R);
- 18 • A MS might be needed in the up and down parts (EC-H) of RICH2.

19 3.6.1 Design

20 At present, two options are being considered.

- 21 • Use one MS per 4 MaPMT: all around the EC (see, for instance, the left picture in figure 4).
22 Cons: it will probably take some more space around the EC and make the pitch between EC larger;
23 it is not easy its mechanical fixation to the rest of the EC. Pros: simple; complete screening all
24 around the MaPMT.

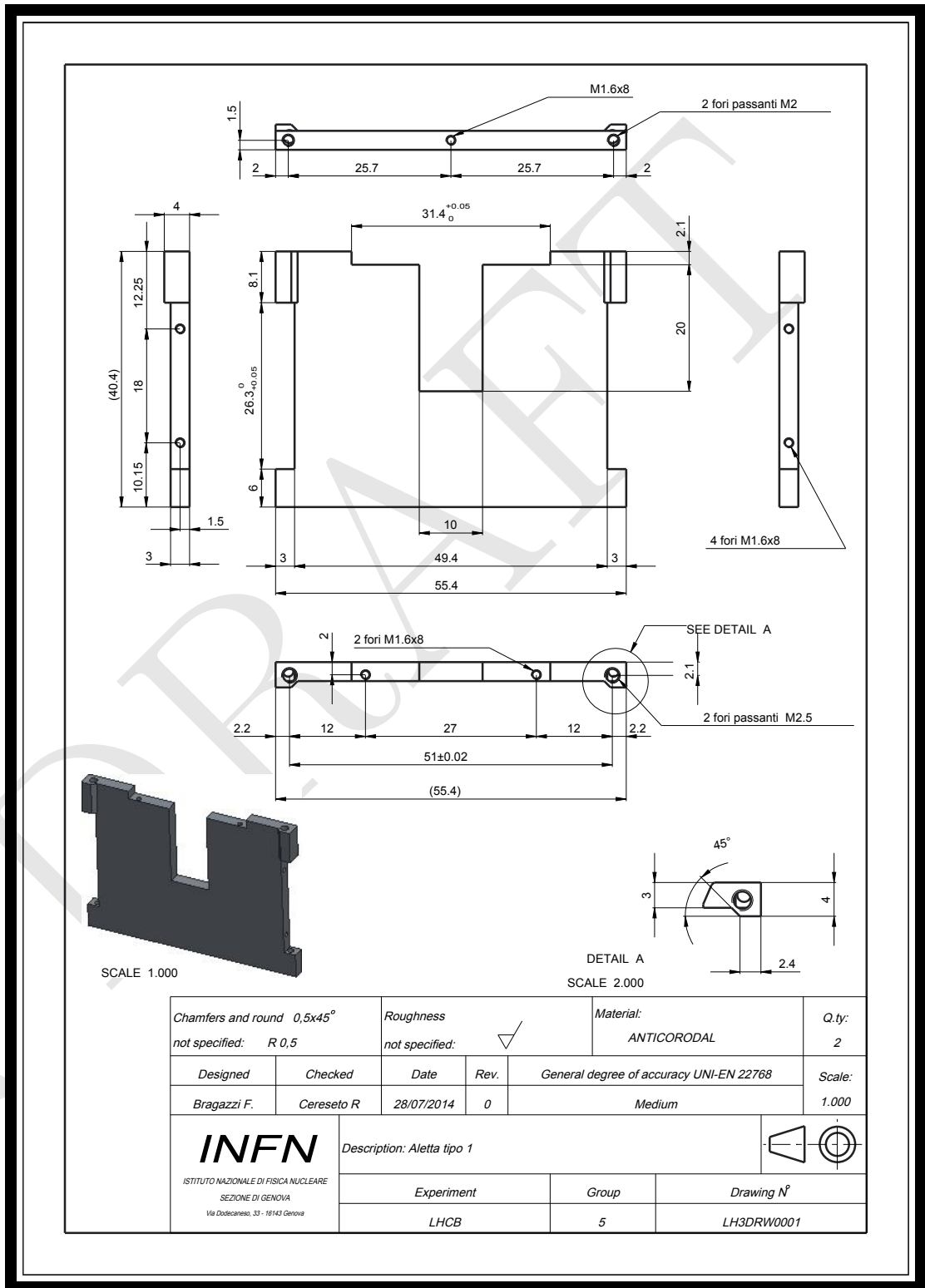


Figure 21: Mechanical design of the EC: sides.

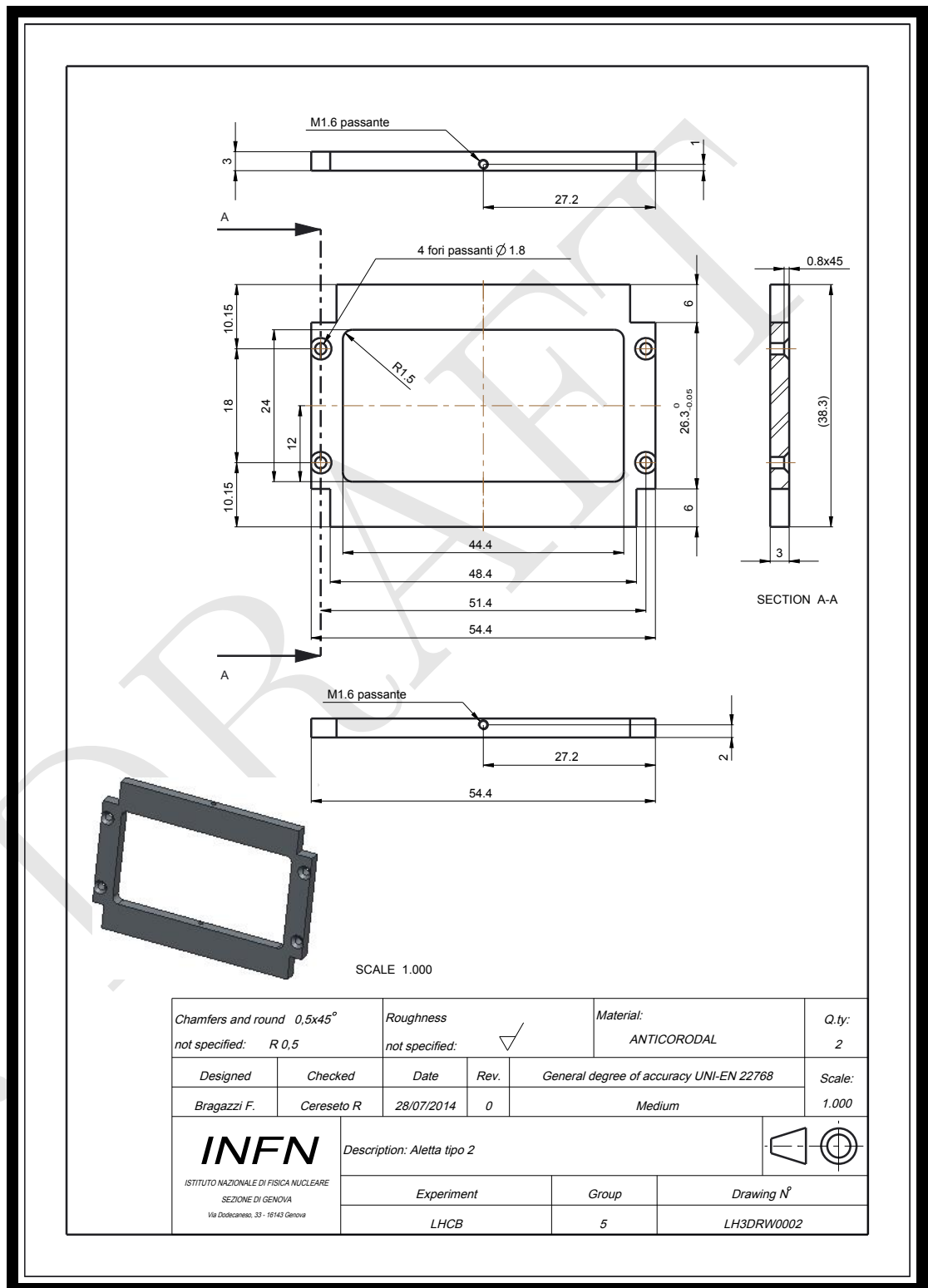


Figure 22: Mechanical design of the EC: bases.

- 1 • Shape one MS per EC crosswise, in between the 4 MaPMT.
- 2 For each MaPMT the MS *square* surrounding 4 MaPMT will be (almost) closed by the three
- 3 neighbouring MaPMT of the three neighbouring EC.
- 4 Cons: about one mm gap at the center of each MS (over 56 mm side length): this is most
- 5 likely negligible, but it has to be tested on prototypes and possibly simulated. Pros: very simple
- 6 construction and mechanical interface; can be made up to 1 mm thick.

7 3.6.2 Integration of the MS into the EC

3.7 Optical adapter system

- 9 Various optical adapter systems were considered and studied (see for instance [5]).
- 10 However, in the baseline design, the inclusion of an optical system is not foreseen; in fact the enormous
- 11 engineering complications required to implement the optical adapter do not seem to be compensated
- 12 by an appealing enough increase of the performance.

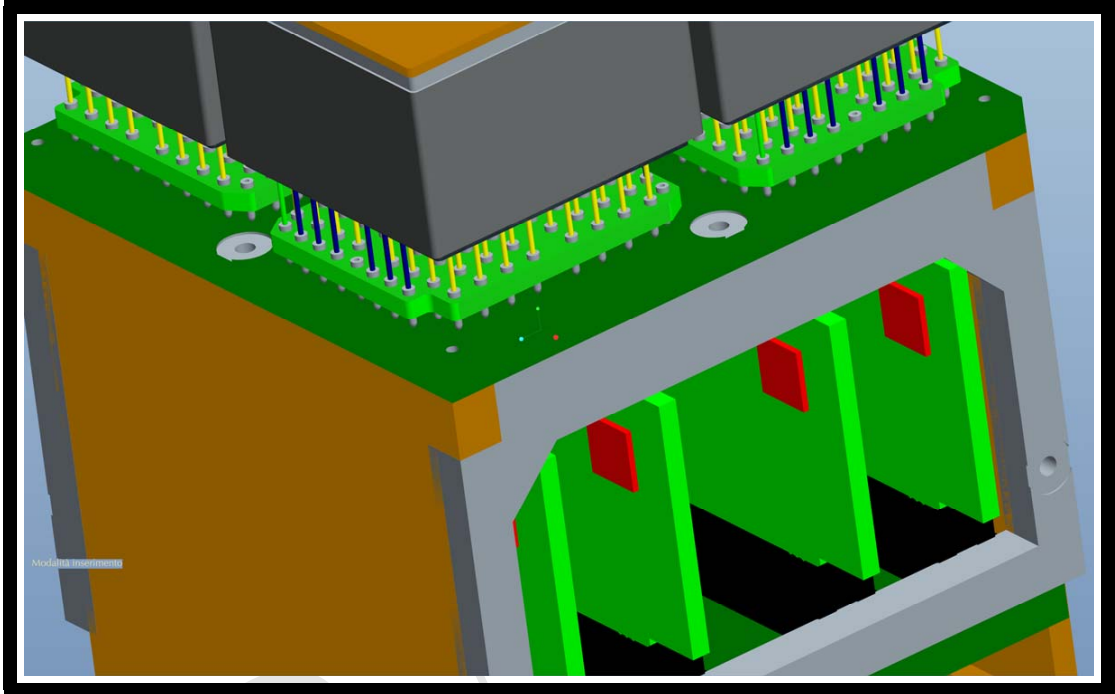
3.8 Drawings

- 14 The full CAD model in STEP format is available at: [Download the EC CAD STEP Model](#). Some
- 15 drawings can be found in section 8.1.
- 16 Details of the design of the mounting of the MaPMT are shown in figures 23a, 23b, 23c.

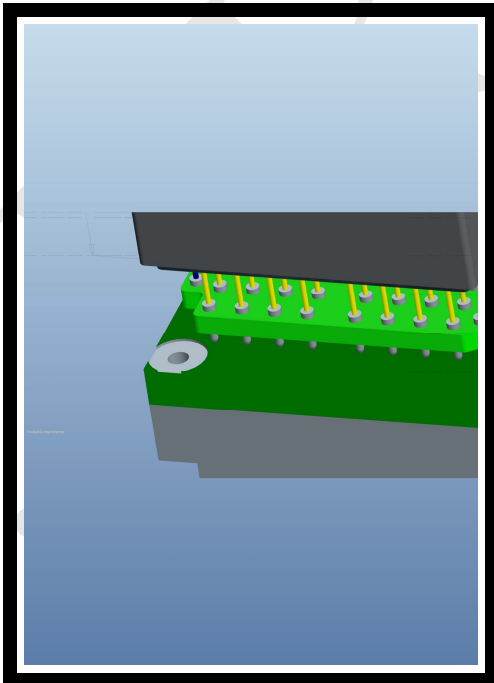
3.9 Critical design issues

4 On-detector electronics overview

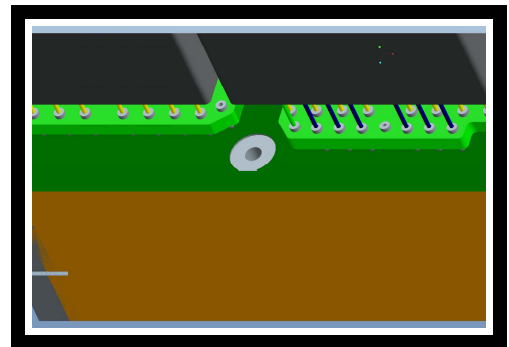
- 19 See [22] for an overview of the on-detector electronics.



(a) Detail of the MaPMT mounting (1)



(b) Detail of the MaPMT mounting (2)

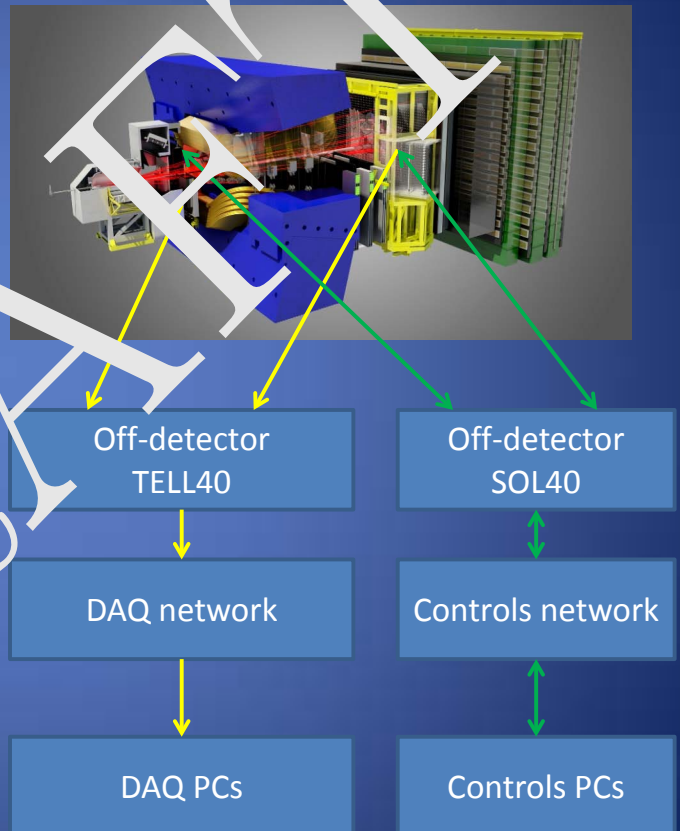


(c) Detail of the MaPMT mounting (3)

Figure 23: Details of the MaPMT mounting.

Architectural overview

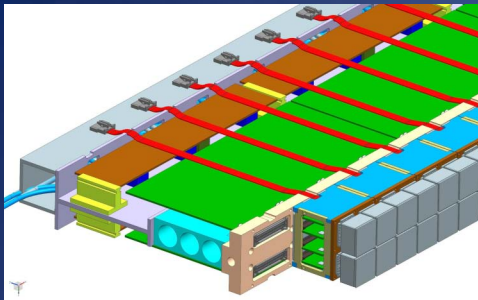
- LHCb RICH detectors capture images of Cerenkov rings.
- 4000, 64-channel multi-anode photomultipliers used as active sensor element.
- Front-end electronics will capture PM signals at rate of 40MHz.
- All captured data transported off-detector to readout network using serial optical links.
- Readout network forwards all data to event PC farm running event selection algorithms.
- Controls (“fast” and “slow”) use same link technology and protocol as DAQ, but is bidirectional with separate infrastructure.



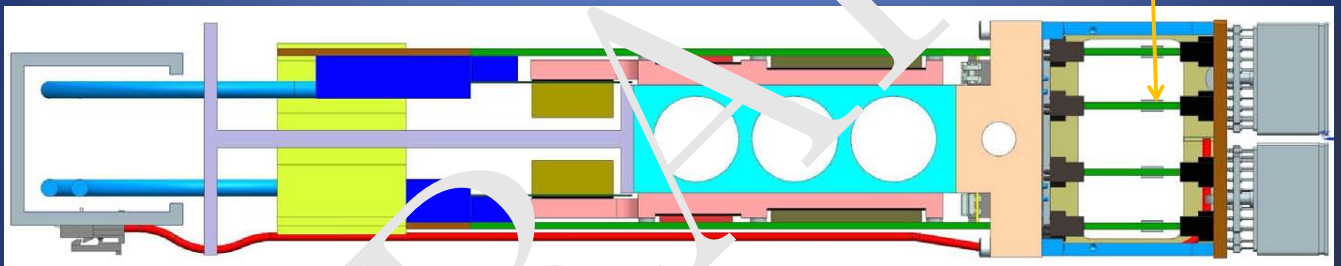
Role of the CLARO ASIC

- Part of the data-acquisition chain for the upgraded LHCb RICH detectors.
- Amplifies and shapes the fast analogue signals from 64-channel multi-anode photomultipliers.
- Applies a threshold to the amplified signals to generate a digital output pulse for each input channel above threshold.

On detector The Front-end Module



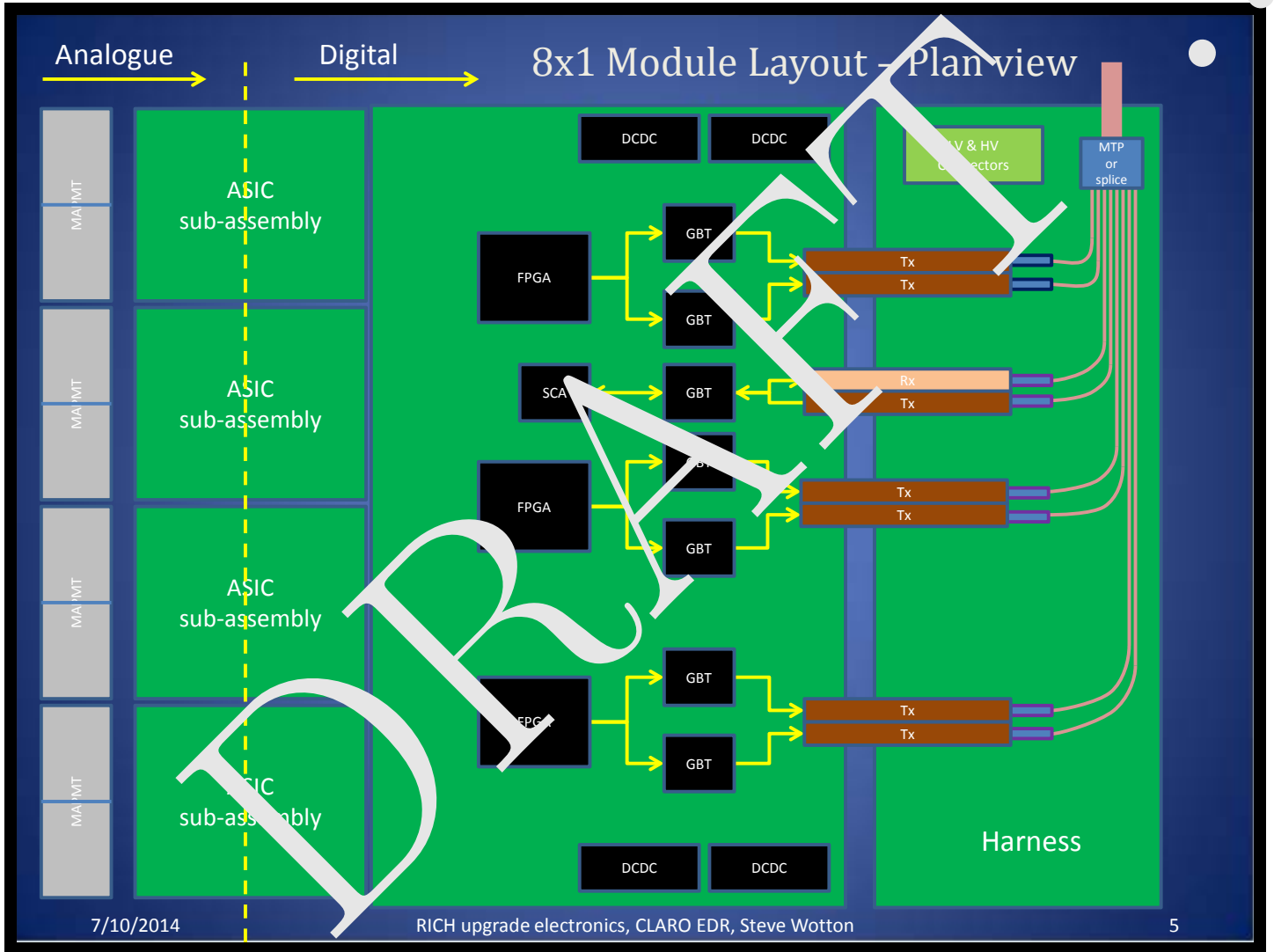
CLAROs mounted on FEBs



Harness
Optical links
LV Cables
HV Cables

Digital Module
Digital Board [1×8]
Support mechanics [2×n]
Cooling [2×n]

Elementary Cell
MAPMT [1×1]
Base Board [2×2]
Front End Board [½×2]
Back Board [2×2]



Environmental Constraints

- Signal integrity
 - Low capacitance coupling requirement between PMT anodes and CLARO inputs to minimise cross-talk
 - Low noise required for good noise rejection with single photon signal.
- Severe space constraints
 - Challenging mechanical integration and installation.
 - Poor accessibility for maintenance, Reliability, fault isolation.
 - Active cooling required in confined space to remove heat from sources in close proximity to sensitive elements (photocathode ages rapidly above 35C).
- Radiation
 - Must tolerate predicted instantaneous and integrated dose.
- Magnetic field
 - restrictions on powering and power filtering (use of inductive elements). Use of DCDC converters and active filters.

Summary of significant dates

- CLARO (+carrier board) EDR Oct 2014
- EC EDR Oct 2014
- Beam tests Oct/Nov 2014
- EC PRR Late Q1 2015
- CLARO (+carrier board) PRR Early Q2 2015
- Production submission July 2015
- Production testing Q2,Q3 2016
- Column assembly/test 2017
- LHC ready to install Sept 2018

- 1 A short overview summary is presented starting at page 27.

4.1 DB

- 3 A scheme of the current DB is shown in figure 24.

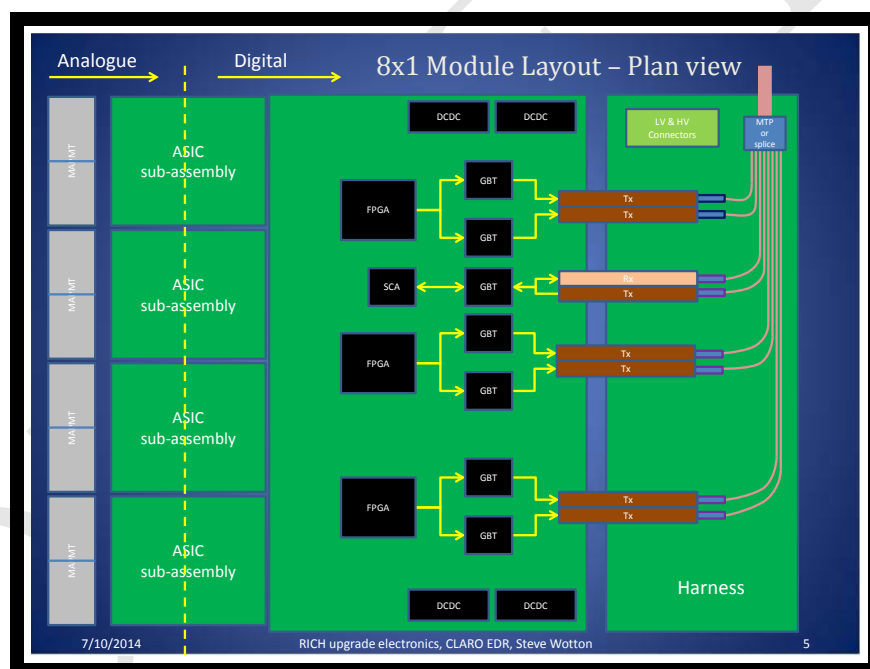


Figure 24: Scheme of the DB

4.2 Grounding and Shielding of the EC

- 5 See [25, 26] for the specifications in LHCb.

6 4.2.1 Base-Board

- 7 An approximate schematics of the shielding and grounding at the BaseB is shown in figure 25

8 Note that, on the BaseB, the signal (i.e. HV) and safety grounds are separated.

9 4.2.2 The Magnetic Shield

10 As the external metal case of the MaPMT is at a high negative potential (the same as the PK) a
11 suitable insulation must be present between the MaPMT case and the magnetic shield.

12 The magnetic shield must be grounded (possibly through a resistor, TBC, Hamamatsu) to the safety
13 ground, for safety reasons, in order not to expose high-voltages.

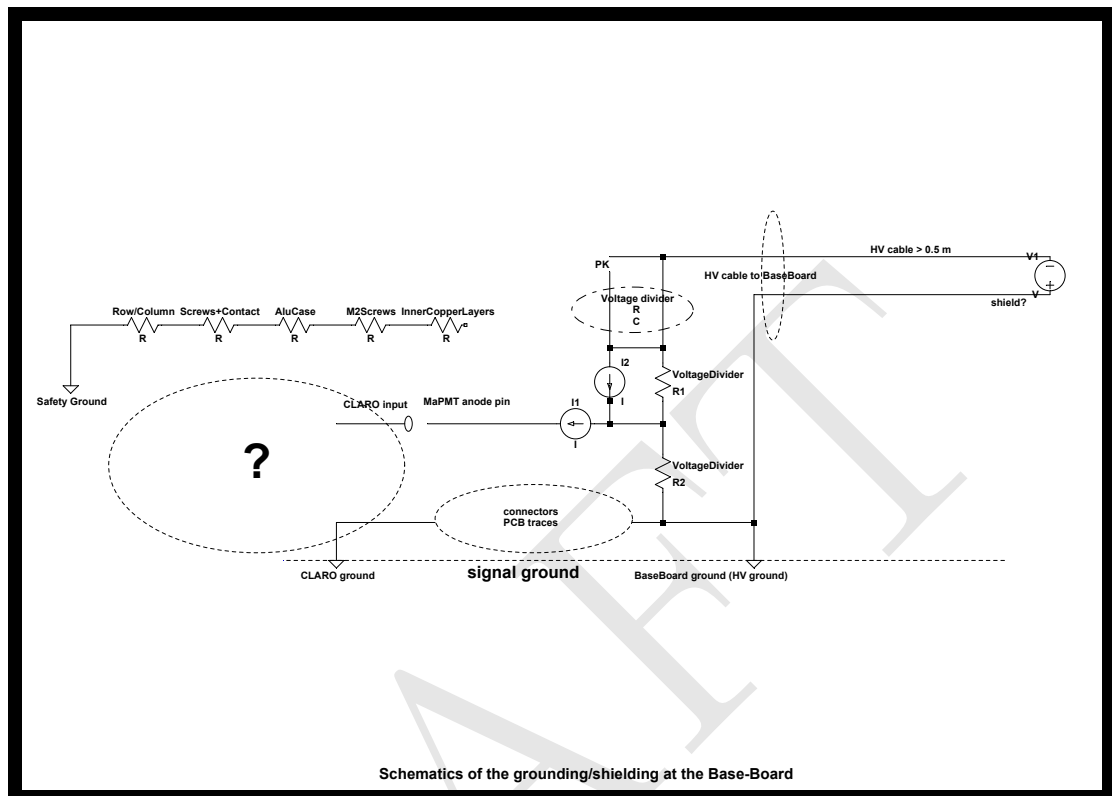


Figure 25

5 Overview of the Photo-Detector Assembly

2 The support structure of all the EC is made of an array of cooled aluminium bars. Each bar is composed
 3 by two machined and/or extruded bars: a bar, called *flange-bar*, parallel to the MaPMT plane, where
 4 the EC are fixed; a *cooling bar*, perpendicular to the first one and facing the DB. The two bars together
 5 form the structural support of the EC and DB assembly and have also the purpose to cool the EC
 6 and DB by circulating cooling fluid in the longitudinal ducts machined in the bars. This assembly is
 7 called *the support bar*. A *double-T* extruded bar, called *the harness bar*, is joined to the support bar
 8 and supports the harness boards. The harness boards are PCB and mechanical supports for the optical
 9 links, HV and LV connections. Another bar in the back acts as cable tray and cable support. This bar
 10 can be mechanically disconnected from the cooled blade and the harness bar in order to decouple the
 11 deformation of the bar that supports the MaPMT from the deformation of the bar that withstands the
 12 weight of cables and cable chains. This can be useful in case of a layout by rows, in order to minimize
 13 the sagittae of the bar supporting the MaPMT, allowing a larger sagitta for the bar supporting the
 14 cables and cable chain. There will be one of the assemblies described above per each column/row of
 15 EC (depending on the layout that will be chosen).

16 The overall dimension of such assembly in the direction perpendicular to the MaPMT plane is of the
 17 order of ≈ 25 cm, much shorter than the one of the current RICH detector. Therefore there will be
 18 enough space on the back of the detector array for routing of services, maintenance, clearance, light
 19 sealing, etc..

20 A view of the linear array of EC (either a column or a row) is shown in figures 26 and 27.

21 In order to ensure a good performance of the MaPMT, it is required to maintain them in a working
 22 condition below 40°C (even better if below 35°C). All the electronics will dissipate heat thus an
 23 case cooling system will be built-in. The heat produced at the PDA might be carried far away due
 24 to convection, thus heating all the RICH detector and giving rise to possible non-uniformities of its
 25 properties and performance. Therefore, while attempting to increase as much as possible the heat flow
 26 to the cooling system via conduction, it will be attempted to reduce as much as possible convection. To
 27 minimize the convection, the cooling elements will be in direct contact with the heating components

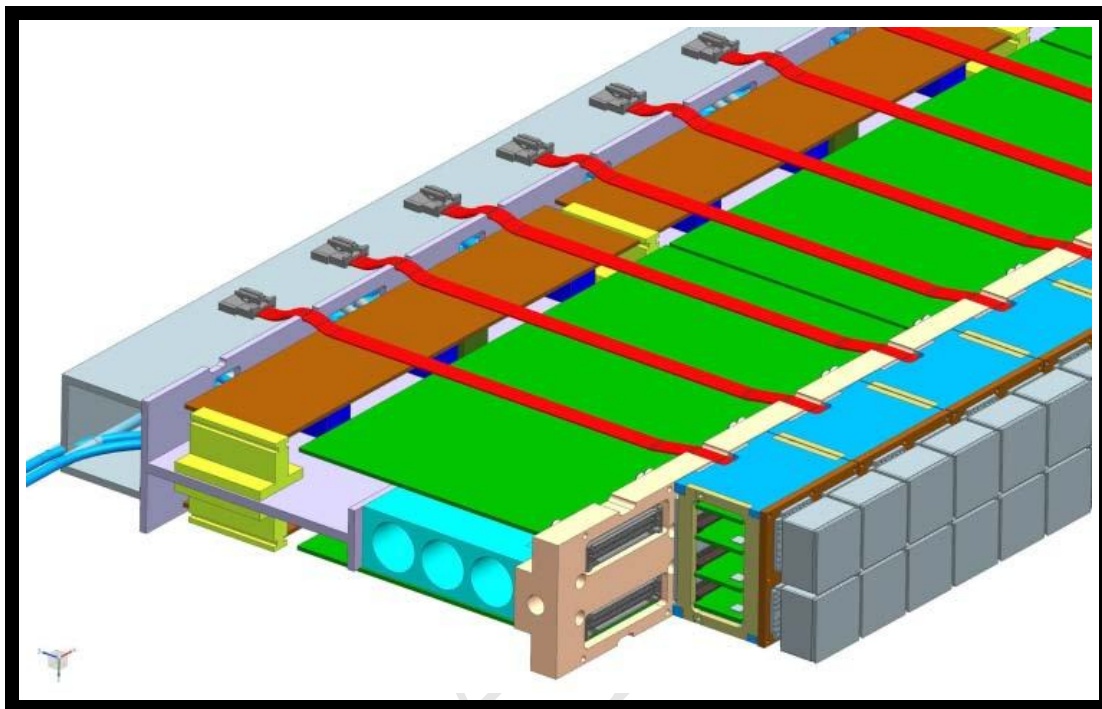


Figure 26: View of the EC array.

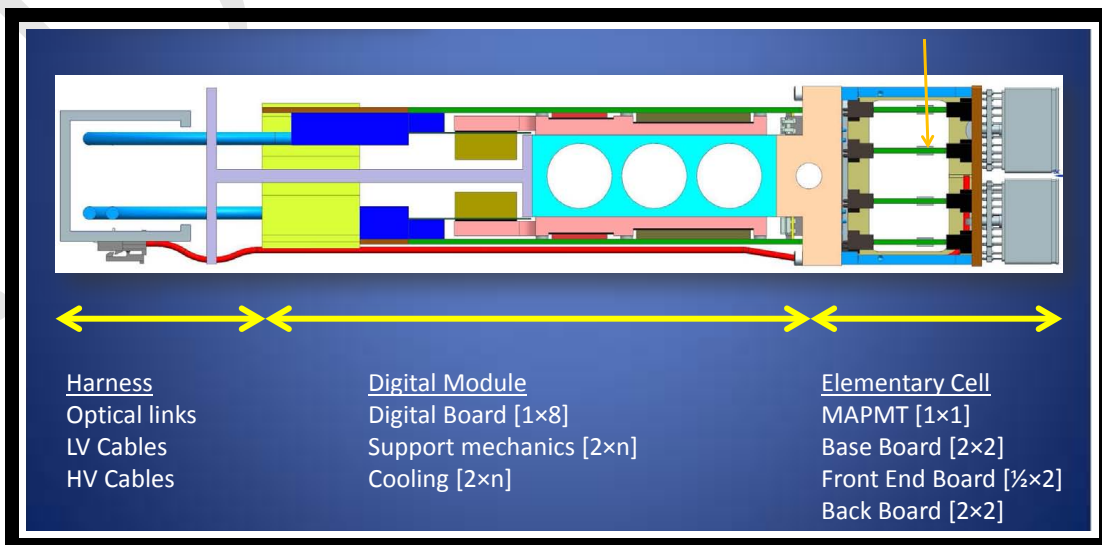


Figure 27: Top view of the EC array.

- 1 to ensure a good thermal conduction. The flow of the coolant fluid will be adjusted in order to get a
- 2 tolerable temperature variation in the PDA.

5.1 Layout of RICH2

4 In case of modularity by rows there will be 24 horizontal bars for each of the two MaPMT array of
5 RICH2. The horizontal bars will be about 700 mm long, each one carrying 12 EC and 3 pairs of DB
6 (3 DB per side). A rough estimate of the weight of a fully equipped row is about 150 N. The sagittae
7 of the horizontal bar due to gravity are expected to be of the order of 0.1 mm, thus smaller or equal
8 than the expected assembly tolerance.

9 In case of modularity by columns there will be 12 bars for each of the two MaPMT array of RICH2.
10 The bars will be vertical, about 1400 mm long, each one carrying 24 EC and 6 pairs of DB (6 boards
11 per side). A rough estimate of the weight of a fully equipped column is about 300 N.

12 The overall weight of each of the two PDA will be of the order of 5000 N.

13 The nominal pitch between bars will be 1 mm more than the EC side dimension. As in the current
14 design the EC has a square footprint of 55.4 mm side, the bar pitch is 56.4 mm, so that the clearance
15 between bars will be 1 mm. The possibility to further reduce this clearance will be checked on the the
16 prototypes.

17 In both cases a modal analysis will be performed in order to asses the mechanical behaviour of the
18 structure in case of induced vibrations.

19 In both cases of either columns or row arrangement, each EC linear array is supported at both ends
20 by means of bearings running on rails. This allows to extract a single EC linear array from the overall
21 MaPMT array and perform maintenance on EC, DB, etc.. The full detector will be mounted inside a
22 rack composed by commercial aluminium extruded profiles and will be mounted on rails in order to
23 fully extract the rack from the magnetic shield. As this arrangement is very similar to the current one,
24 the possibility to reuse the current racks with their bearing and rails system will be investigated as
25 well.

26 Cables and optical fibres will be routed from the rack to the patch panel on the magnetic shield by
27 means of commercial cable chains. There will be one small cable chain for each linear array in order to
28 allow the extraction and maintenance of each single row or column. This cable chains will route cables
29 and fibres to a patch panel positioned on top the rack in case of column layout, otherwise on the side
30 of the rack in case of an arrangement by rows. The full bunch of services will then be routed to the
31 patch panel on the magnetic shield by means of a common cable chain.

5.2 Layout of RICH1

33 The engineering of RICH1 is much more complex than the one for RICH2, due to the many constraints.
34 It will be attempted to make both detectors as similar as possible. However a final layout for RICH1
35 is not available yet.

6 EC₆ Interface to the super-structure

37 In this section EC will mean EC-R, unless specified otherwise.

6.1 Mechanical interface

39 The EC is mechanically connected to the row/column super-structure via four M2.0(M2.5?) (TBC)
40 screws for easy installation/de-installation as long as any row/column has been shifted along its rails
41 away from the focal plane. Moreover each EC is electro-mechanically connected to two different DB,
42 via the two connectors on the BackB. A sufficient mechanical precision of all the parts is essential with
43 this arrangement.

- 1 In case of mounting of the EC, the two connectors will be connected first, to try to minimize stresses
- 2 on their soldering, and screws will be fastened afterwards. The holes for screws will have the required
- 3 tolerance. Dismounting will go the other way round.
- 4 In case of mounting of the DB the same procedure (the four connectors first, screws afterwards) is
- 5 foreseen; the other way round for dismounting. In case this turns out to be problematic, due to the
- 6 presence of four connectors, it will be assumed that the DB is always fixed with no EC present, and
- 7 EC are mounted afterwards (the other way round for dismounting).
- 8 Tests on prototypes will be carried on to validate all the procedures.

6.2 Thermal interface

10 Taking out the heat produced inside the EC requires a lot of care, as it is produced inside a relatively
11 small volume with a large number of EC close-packed.

12 The main heat sources of the EC are the voltage dividers on the BaseB, with an assumed power
13 dissipation of 0.4 W/MapMT. For the CLARO chips on the FEB, the assumed power dissipation is
14 16 mW/CLARO, that is 128 mW/MapMT. Even if the voltage divider dissipate more power than the
15 CLARO chips, it is easier to build a low thermal impedance path to the cooling system for the voltage
16 divider than for the CLARO chips. Moreover it has to be avoided, by a suitable design, that the
17 heat produced by the CLARO chips flows towards the MapMT instead of flowing towards the cooling
18 system.

19 The cooling is provided by flowing coolant inside the cooling bar. The heat is removed from the EC
20 back-side via thermal conduction on the four machined surfaces in contact with the machined flange-
21 bar. The thermal contact is also ensured by the four M2.0(M2.5?) (TBC) screws that fasten the EC
22 back-side to the flange-bar. The main heat paths are:

- 23 • from the voltage divider to BaseB, then to the EC case, then to the EC back-side;
- 24 • from the CLARO chips to FEB, then to the connectors to BaseB and BackB, then to the EC
25 case, then to the EC back-side.

26 It is of paramount importance the evaluation of the regime temperature, in order to have a reasonable
27 confidence that the EC, as it is currently designed, can evacuate the heat, as the power values are
28 relatively small but the heat paths are mainly composed by boards that are thermally insulating.
29 Localized high temperatures might imply shorter life of components and the development of convective
30 flows inside the gas volume. Relevant convective motion in the gas would imply higher temperature on
31 the top part of the detector with negative consequences on the lifetime of components positioned on
32 the top sectors, non-uniform thermal expansions and detector behaviour.

33 Preliminary simulations have been performed in order to evaluate the cooling efficiency of the EC.
34 The simulations assume that some contribution is negligible while other contributions were neglected
35 because the parameters could be hardly reliable: contact resistances, convection and irradiation. The
36 capability to cool the CLARO chips and voltage dividers depends on the thermal conductance of the
37 PCB and connectors. These parameters are quite difficult to input to the FEA as they depend on
38 contact shapes and thickness inside the connectors and on the numbers and shapes of the copper
39 planes and shape of copper tracks on the PCB. As a first approximation the connectors have been
40 assumed as bulk bodies with the same thermal conductivity of the PCB. The thermal conductivity
41 have been estimated assuming that the PCB are composed by FR4 having a thermal conductivity of
42 0.3 W/mK. The PCB thermal conductance on the plane can be strongly influenced by the amount of
43 ground planes and by the length, shape and dimensions of the tracks.

44 FEB and BackB are expected to have $2 \times 35 \mu\text{m}$ of copper layers on 1.6 mm of PCB thickness; then the
45 amount of copper in the thickness is about 5% and thermal conductivity on the plane can be estimated
46 as $\approx 8 \text{ W/mK}$. The BaseB is expected to have $6 \times 105 \mu\text{m}$ copper planes, but such planes have many
47 holes; therefore, assuming a factor two of reduction due to the holes, the amount of copper is about
48 10% of the thickness and the thermal conductivity on the plane can be estimated as $\approx 40 \text{ W/mK}$. The
49 thermal conductivity through the thickness is affected by vias, traces, etc.. As guess, a copper content

1 along the thickness from 0% to 1% of the overall cross section can be assumed, that is a thermal
2 conductivity of $(0.3 \div 4)$ W/mK; therefore the thermal conductivity of PCB changes dramatically with
3 a small change in the amount of copper content.

4 Some preliminary simulations have been performed, assuming a reasonable influence of the copper
5 content of the PCB. Even applying to such values a safety factor four of reduction, the delta temperature
6 between the hottest regions (BaseB and CLARO chips) and the cooling duct wall is below $\approx 12^\circ$.

7 These results will be cross-checked and validated with the first prototypes. If necessary, suitable copper
8 thermal bridges for the CLARO chips will be used.

9 Thermal adhesive tapes and films and thermal adhesive pastes will be used to improve the thermal
10 conductance at the interfaces.

6.3 Electrical interface

6.4 High Voltage distribution

13 Each R11265-M64 needs a voltage up to 1.1 kV and a current up to 0.37 mA (with the standard voltage
14 divider), implying a total current of the order of 1.5 mA for each EC-R (see section B.1).

15 Each R12699-M64 needs a voltage up to 1.1 kV and a current up to 0.23 mA (with the standard voltage
16 divider), corresponding to the same total current for each EC-H.

17 To limit the number of HV channels to a manageable level every PDM will be powered with an
18 independent HV channel. MaPMT will be selected for similar characteristics inside each PDM.

19 In the present system there are 3 cables type 04.31.52.075.9 (CERN store), each one containing 37
20 unipolar conductors rated at 3 kV for RICH2 and 3 similar cables for RICH1. In addition there are
21 18 HV cables on RICH2 and 14 on RICH1 (currently powering the HPD) which can be rerouted to
22 the new PDA. If this solution will prove difficult to implement, we will consider to deploy new cables
23 (similar to the existing multi-conductor ones) to obtain a tidy voltage distribution scheme.

24 The detailed implementation will depend on the final architecture and detector partitioning.

25 6.4.1 Power supplies

26 We require the following specifications.

- 27 • The system will be remotely controlled and its interface should be compatible with the CERN
28 environment.
- 29 • Each channel will be able to provide at least 1.1 kV with sufficient current to drive either one
30 PDM containing 4 EC equipped with R11265-M64 or a small group of PDM equipped with the
31 R12699-M64.
- 32 • In order to reduce the possibility of having ground loops caused by the HV connections, the HV
33 channels will be floating with respect to the ground of the crate.

34 CAEN proposes a system based on the A1538 board (12 channels , 1.5 kV, 10 mA, off-the-shelf) and
35 the SY4527 crate.

36 ISEG proposes a system based on EHS F013n_SHV modules (16 channels, 1.3 kV, 7 mA, custom made)
37 and the ECH 44A_1200W crate.

38 At first sight both seem to meet the requirements.

39 See [HV distribution for the R11265-M64](#) for more details.

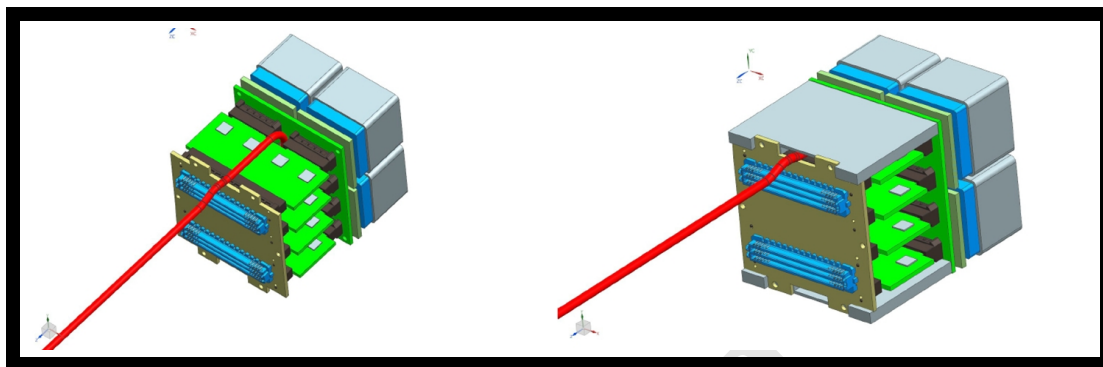


Figure 28: Routing of the HV cable.

7 EC₁ assembly and disassembly

2 In this section EC will mean EC-R, unless specified otherwise.

3 The EC assembly procedure will go as follows:

- 4 • the FEB are mounted on the connectors of the BaseB;
- 5 • the sides of the case are screwed to the BaseB;
- 6 • the bases of the case are screwed to the sides and, TBC, to the BaseB;
- 7 • the FEB are inserted on the connectors of the BackB which is then screwed to the sides and/or
- 8 bases of the case;
- 9 • the MaPMT are mounted on their custom socket on the BaseB;
- 10 • the MS is installed.

11 Disassembly goes the other way round.

12 A simple mechanical tool will be realized to easily extract the MaPMT from its socket on the BaseB
13 (such as a small fork lift inserting between the MaPMT base and the MaPMT socket), in order to
14 make the operation simpler, safer and avoid distortion of the anode pins. Note that, due to the 2×2
15 layout of the EC-R, every MaPMT has two of its sides exposed so that removal will not be difficult.

8 Budgets

17 In this section EC will mean EC-R, unless specified otherwise.

8.1 Geometry

19 Beware: all the longitudinal distances (i.e. along the axis of the EC/MaPMT) must be cross-checked
20 on the prototypes for the height of the soldering of the connectors and the MaPMT socket).

21 Drawings of the geometry are shown in figures [29](#), [30](#), [31](#), [32](#), [33](#).

8.2 Mass

8.3 Power

9 Possible Radiation issues

25 All the EC components that may be sensitive to radiation damage in the LHCb environment have to
26 pass radiation hardness tests, in order to ensure stable operation of the upgraded RICH detectors over
27 15 years [[27](#)].

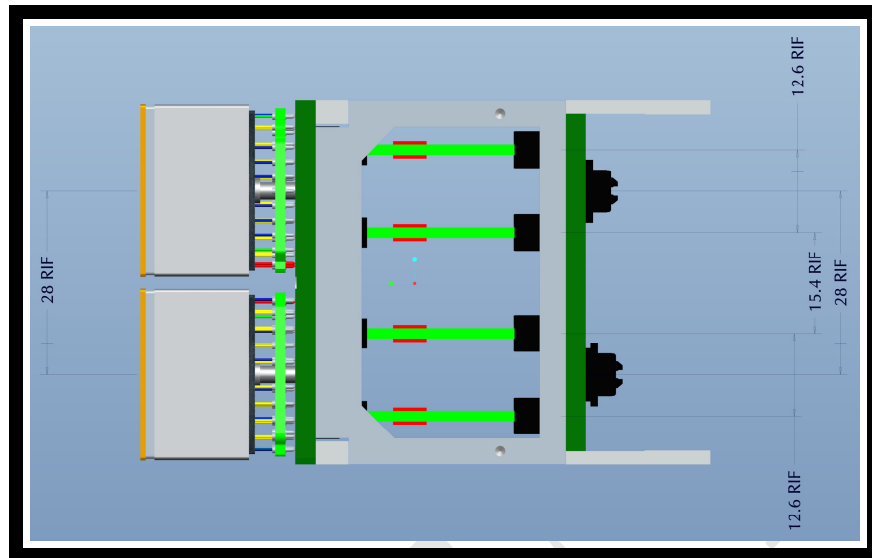


Figure 29: EC sizes: top view (longitudinal sizes to be checked/confirmed).

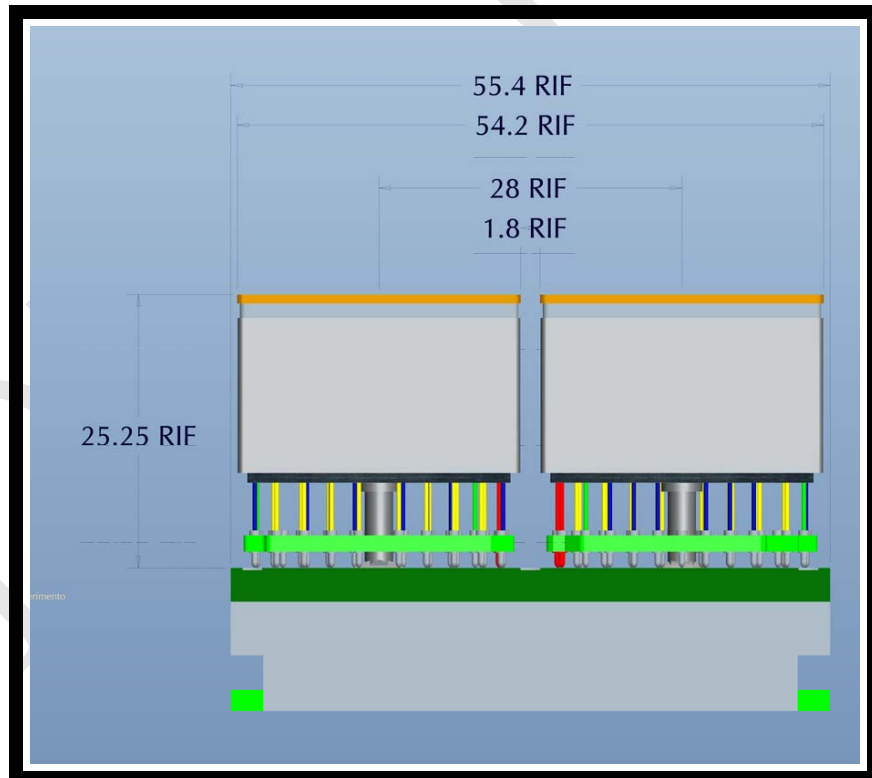


Figure 30: EC sizes: side view, detail of the MaPMT housing (longitudinal sizes to be checked/confirmed).

Component	Power	Notes
4 MaPMT	108 g	•
1 BaseB	g	•
4 FEB	g	•
1 BackB	g	•
mechanical structure	g	•
4 magnetic shield	g	TBD
Total	g	•

Table 1: Mass budget for one EC

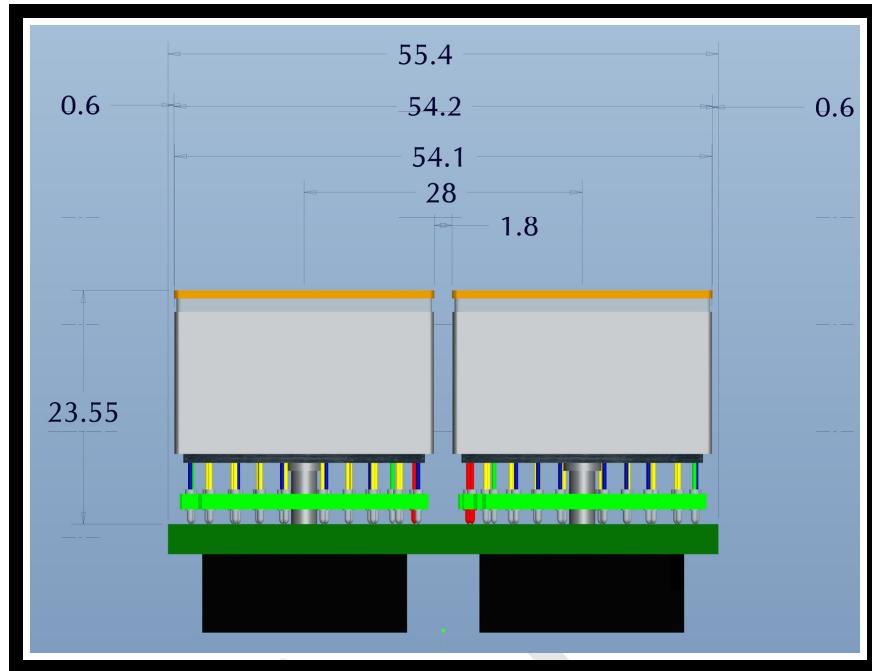


Figure 31: EC sizes (longitudinal sizes to be checked/confirmed).

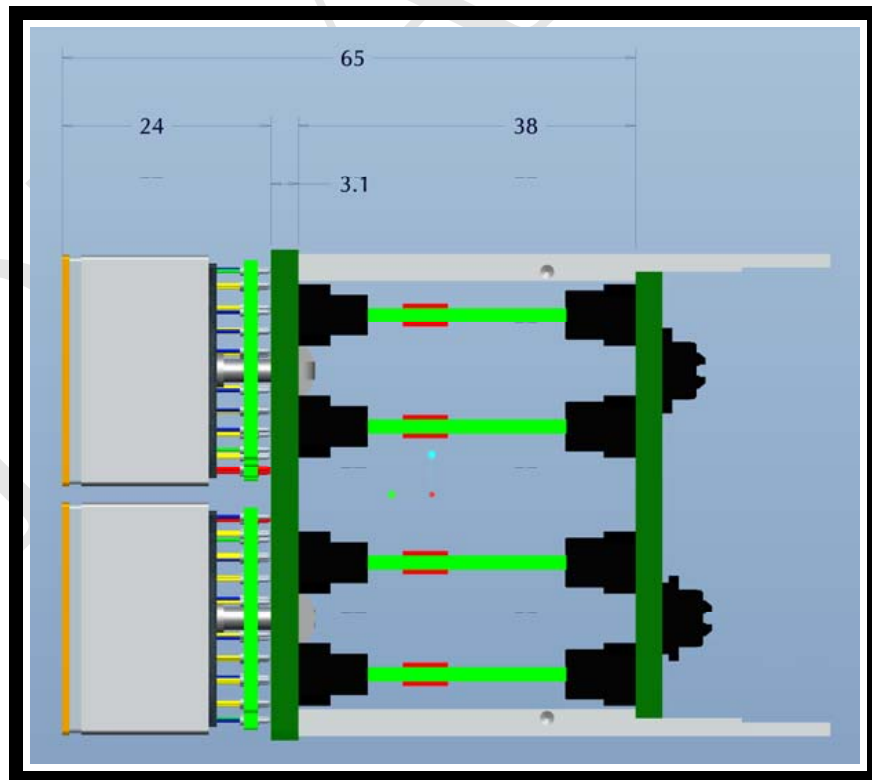


Figure 32: EC sizes (longitudinal sizes to be checked/confirmed).

Component	Power	Notes
4 MaPMT	1.6 W	
4 FEB (including the CLARO chips)	0.5 W	
1 BackB	0.004 W	
Total	2.1 W	

Table 2: Power budget for one EC

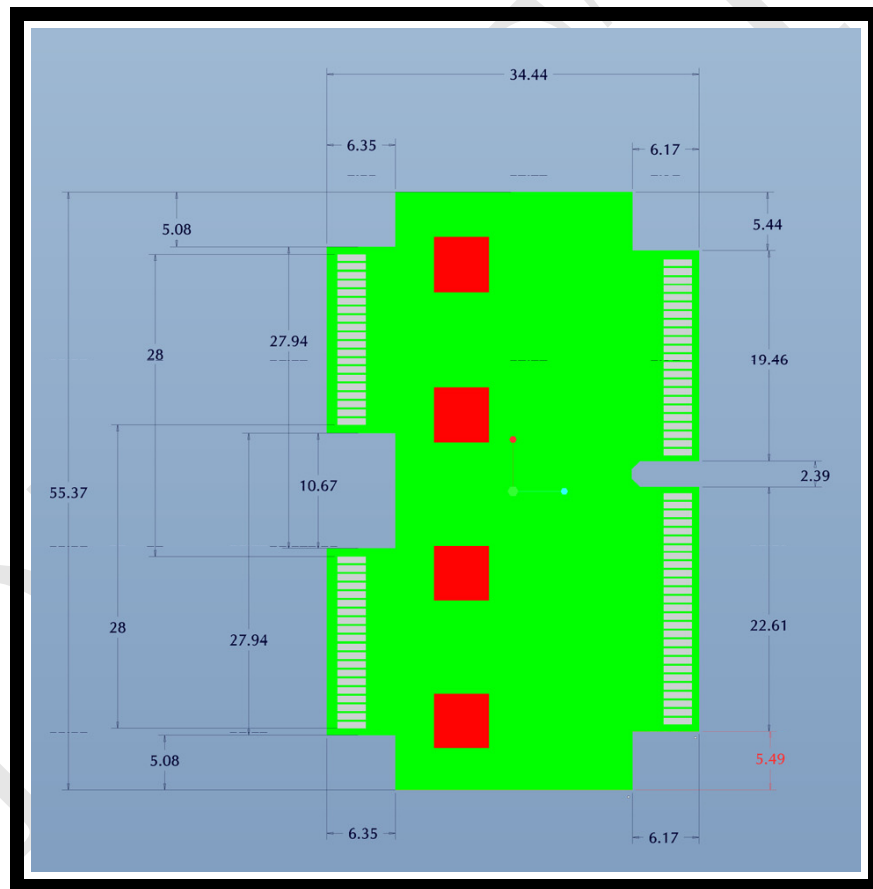


Figure 33: FEB sizes (longitudinal sizes to be checked/confirmed).

1 The radiation levels that will be present in the upgraded LHCb experiment might deteriorate the
2 performance of the components in terms of Total Ionising Dose (TID) and Single Event Effects (SEE).
3 According to FLUKA simulations of the existing RICH detectors, adapted to the LHCb run scenario
4 after the upgrade, we should expect a neutron fluence of 6.1×10^{11} 1 MeV n_{eq}/cm^2 and a total ionising
5 dose of 40 kRad, for 1 year of running.
6 These estimates are based on the worst case radiation level for single proton-proton collisions, assuming
7 one year of LHCb operation (10^7 s), a luminosity of $2 \times 10^{33} \text{cm}^{-2}\text{s}^{-1}$ and a proton-proton collision
8 cross section of 84 mbarn [1].
9 In the present simulation, the final geometry and materials are not implemented yet, and numbers have
10 typical statistical errors of 10% ÷ 30%. In addition no safety factor is included.
11 In a very conservative approach several CLARO chips were irradiated up to a level 10 times larger
12 than the radiation levels expected in 10 years of LHCb. The radiation hardness tests were performed
13 by irradiating the prototype 4-channels CLARO chip with neutrons, X-rays and protons and more
14 information can be found in [2]. Tests of the 8-channel version of the CLARO chip are planned in the
15 near future.
16 Another electronics component that is very sensitive to radiation is the FPGA that is going to be used
17 in the DB. A dedicated test board has been developed and tests are planned to measure SEE rates in
18 a high radiation environment.
19 Temperature sensors will be mounted in the EC to monitor heating and avoid damage and keep
20 the appropriate operating temperatures of the MaPMT and front-end electronics during operations.
21 Radiation resistance of these devices should be measured before production starts.
22 An irradiation of a few samples of MaPMT windows (UV-glass and borosilicate-glass) has been done
23 and a wavelength dependent transmittance degradation has been measured. UV-glass is found, as
24 expected, to be much more resistant than borosilicate-glass.
25 Whenever possible the components will be tested separately, however an irradiation of a few complete
26 EC would be done in order to assess the radiation hardness of the complete system.

9.1 Expected Radiation Levels

28 Radiation doses expected at the upgraded LHCb [23] show 42 kRad (7 kRad) for the worst (best) case
29 for RICH1 and 4.0 kRad (1.5 kRad) for the worst (best) case for RICH2, not including variations due
30 to the final LHCb geometry and materials and with no safety factors. The statistical errors on the
31 expected radiation dose are of the order of 10% ÷ 30%. After 15 years of operation the integrated
32 radiation dose in RICH1 is expected to be about 630 kRad.

10 Prototyping

34 In this section EC will mean EC-R, unless specified otherwise.
35 A first version of the EC and PDM was developed starting during 2012 for use with a readout system
36 based on the MAROC chip (see figure 5), before the CLARO chip turned out to be a better option.
37 This allowed to test extensively the BaseB. Thanks to these efforts its design was improved under many
38 respects, when reverting to development of the design of the BaseB for reading-out the CLARO chip.

10.1 Mockup

10.2 Mechanical measurements on the BaseB

41 Mechanical stress measurements will be carried out on the EC prototypes to validate both the mechan-
42 ical robustness and the mechanical precision of the assembly.

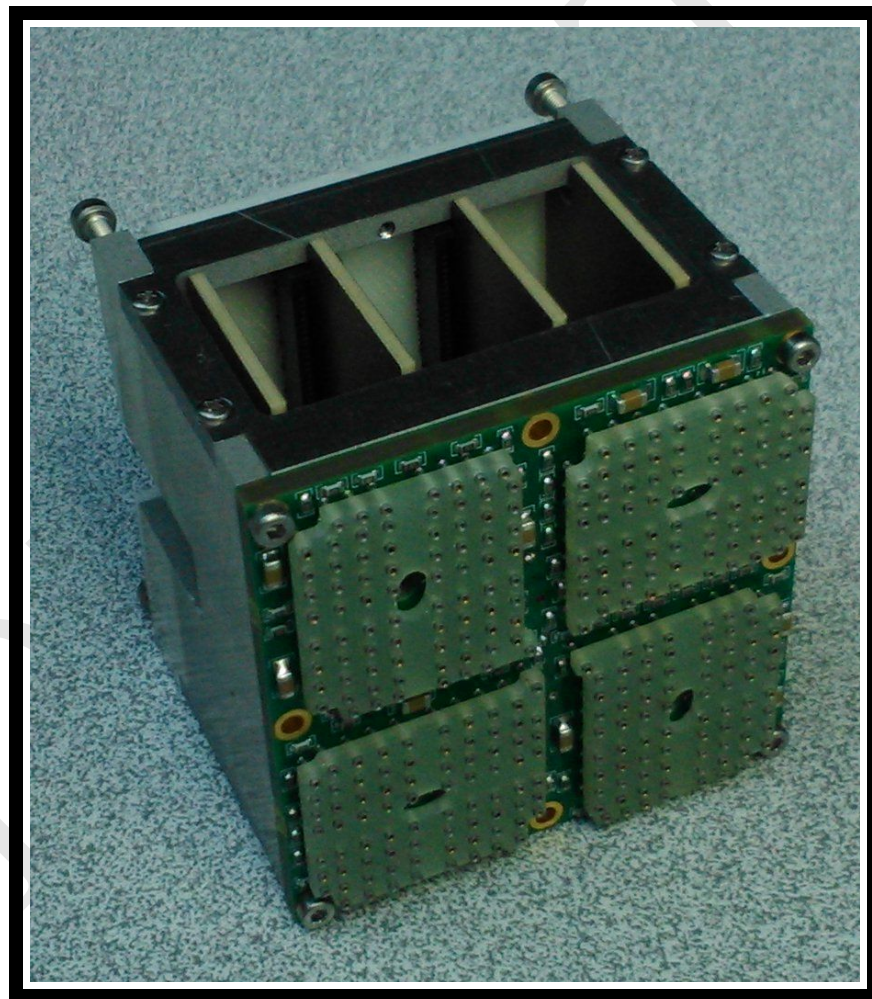


Figure 34: Mockup of the EC.

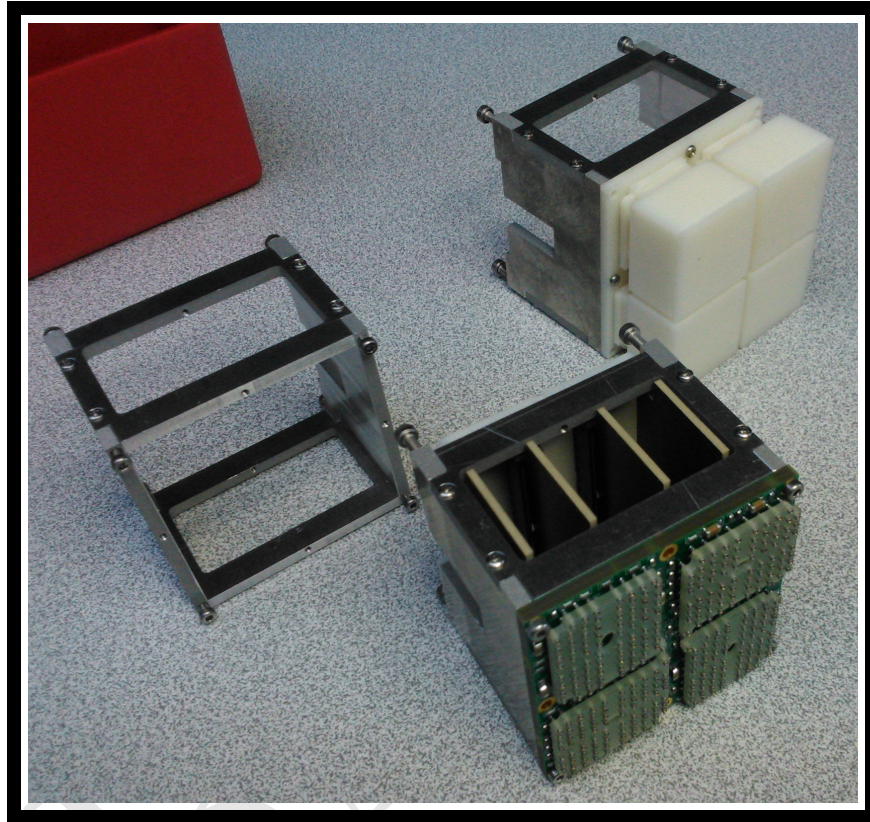


Figure 35: Various mockups, front-side.



Figure 36: Various mockups, back-side.

10.3 Electrical measurements on the BaseB

- 2 The conformity of the PCB of the BaseB to specifications was checked after delivery.
- 3 The current flowing in the voltage divider as a function of the HV has been monitored as well as the
- 4 HV at the last and last-but-one dynodes was measured.
- 5 All measurements were found to be compatible both among different PCB and with the expected
- 6 values.
- 7 Once the circuital part of the PCB has been verified, the pin-out from the MaPMT socket to the FEB
- 8 connector has been checked in order to verify the electrical continuity.
- 9 Finally a R11265-M64 MaPMT has been mounted on each MaPMT socket of each PCB and illuminated
- 10 with a LED, in order to check the single-photon spectrum for a few pixels.

10.4 Thermal measurements on the BaseB

- 12 A few very preliminary thermal measurements were done on the BaseB with/without its case.
- 13 The main heat sources on the BaseB are the resistors of the voltage divider, because the temperature
- 14 sensors dissipate a negligible power.
- 15 In the real operating conditions convection might be non negligible; therefore the experimental setup
- 16 has been placed inside a closed box to reduce convection; no additional cooling is applied. The temper-
- 17 ature was monitored by means of an IR thermal camera, as well as a thermocouple and a pyrometer.
- 18 Aluminium surfaces were covered with a black tape to make their emissivity larger a more similar to
- 19 the one of the FR4.
- 20 The first measurement was performed mounting the BaseB on the case of the EC. The ambient temper-
- 21 ature before switch-on was 27 ° C. When the HV high voltage was turned on to 950 V a temperature
- 22 plateau was reached after about half an hour. The PCB top and bottom layers in steady conditions are
- 23 shown in figure 37a and 37b. The temperature of the MaPMT socket reached about 30 ° C. The peak
- 24 temperature, as expected, are reached near the resistors, as shown in figure 38a. The top and bottom
- 25 layers of the PCB reach about the same temperature, showing that thermal conduction of the BaseB
- 26 is good enough (see figure 38b).

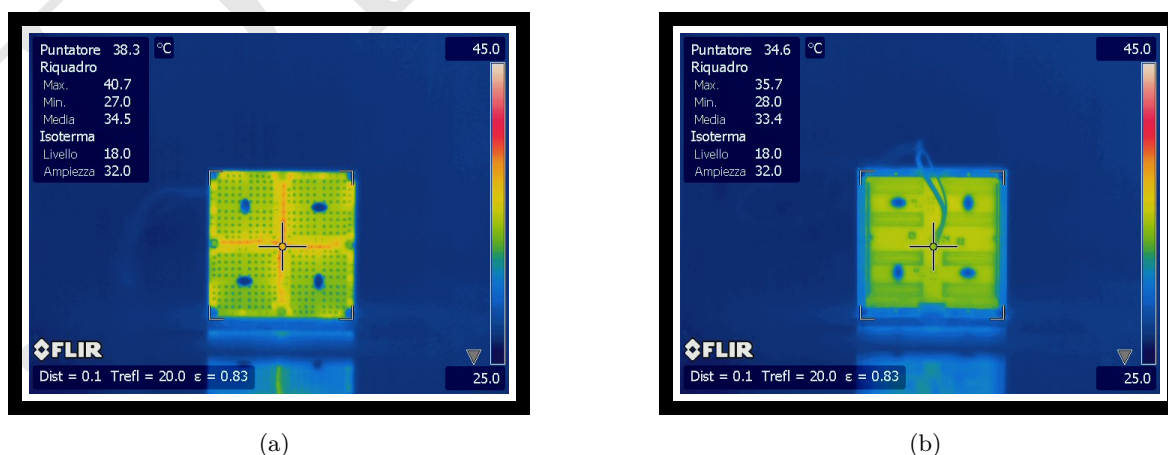


Figure 37: Top and bottom layers of the BaseB in steady-state. The BaseB is mounted on the case of the EC.

- 27 In order to check that heat flows to the Aluminium case the temperature of the case was measured with
- 28 both a thermocouple and a PT100. The average temperature of the PCB is about 5 ° C higher than
- 29 the temperature of the case.
- 30 Finally, the temperature of the PCB was measured without the case. The result is shown in figures 39a
- 31 and 39b. As expected, both the top and bottom layers of the PCB reach higher temperatures with
- 32 respect to the previous measurement.

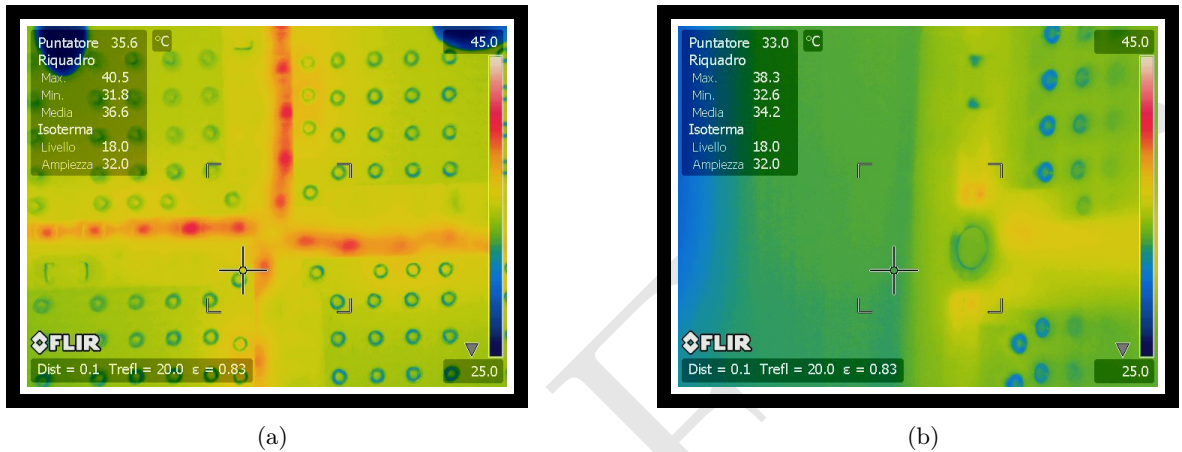


Figure 38: Left: view of the middle of the PCB. The resistors of the voltage divider are clearly visible as the hottest components while the socket temperature is colder. Right: view of the side of the BaseB showing how the PCB stabilizes at a rather uniform average temperature.

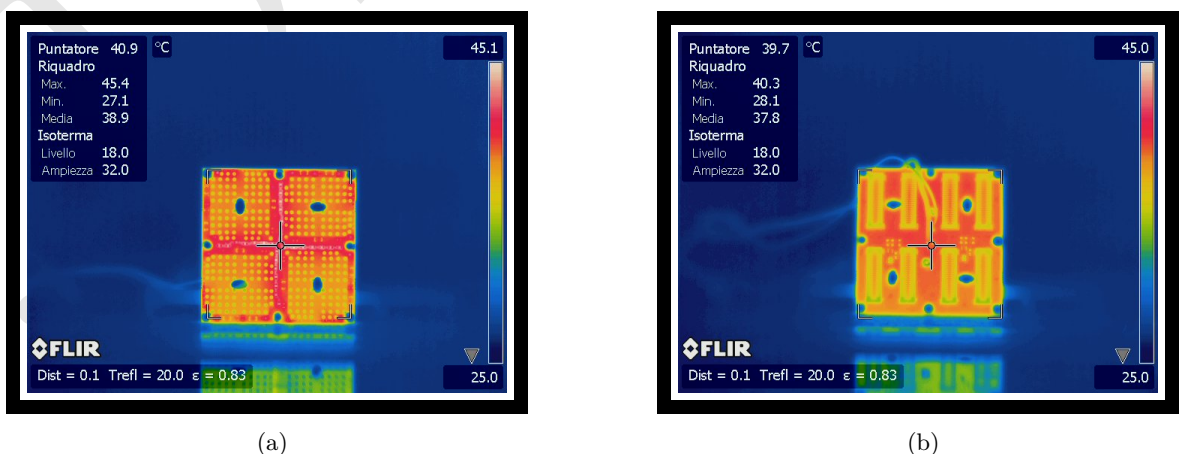


Figure 39: Top (left) and bottom (right) layers of the PCB. The BaseB is not mounted on the case of the EC.

10.5 Stress tests on the BaseB

- 2 In order to qualify the BaseB for the long required operation time in the harsh LHCb environment,
- 3 stress tests will be made on the prototypes. Among other things, these tests will be useful to check the
- 4 reliability of the soldering of the MaPMT sockets, which cannot be visually inspected.
- 5 A test protocol will be defined, including operation at the extreme LHCb environmental temperatures
- 6 with sudden thermal cycles
- 7 Radiation hardness tests will be made as well (see section 9).

11 Quality Assurance

- 9 Basic QA tests of the BaseB will be asked to the producer.
- 10 In addition to that, an automatized burn-in system for testing the BaseB after production and prior
- 11 to assembly will be developed. It will automatically test for electrical continuity (also at the MaPMT
- 12 socket) and voltages of the voltage divider; it will look for possible short-circuits between anodes; it will
- 13 also carry on basic electrical stress tests (operation at a voltage larger than the nominal one); it will
- 14 include medium-term operation for a minimum time under HV, in order to identify possible early-life
- 15 failures of components.

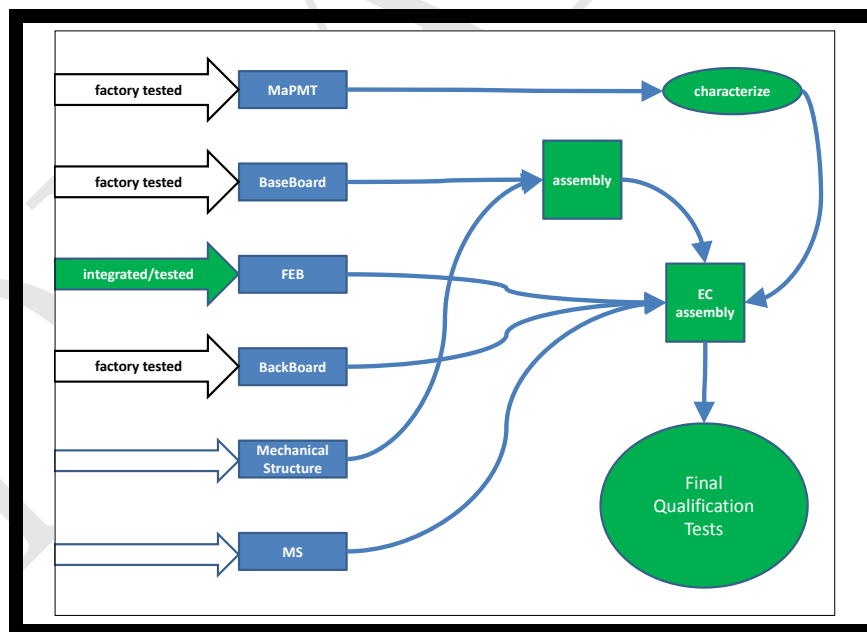


Figure 40: QA flow chart for the EC

- 16 See the presentation by Carmelo on July, 30th 2014: [QA of the EC](#).
- 17 Quality assurance of the complete EC can be done using a dedicated test station made of a blue laser
- 18 with repetition rate of 40 MHz, in addition to fibre-optics and motorised stages to deliver laser light
- 19 on specific MaPMT pixels.
- 20 A pulsed laser, set at constant power (e.g. corresponding to 1 p.e.) and controlled by a PC, can illumi-
- 21 nate one pixel of the MaPMT, set at a fixed high voltage, pre-determined by separate qualifications.
- 22 By making a threshold scan on several DAC values we can measure the single photon spectrum for
- 23 each pixel. Assuming that about 20 seconds are sufficient to test 1 pixel, then about 1.5 hours will be
- 24 needed per single EC, and therefore 225 days (8 hours per day) to test all 1267 EC (roughly assuming
- 25 all EC-R type). A total of about 12 months are needed to test the full EC production assuming a single
- 26 test station, and about 4 months would be needed to prepare the complete test setup.

12 Repair and Maintenance

2 Each EC will be mounted on a row/column. Then this row/column will be installed on a larger structure
3 in the Photo-Detector enclosure of the RICH detector. In case of problem with some EC, it will be
4 needed to have access to this row/column to replace the faulty element. It is planned to replace only
5 a complete EC in the LHCb framework. The repair of the faulty components (like a MaPMT) of the
6 EC will be done in laboratory with dedicated tools and facilities for testing it. Such intervention will
7 be done, in principle, when at least few EC show an issue (as one EC is about 1‰ of the overall
8 sensitive area of the RICH). Of course maintenance can be done only during an LHC stops or shut-
9 down periods. According to the experience learned with the present RICH system, a minimum of one
10 day will be required for carrying out this job.

11 The replacement of the faulty EC will require to open the Photo-Detector enclosure and first extract
12 a complete row/column (eventually after disconnecting services: power, control, monitoring, HV and
13 optical fibres). This dismounting will be done by means of the four M2.0(M2.5?) (TBC) screws that
14 attach the EC to the flange bar. This operation requires to unplug the HV connector on the harness
15 board and unplug the EC from the two DB connectors.

16 The repair of the EC will be done in a lab. One can assume that the mechanical components present
17 poor risk of failure. The spare parts which should be produced concern mainly the MaPMT, the FEB,
18 the BaseB and the BackB.

19 The figure 41 shows an exploded view of the EC.

20 To replace one MaPMT, one simply needs to unplug it. As the four MaPMT are closely packed, a
21 dedicated tool will be prepared for helping their extraction. The replacement of any DB requires to
22 unscrew the M2.0(M2.5?) (TBC) screws and unplug them.

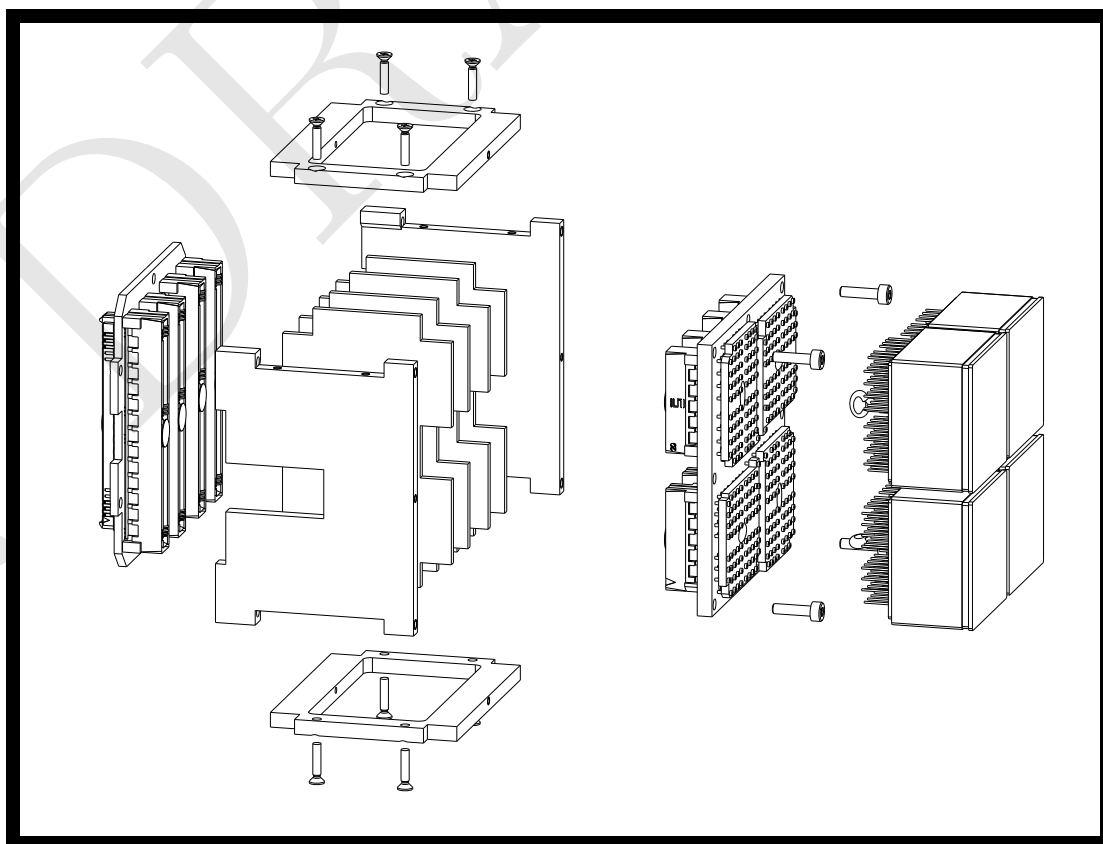


Figure 41: Exploded view of the EC.

23 After the repair the EC will be fully tested as described in section 11.

13 Project schedule

2 As the EC-H design will follow the same principles of the EC-R one, and, moreover, it is going to be
3 much easier, due to the less tight space constraints and smaller number of pixels/channels, a complete
4 EDR for the EC-H is not foreseen. On the other hand an addendum to the present documentation will
5 be submitted.

6 A test-beam is foreseen in October 2014 where a few full EC-R will be tested with real Cherenkov
7 light. Some aspects at system level, such as grounding schemes and shielding of the HV cables, will
8 be tested in situ. Moreover, other important aspects, already extensively tested in laboratory, will be
9 tested in a real setup, such as gain linearity of the MaPMT, gain dependence on the voltage, dark
10 current rates (see a summary at the CLARO EDR meeting [22]). Drawings of the test-beam setup are
11 shown in figures 42, 43, 44.

12 The PRR for the EC-R is foreseen in the 2nd quarter of 2015 and production to start in the 3rd of
13 2015 (TBC).

14 The PRR for the EC-H is foreseen in the 3rd quarter of 2015 and production to start in the 4th of
15 2015 (TBC).

14 Project validation via test-beam

17 The setup designed for the October 2014 test-beam is shown in figures 42, 43 and 44.

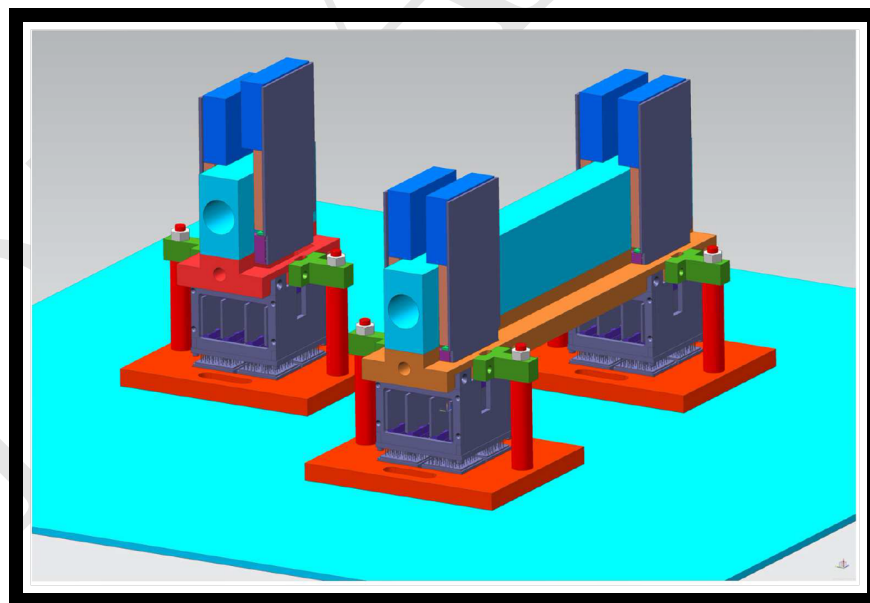


Figure 42: Test-Beam Setup (1).

15 Inventory and bookkeeping during production and operations

19 See also comment number (10) for the referees (section F).

20 The large number of components involved require an efficient inventory and bookkeeping system, which
21 is begin developed. The main requirements are as follows.

- 22 • Full detector inventory and bookkeeping, accounting for the hierarchical structure of all the sub-
23 assemblies and for the changes in time of the composition of the assemblies and their calibration
24 data.

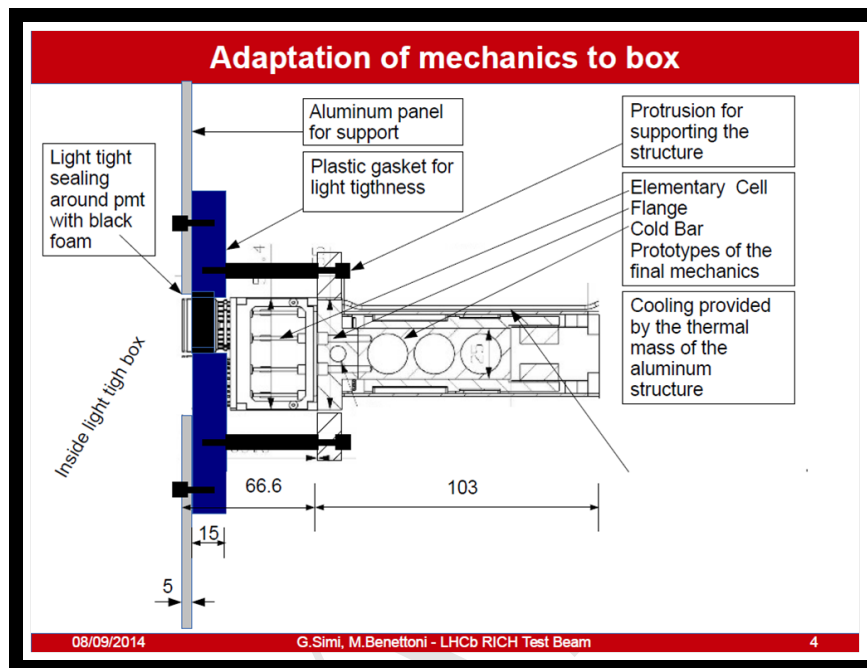


Figure 43: Test-Beam Setup (2).

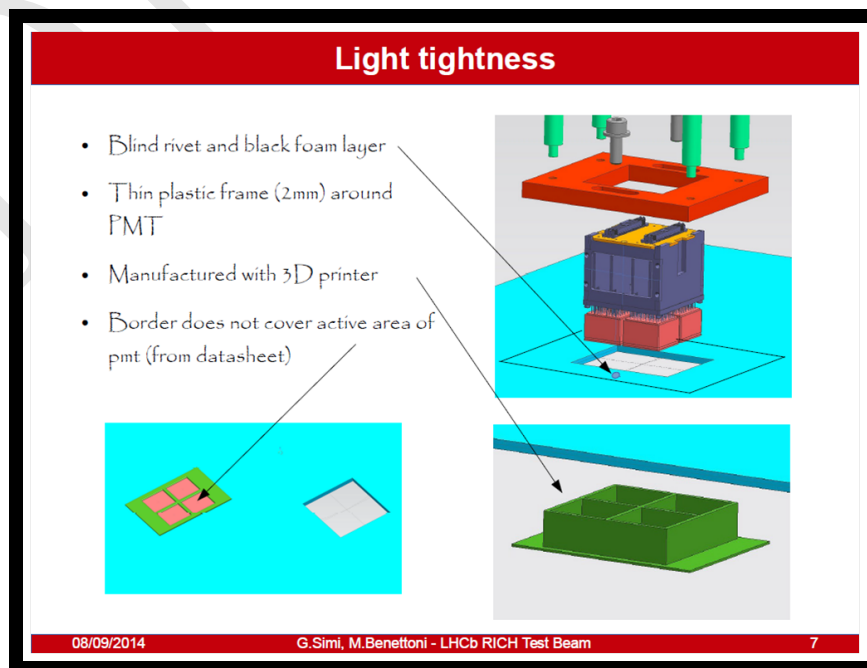


Figure 44: Test-Beam Setup (3).

- 1 • Save records with valid-datetime-range and transaction datetime, to allow changes in time of the
2 assembly content, improved calibration data, and mistake corrections without losing track of
3 the historical records.
- 4 • Users cannot delete records, they can only insert a new record with appropriate valid-datetime-
5 range (i.e. need to keep track of the full history).
- 6 • Capability to take a snapshot of all detector data, retrieving all and only the data valid at a
7 certain datetime.
- 8 • Trending plots/tables for numerical/non-numerical data.
- 9 • System-maintained referential integrity and transaction datetime (versioning may be needed to
10 cope with mistakes).
- 11 • Multi-user access, with access control and logging of date-time and user for any transaction.

16 The EC-H for the new R12699-M64 Flat Panel MaPMT

13 The EC-H is described in all details in the documents produced for the CLARO/FEB EDR [24].
14 At the level of the EC it seems to be difficult to keep anything exactly the same as for the EC-R.
15 The EC-H concept design is presented in figure 45.
16 It is based on the attempt to keep the traces from the anodes to the input of the CLARO chip as short
17 as possible.
18 In the current baseline, the same pitch is kept for the EC-H as for the EC-R (28.0 mm).
19 The BaseB will be equipped with one single SMD socket through which the R12699 MaPMT receives
20 the bias voltages and delivers the anode signals. The opposite side of the BaseB would be equipped with
21 four SAMTEC HSEC8-110-01-L-DV-A-K connectors through which the anode signals will be routed
22 to the FEB. The view of the connectors on the back of the BaseB is presented in figure 46.
23 Note that the R12699-M64, unlike the R11265-M64, is sold with a socket that is not larger than the
24 MaPMT case itself, so that it is possible, a priori, to use the socket sold by the manufacturer, which
25 includes a biasing circuit. However, the biasing circuit is an active voltage divider, which might not
26 be suitable in the LHCb environment (both for radiation and for reliability). Moreover, the need to
27 mechanically support the R12699-M64 would require to design a BaseB in any case, resulting in two
28 (instead of one) PCB behind the R12699-M64. The case will be investigated.
29 Placement of the connectors on the BaseB would require to use two FEB in the EC-H design. Figure 47
30 shows the FEB. With four CLARO chips (two per side of the FEB) each FEB is plugged into two
31 HSEC8-110-01-L-DV-A-K connectors (BaseB side) and one single HSEC8-140-01-L-DV-A-K connector
32 (BackB side).
33 The BackB consists of one single SEAM-30-02.0-L-06-2-A-K connector for the DB and two HSEC8-
34 140-01-L-DV-A-K connectors for the FEB. The connector to the DB will be shifted sideways to let it
35 have the same positioning of the analogous connector for the EC-R, so that the rest of the mechanical
36 assembly will be unchanged.

17 The LHCb environment

17.1 Expected occupancy

39 Data from simulations by Sajan and Jibo.
40 Peak occupancies are reached in a small number on MaPMT only. For instance, (from Jibo, as of:
41 August 12, 2013)

- 42 • RICH1

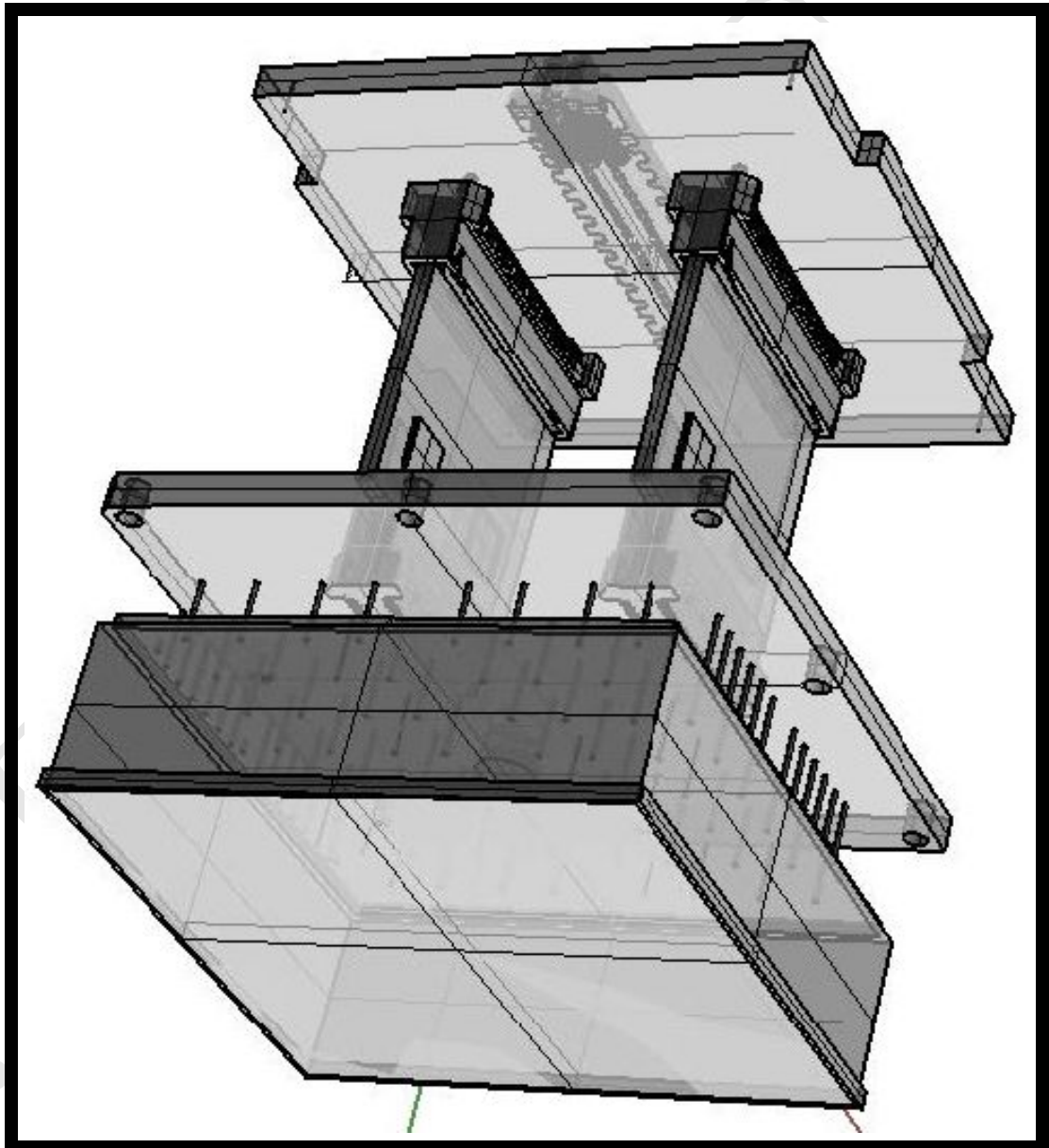


Figure 45: The EC-H concept design.

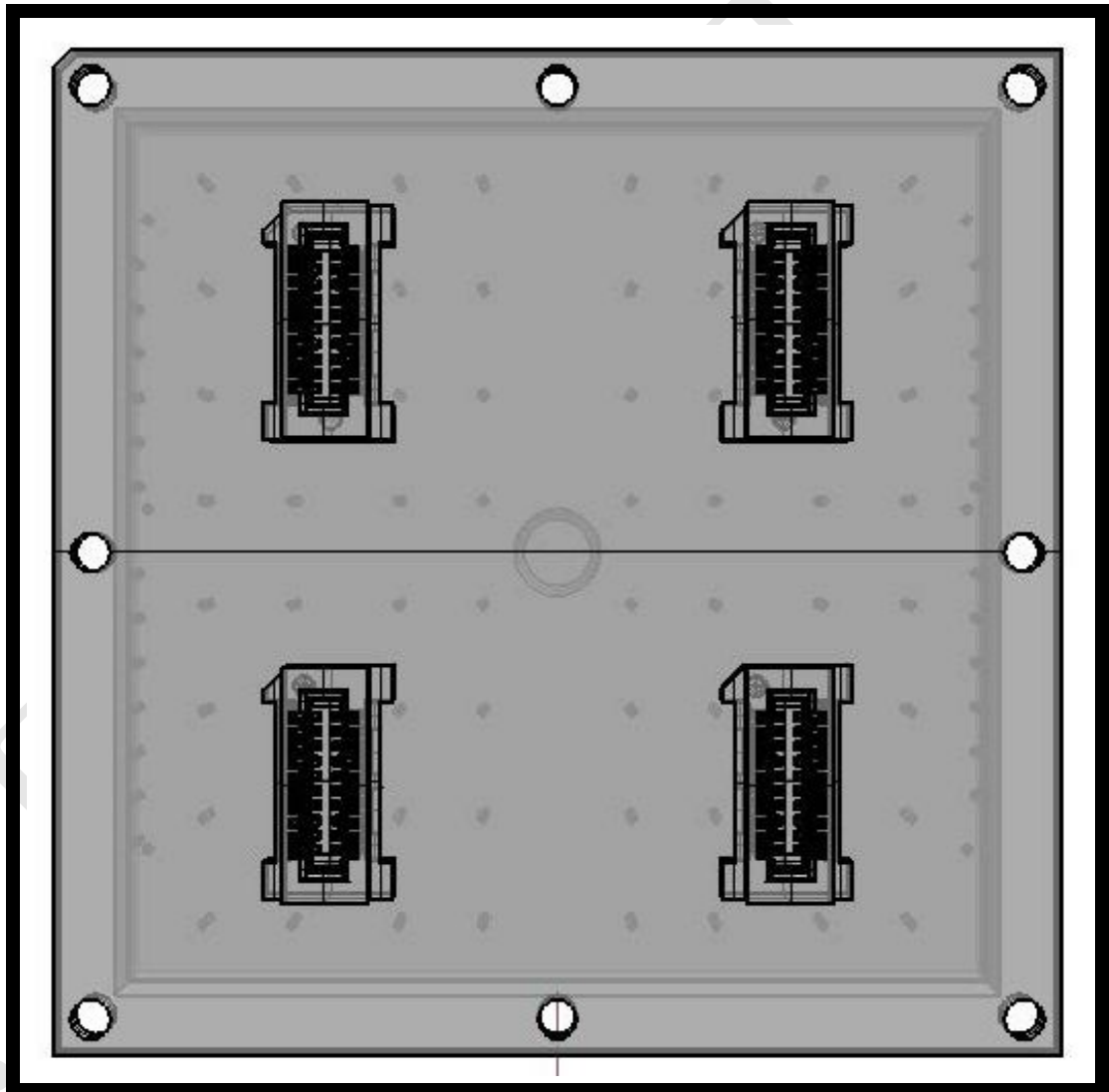


Figure 46: View of the connectors on the back of the BaseB.

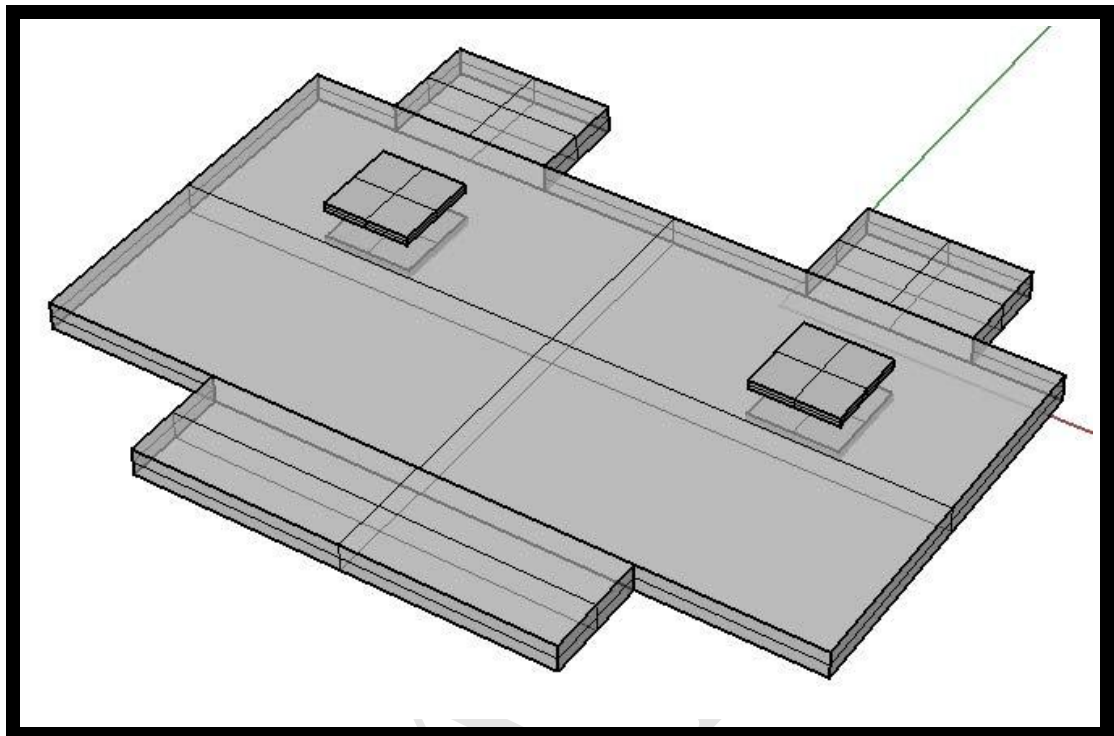


Figure 47: FEB for the EC-H.

- 1 – 0.000 of the MaPMT have occupancy > 25%;
- 2 – 0.003 of the MaPMT have occupancy > 20%;
- 3 – 0.029 of the MaPMT have occupancy > 10%.
- 4 – 0.054 of the MaPMT have occupancy > 5%.
- 5 – 0.130 of the MaPMT have occupancy > 2%.
- 6 • RICH2
- 7 – 0.000 of the MaPMT have occupancy > 8%;
- 8 – 0.006 of the MaPMT have occupancy > 6%;
- 9 – 0.042 of the MaPMT have occupancy > 4%;
- 10 – 0.112 of the MaPMT have occupancy > 2%;
- 11 – 0.202 of the MaPMT have occupancy > 1%;

18 References

- 13 [1] M. Karacson, *Radiation levels in the LHCb cavern*, Presentation at the *LHCb Upgrade Electronics*,
14 February 2013, <https://indico.cern.ch/event/225746/>. 9
- 15 [2] M. Fiorini et al., *Radiation hardness tests and characterization of the CLARO-CMOS, a low power*
16 *and fast single-photon counting ASIC in 0.35 micron CMOS technology*, in press, Nucl. Instrum.
17 Meth. A, DOI: 10.1016/j.nima.2014.04.072 9
- 18 [3] . L. Cadamuro et al., *Characterization of the Hamamatsu R11265-103-M64 multi-anode photo-*
19 *multiplier tube*, JINST, 03/2014; 9(06). DOI: 10.1088/1748-0221/9/06/P06021. B.4
- 20 [4] *TWEPP 2014: The GBT-SCA, a Radiation Tolerant ASIC for Detector Control and Monitoring*
21 *Applications in HEP Experiments* 3.2.3
- 22 [5] ... et al., *RICH TDR* 1, 1, 3.7

- 1 [6] M. Adinolfi et al., *Performance of the LHCb RICH detector at the LHC*, Eur. Phys. J. C 73 (2013)
2 2431; arXiv:1211.6759. 3.6
- 3 [7] LHCb 2000-005 RICH - 19/02/2000. 1
- 4 [8] A. Petrolini, Nucl. Instr. and Meth. A 497 (2003) 314 330. 1
- 5 [9] P. Musico, et al., Nucl. Instr. and Meth A 518 (2004) 210 212. 1
- 6 [10] P. Musico, et al., Nucl. Instr. and Meth A 550 (2005) 559 566. 1
- 7 [11] *Framework TDR for the LHCb Upgrade: Technical Design Report*, CERN-LHCC-2012-007 and
8 LHCb-TDR-12; <http://cds.cern.ch/record/1443882/files/LHCB-TDR-012.pdf>.
- 9 [12] D'Ambrosio, C. et al., *RICH2019: a proposal for the LHCb-RICH upgrade*, CERN-
10 LHCb-PUB-2013-011 and LHCb-PUB-2013-011; [http://cds.cern.ch/record/1560529/files/](http://cds.cern.ch/record/1560529/files/LHCb-PUB-2013-011.pdf)
11 [LHCb-PUB-2013-011.pdf](http://cds.cern.ch/record/1560529/files/LHCb-PUB-2013-011.pdf). 1
- 12 [13] R. Forty, *Ring-Imaging Cherenkov Detectors for LHC-B*, CERN-PPE/96-176, 4 September 1996.
- 13 [14] LHCb RICH Collaboration, *LHCb RICH1 Engineering Design Review Report*, LHCb-2004-121;
14 <http://cds.cern.ch/record/897981/files/lhcb-2004-121.pdf>.
- 15 [15] Courtesy of Christoph Frei. (document), 4
- 16 [16] LHCb RICH Collaboration, *LHCb RICH2 Engineering Design Review Report*, LHCb-2002-009
17 <http://cds.cern.ch/record/691478/files/lhcb-2002-009.pdf>.
- 18 [17] Courtesy of Roberta Cardinale.
- 19 [18] Dave Websdale, private communication.
- 20 [19] Courtesy of Sajan Easo.
- 21 [20] LHCb Collaboration, A. A. Alves Jr. et al., JINST 3 (2008) S08005; LHCb/RICH Collaboration,
22 M. Adinolfi et al., Eur. Phys. J. C 73 (2013) 2431.
- 23 [21] S. O. Flyckt and C. Marmonier, *Photomultiplier Tubes: Principles and Applications*, Philips Pho-
24 tonics, Brive, France, 2002 B.2
- 25 [22] CLARO/FEB EDR 1, 1.1, 2, 3.1, 3.2.1, 3.6, 4, 13, B.4
- 26 [23] M. Karacson, private communication. 9.1
- 27 [24] P. Carniti et al., *CLARO Front End Board (FEB) manual*, CLARO EDR;
28 P. Carniti et al., *Back-Board (BackB) v0.1*, CLARO EDR;
29 P. Carniti et al., *Elementary Cell for R12699-M64 (EC-H) v0.1*, CLARO EDR. 3.3, 3.4, 16
- 30 [25] J. Christiansen et al., *Grounding, shielding and power distribution in LHCb*, LHCb Project Doc-
31 ument No EDMS 584310, LHCb subsystem ELECTRONICS. 4.2
- 32 [26] K. Wyllie, *Grounding, power distribution and shielding of the LHCb RICH detectors*, [https://](https://edms.cern.ch/document/792758/1)
33 edms.cern.ch/document/792758/1. 4.2
- 34 [27] K. Wyllie, http://lhcb-elec.web.cern.ch/lhcb-elec/html/radiation_hardness.htm. 9

A The R11265-M64 MaPMT

36 The baseline photo-sensor is the R11265-M64 MaPMT from Hamamatsu, readout by new (external)
37 front-end electronics. For RICH2, the newly announced R12699-M64 from Hamamatsu, readout by new
38 (external) front-end electronics, is under study as well.

39 The main characteristics relevant to the RICH upgrade design are presented this section.

A.1 Data-sheet

2 The R11265-M64 MaPMT from Hamamatsu is a one-inch square 8×8 multi-anode, fast time-response,
3 0.8 mm thick UV/borosilicate input window, with bialkali/SBA/UBA photo-cathode, 12-stage metal
4 channel dynodes, head-on MaPMT. It is shown in Figure 5a, installed on the custom socket (BaseB)
5 for 4 MaPMT developed for the LHCb RICH upgrade.

6 The minimum geometrical sensitive area is $23 \text{ mm} \times 23 \text{ mm}$, giving a geometrical acceptance of the
7 bare MaPMT of 0.82. Low efficiency regions ($\approx 0.2 \mu\text{m TBC}$) are present between pixels.

8 Typical channel to channel uniformity is 1:3; maximum is 1:5.

9 The typical dark current, at 25°C , is 0.4 nA per anode pixel; maximum is 4 nA (about one order of
10 magnitude less than typical currents on pixels with 0.01 occupancy).

11 The mass is 0.027 kg.

12 The maximum operating temperature is 50°C .

13 The typical gain with a standard voltage divider optimized for single-photon detection (that is non
14 tapered, except for the first and last stages) is: $G = 1.0 \cdot 10^6$ at 1.0 kV supply voltage; $G = 0.5 \cdot 10^6$ at
15 0.93 kV supply voltage. The gain increase per 0.1 kV voltage increase is ≈ 2.5 (TBC).

16 The maximum supply voltage between anode and cathode is 1100 V (TBC) and the maximum anode
17 output current is $100 \mu\text{A}$.

A.2 Total Photo-Detection efficiency

19 The R11265-M64 MaPMT is provided by Hamamatsu with different bialkali photo-cathodes and dif-
20 ferent input windows. A trade-off between performance and cost has to be done. In particular photo-
21 electron yield, chromatic error and radiation hardness have to be taken into account.

22 Three different bialkali photo-cathodes are available for the R11265-M64 with increasing quantum
23 efficiencies (QE): the normal bialkali, the super bialkali (SBA) and the ultra bialkali (UBA). UBA
24 features higher QE and higher cost but it does not seem to be available for mass production (TBC),
25 so that SBA appears to be a good compromise.

26 The two possible input windows which are under study are made of borosilicate or UV glass.

27 The spectral response (QE of the photo-cathode and glass transmission combined) for the R7600
28 MaPMT, which is claimed to be the same as R11265-M64, as measured by Hamamatsu is shown in
29 Figure 48.

30 A.2.1 Comparison of the SBA with UV/borosilicate spectral responses

31 In the choice of the entrance window, between borosilicate glass and UV glass, a trade-off is required
32 among light transmission (maximized by the UV glass when considering the Cherenkov light energy
33 spectrum), chromatic error (increasing with the UV glass), ageing due to radiation damage (better for
34 UV glass) and cost (UV glass is a bit more expensive).

35 The SBA borosilicate and SBA UV spectral curves are reported in Figure 49. The SBA borosilicate
36 curve has been extrapolated below 270 nm while the SBA UV curve has been cut at 200 nm. The cut
37 of the SBA UV curve at 200 nm can wrongly reduce the estimated chromatic error. However, currently
38 no data below 200 nm is available for the reflectivity of the mirrors and the quartz plane has a cut-off
39 at 200 nm.

40 The numerical values for borosilicate and UV glass windows with SBA photo-cathode are summarized
41 in Table 3.

42 A back-of-the-envelope estimate of the yield and of the resolution using borosilicate and UV glass
43 windows has been performed. In RICH1 a rough estimation of the yield per unit of length gives
44 30 photons/m with borosilicate and about 40 photons/m with UV glass.

45 On the other hand UV glass gives larger chromatic error for single photon resolution. For borosilicate
46 a $\Delta\theta_{\text{borosilicate}} \approx 0.48 \text{ mrad}$ has been obtained, to be compared to the UV error which is $\Delta\theta_{\text{UV}} \approx$

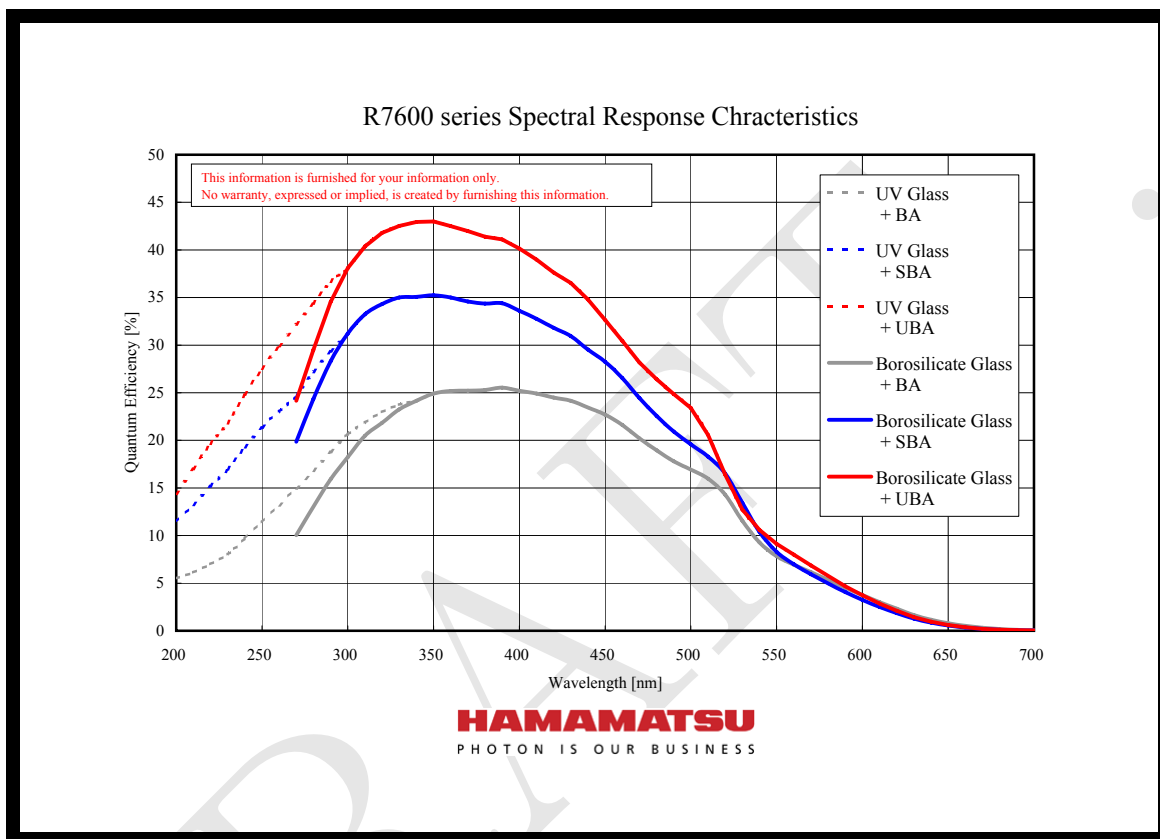


Figure 48: Spectral response of the R7600 MaPMT for the different photo-cathodes and entrance windows available from Hamamatsu.

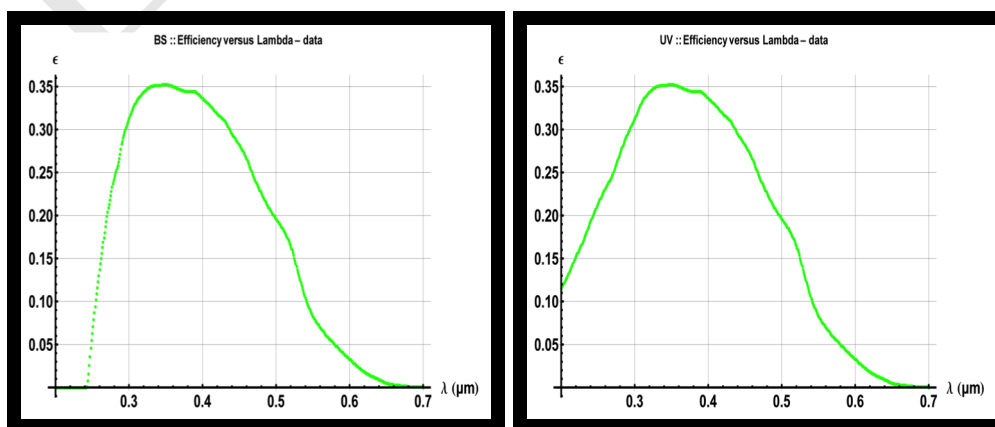


Figure 49: borosilicate (left) and UV (right) spectral response used to compare the yields and the resolutions.

λ (μm)	$\epsilon_{\text{borosilicate}}$	ϵ_{UV}
0.200	0.000	0.115
0.210	0.000	0.132
0.220	0.000	0.152
0.230	0.000	0.170
0.240	0.000	0.193
0.250	0.063	0.213
0.260	0.137	0.231
0.270	0.199	0.247
0.280	0.243	0.272
0.290	0.283	0.294
0.300	0.312	0.312
0.310	0.332	0.332
0.320	0.343	0.343
0.330	0.350	0.350
0.340	0.351	0.351
0.350	0.352	0.352
0.360	0.350	0.350
0.370	0.346	0.346
0.380	0.344	0.344
0.390	0.344	0.344
0.400	0.336	0.336
0.410	0.328	0.328
0.420	0.318	0.318
0.430	0.310	0.310
0.440	0.295	0.295
0.450	0.282	0.282
0.460	0.266	0.266
0.470	0.244	0.244
0.480	0.226	0.226
0.490	0.209	0.209
0.500	0.196	0.196
0.510	0.183	0.183
0.520	0.165	0.165
0.530	0.134	0.134
0.540	0.104	0.104
0.550	0.083	0.083
0.560	0.070	0.070
0.570	0.059	0.059
0.580	0.050	0.050
0.590	0.041	0.041
0.600	0.033	0.033
0.610	0.025	0.025
0.620	0.018	0.018
0.630	0.013	0.013
0.640	0.009	0.009
0.650	0.005	0.005
0.660	0.003	0.003
0.670	0.002	0.002
0.680	0.001	0.001
0.690	0.001	0.001
0.700	0.000	0.000

Table 3: The spectral response efficiency for borosilicate and UV glass window.

1 0.84 mrad. As a baseline UV glass has been assumed, further investigation is being carried out. It has
 2 to be pointed out that the increased chromatic error for the UV is compensated by the bigger yield
 3 when estimating the error on the track. The back-of-the-envelope estimated total error per track gives
 4 $N_{borosilicate}^{track} = \Delta\theta_{borosilicate}/\sqrt{30} = 0.16$ for the borosilicate and $N_{UV}^{track} = \Delta\theta_{UV}/\sqrt{40} = 0.17$
 5 which are similar.

6 Another characteristics which has to be taken into account in the final decision is the radiation hardness.
 7 The Photo-Detectors in the central region of RICH1 are currently subject to about 3 Krad dose per
 8 year. The upgrade environment will be much more harsh. The MaPMT window after being subject to
 9 radiation will start to reduce its transmittance. The reduced transmittance will decrease the photon
 10 yield. The damage as a function of the integrated radiation dose for the UV and the borosilicate
 windows is reported in Figure 50. The UV window is much more radiation hard than the borosilicate

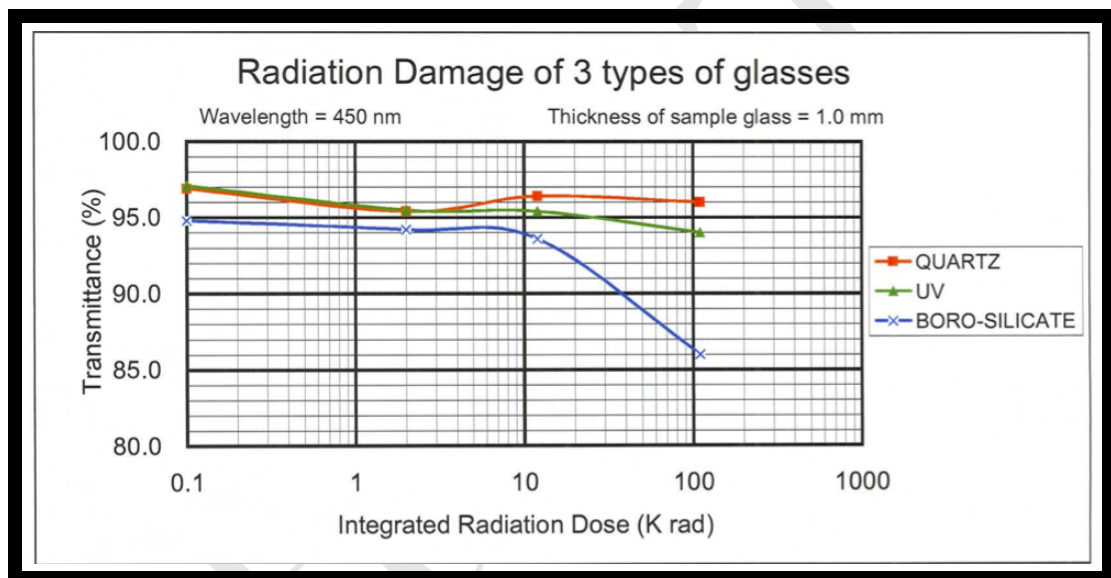


Figure 50: Window transmittance degradation due to the radiation damage.

11 window. In fact, at an integrated radiation dose of about 630 kRad, the UV window transmittance will
 12 be about 93% compared to 79% of the borosilicate glass window.

14 In addition to the Quantum Efficiency the photo-electron collection efficiency at the first dynode affects
 15 the total photo-detection efficiency. For this type of MaPMT a figure of about 0.9 (TBC) is usually
 16 assumed.

A.3 Dark current

18 TO BE WRITTEN...

B The R11265-M64 MaPMT in the RICH of LHCb

B.1 Operating voltage, gain and ageing

21 In order to define the operating parameters of the MaPMT (voltage divider ratios and operating
 22 voltage) one has to take into account: the MaPMT gain; the corresponding anode current, depending
 23 on the occupancy of the MaPMT and to be compared with the maximum allowable total anode current
 24 of 100 μ A (from specifications); the corresponding ageing; the current of the voltage divider, affecting
 25 both the power consumption and the gain non-linearity; the largely varying occupancies of the MaPMT
 26 at different locations; the spread of gain and other parameters from MaPMT to MaPMT and from
 27 pixel to pixel; the change of parameters with ageing; the parameters of the front-end electronics.

- 1 In order to limit as much as possible the ageing and to avoid to exceed the maximum current limit of
2 the MaPMT, it is safe to work at the lowest possible voltage, so that ageing is limited and the ageing
3 can be counteracted by increasing in steps the operating voltage. In fact, the ageing of the MaPMT is
4 uncertain over the long time-scale involved (fifteen years operation (TBC)) with the expected anode
5 currents. Moreover, occupancies in real data might be larger than simulated occupancies, so that a
6 suitable safety margin must be introduced in all these calculations.
- 7 The anode currents for the different occupancy MaPMT, taking into account a safety factor of 2 and
8 at the nominal gain quoted by Hamamatsu, are reported in Table 4. It is important to stress that the
maximum allowable total anode current is $100 \mu\text{A}$.

Occupancy (%)	V	$I_a [\mu\text{A}]$
5	900	34.0
5	950	25.8
5	980	34.0
10	900	32.8
10	950	51.6
10	980	68.0
15	900	49.2
15	930	65.1
15	950	77.4
15	980	102.0
20	900	65.5
20	930	86.8
20	950	103.2
23	900	75.4
23	920	90.4
23	930	100
25	900	81.9
25	920	98.3

Table 4: Total anode current for different occupancies at nominal gain and with a safety factor 2.

- 9
10 The maximum operating voltage is -1.1 kV .

B.2 Biasing of the MaPMT

- 12 The standard voltage divider suggested by Hamamatsu is a voltage divider non-tapered, except for
13 first and last stage, optimized for maximum gain, that for single-photon detection. The voltage divider
14 ratios suggested by Hamamatsu are, in fact:

$$(PK) \quad R_0 \{2.3, 1.2, 1, 1, 1, 1, 1, 1, 1, 1, 1, 1.5\} \quad (A). \quad (1)$$

- 15 When using $R_0 = 200 \text{ k}\Omega$, so that the total resistance of the voltage divider is $R = 3 \text{ M}\Omega$, the total
16 power is $P = 0.33 \text{ W/MaPMT}$ at $\Delta V = 1.0 \text{ kV}$.

- 17 Using the approximate relation

$$\Delta G / G \approx I_a / I_{VD} \quad (2)$$

- 18 (see for instance [21]) one finds a gain non-linearity $\Delta G / G = 0.12$ at the occupancy 0.1.

- 19 The system is designed such that one can power the last and last-but-one dynodes, because in the
20 highest occupancy regions one should assume, conservatively, that this is necessary in order to keep the
21 MaPMT in the linear region of gain; this requires two additional HV lines with a maximum voltage of
22 110 V and 184 V .

- 23 In the high-occupancy regions of RICH1 (for instance, $f > 0.1$, that is about 3% of the MaPMT for
24 RICH1, that is about 60 MaPMT in total) one can use either a second or a second plus a third power
25 supply to improve the gain linearity at the same power consumption to obtain: $P \approx 0.33 \text{ W/MaPMT}$
26 at $\Delta V = 1 \text{ kV}$ and gain non-linearity $\Delta G / G = 0.04$ at occupancy 0.3.

- 1 Given the lower occupancies this workaround might be unnecessary in RICH2.
- 2 Various other solutions are available to further reduce the power consumption (if necessary) and/or
- 3 improve the gain non-linearity, by employing more elaborate power supply schemes using more power
- 4 supplies. These alternative will be evaluated in case of problems with the one proposed here.
- 5 The gain versus voltage is shown in figure 51. The nominal gain at $\Delta V = 0.9(1.0)$ kV, $G =$
- 6 $0.4 \cdot 10^6(1.0 \cdot 10^6)$.
- 7 Gain linearity for different MaPMT occupancies at different voltages is reported in Table 5, showing
- 8 that, in order to have a worst-case gain linearity of the order of 10%, the MaPMT with occupancy
- 9 greater than 15% need a second voltage applied.

Occupancy (%)	V	$\Delta G/G(\%)$
5	900	5.0
5	950	7.8
5	980	10.3
10	900	10.0
10	950	15.6
10	980	20.6
15	900	14.9
15	950	23.5
15	980	30.9
20	900	19.8
20	950	31.3
23	900	22.8
23	930	30.3
25	900	24.8
25	920	29.8

Table 5: Gain linearity for different occupancies

B.3 Prototyping

- 11 The current BaseB prototype strictly follows the standard Hamamatsu design. Moreover the BaseB is
- 12 already designed to allow a second power supply, on the last dynode, and a third power supply, on the
- 13 next to last dynode. The schematics is shown in figure 8

B.4 Ageing

- 15 The conclusions of this section should be compared with the recent measurements presented [22].
- 16 The MaPMT are expected to operate with high efficiency in the high-occupancy RICH upgrade en-
- 17 vironment. The performance of the MaPMT degrades as they are exposed to large amount of light.
- 18 The ageing, which depends on the total collected charge, normally decreases the gain of the MaPMT
- 19 (but compare with reference [22], where measurements are shown such that, at the beginning of their
- 20 lifetime, the MaPMT gain increases.). An estimate of the expected MaPMT degradation is necessary
- 21 in order to estimate the MaPMT lifetime and to set the operating gain and voltages.
- 22 In order to carry on a back-of-the-envelope estimate, a LHC operation time of about 1500 h/year has
- 23 been assumed. In order to be as conservative as possible a safety factor on the operation time of 2 has
- 24 been applied. Moreover a safety factor of 2 has been applied when calculating the anodic current in
- 25 order to take into account possible discrepancies between the LHCb simulations and real data.
- 26 The initial operating high voltage has been set to 900 V, which is the lowest possible voltage according
- 27 to specifications in order to be as conservative as possible. The high voltage operating range extends up
- 28 to 1100 V (TBC). Clearly, the low operating high voltage and gain impacts on the front-end electronics
- 29 design.
- 30 As it can be seen in Figure 51, the typical gain at 900 V for a standard MaPMT is $G = 4 \cdot 10^5$ while
- 31 at 1100 V is $2.1 \cdot 10^6$. The gaining factor is about 5.

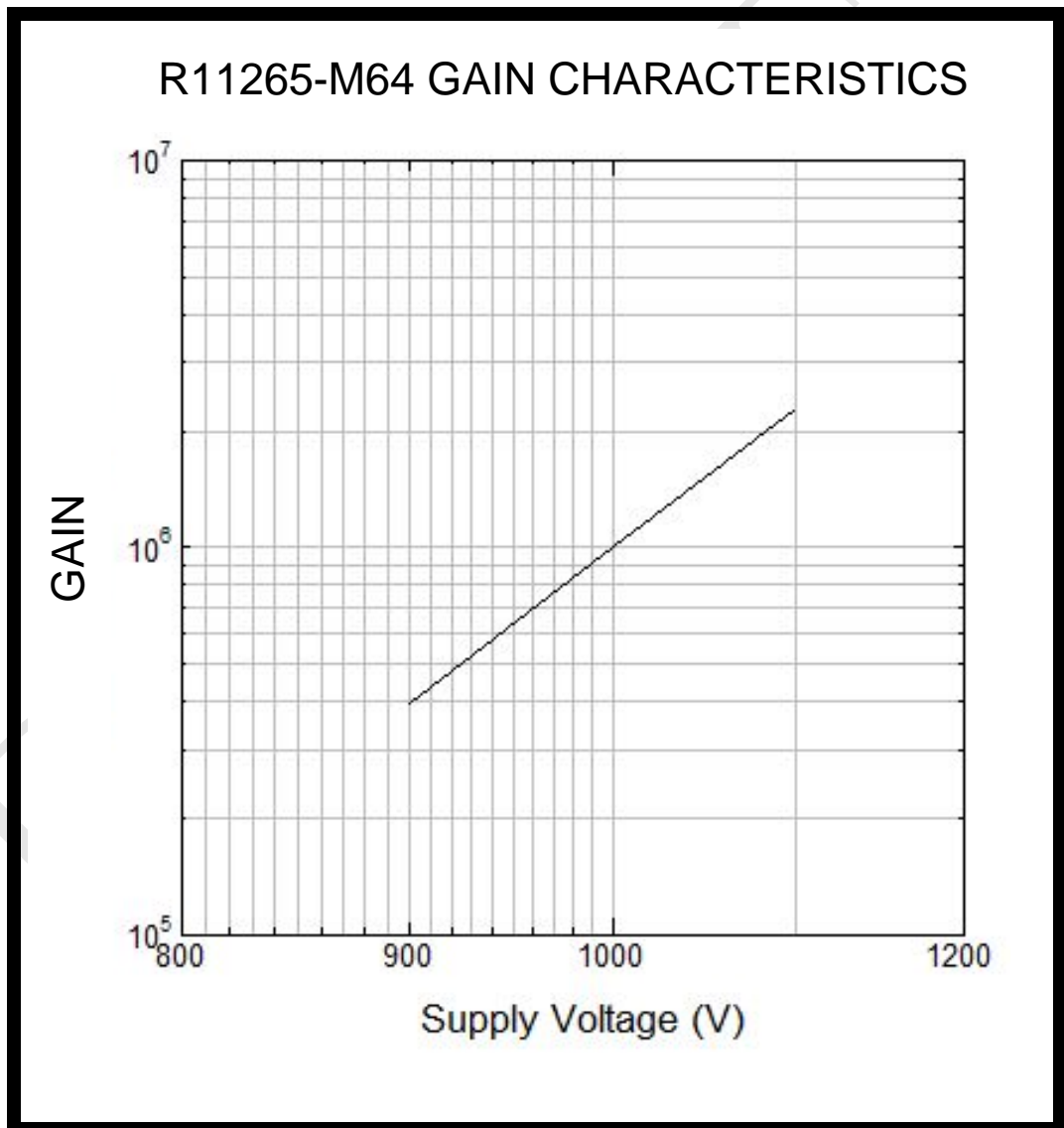


Figure 51: Nominal gain versus supply voltage with the standard voltage divider (from Hamamatsu).

- The change of the relative anode sensitivity as a function of the operating time provided by Hamamatsu is reported in Figure 52. The curve refers to an initial anode current of $100 \mu\text{A}$, the maximum allowed,

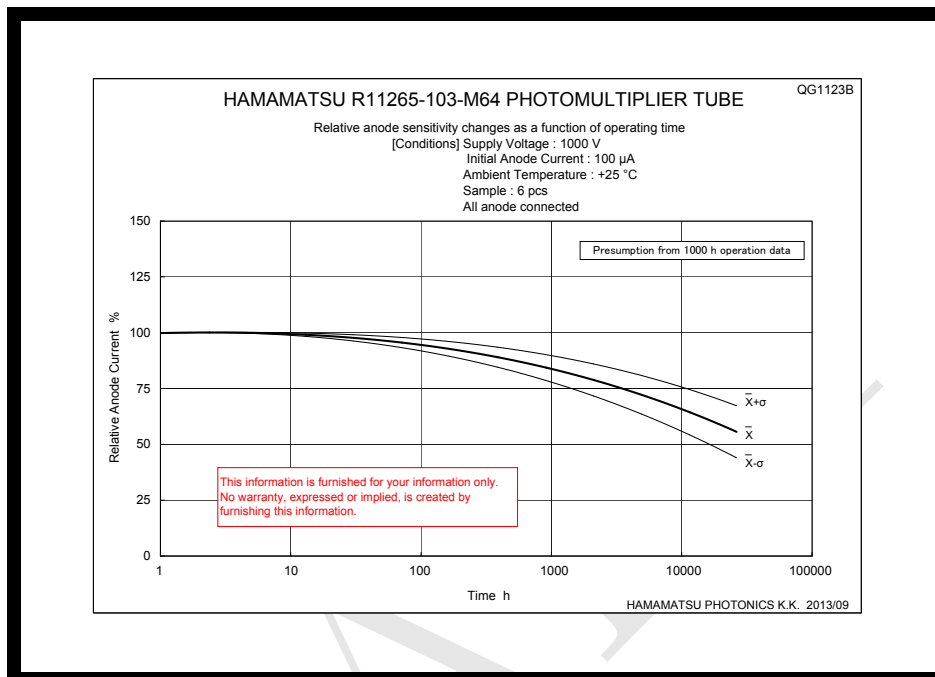


Figure 52: Relative anode current as a function of the MaPMT operating time.

- according to specifications.
- After 20000 h which corresponds to an integrated charge of $Q \approx 4700 \text{ C}$, the gain is reduced to $\approx 55\%$ ($\approx 44\%$) of the initial gain for the average curve (-1σ) curve. In order to recover the gain loss, it has been calculated that the voltage has to be increased of $\approx 65 \text{ V}$ ($\approx 80 \text{ V}$).
- Approximately 97% of MaPMT of RICH1 will have an occupancy less than 10%. The current for a MaPMT which is subject to a 10% occupancy at $V = 900 \text{ V}$ is $\sim 16 \mu\text{A}$ and after 20000 h, it has collected a charge $Q_{10\%} \approx 1550 \text{ C}$. This means that after ~ 20 years of operation, the gain has dropped to 55% (44%) of the initial gain for the average curve (-1σ curve). In order to have the same gain as at the initial operation gain, it is necessary to increase the applied voltage of 3 V (4 V) every year.
- Only 3% of the MaPMT (≈ 60 MaPMT in RICH1) having an occupancy greater than 10% will be more subject to ageing. Considering a 23% occupancy MaPMT (99.9% of the MaPMT are subject to less than 23% occupancy), the voltage has to be increased of 10 V (considering the -1σ curve) every year.
- In Table 6, the expected lifetime for MaPMT in different positions of the focal plane which are then subject to different occupancies is calculated.
- In any case the number of MaPMT which will have to be replaced due to ageing effects is negligible also compared to other possible failures, not related to ageing, which has to be taken into account when the number of needed spares MaPMT is estimated.
- It is important to point out that different MaPMT might age differently. However, from preliminary measurement, it is expected that MaPMT with similar initial gain will age with a similar trend (REFERENCE???)
- Swapping of the MaPMT between regions with high and low occupancy could be implemented.
- A dedicated measurement of the ageing is crucial for a proper design and it is being performed [3].

C The new R12699-M64 Flat Panel MaPMT

- A new flat panel MaPMT, the R12699-M64, is under development at Hamamatsu. The new R12699-M64, with an improved photo-electron collection efficiency of $\approx 87\%$, is an improved version of the

Occupancy [%]	HV (V)	Exp. Lifetime [years] (average curve)	Exp. Lifetime [years] (-1σ curve)
10	900	55	40
10	930	34	25
15	900	36	27
15	930	22	16
20	900	27	19
20	930	17	12
23	900	24	17
23	930	15	11
25	900	18	13
25	920	15	11

Table 6: MaPMT expected lifetime for different occupancy for the average curve and for the -1σ curve. The last column indicates the number of MaPMT in RICH in percentage which are subject to that occupancy.

1 H8500 Flat Panel MaPMT and from the first tests performed by Hamamatsu it looks suitable for single
2 photon counting applications. It is a 2-inches, 8×8 multi-anode, 1.5 mm thick borosilicate (UV?) input
3 window with bialkali (SBA?) photocathode, 10-stage dynodes, head-on MaPMT. It has an effective
4 sensitive area of $48.5 \text{ mm} \times 48.5 \text{ mm}$ reaching a packing density of 0.87. The pixel size is 5.8 mm. The
5 expected cost is about twice the cost of the R11265-M64 but the covered area is four times as large. The
6 weight is 0.146 Kg. The maximum operating temperature is 50°C . The maximum supply voltage is
7 -1100 V and the maximum output current is $100 \mu\text{A}$. The typical gain with a standard voltage divider
8 optimized for single-photon detection is $G = 1.0 \cdot 10^6$ at 1.0 kV. Typical channel to channel uniformity
9 is 1:2, maximum 1:3. Typical cross-talk is 3%. The typical dark current is 0.1 nA per anode pixel; 6 nA
10 in total and 50 nA maximum.

11 The R12699-M64 flat panel is under investigation as the photo-sensor for the RICH2 detector instead
12 of using the R11265-M64 in the edge regions (that is top and bottom of the focal planes) where the
13 occupancy is lower. In fact, in order to reduce the number of MaPMT in RICH2 one might use a
14 MaPMT with a larger pixel size, such that the total error on the reconstructed Cherenkov angle in
15 RICH2 is not significantly increased. A larger MaPMT will reduce the number of necessary MaPMT,
16 with a cost saving, and will simplify the system, instead of increasing its complexity as it would be
17 the case if using a lens system. Moreover using larger MaPMT would decrease the number of gaps
18 between the MaPMT with an increase the case area coverage.

19 As a first approximation, an Elementary Cell made of 2×2 R11265-M64 MaPMT could be replaced by
20 one single R12699-M64, gaining a factor four in the number of MaPMT. Therefore the current baseline
21 is to install both the R12699-M64 and the R11265-M64 in RICH2 depending on the occupancy of
22 the different regions. The only significant difference of the R12699-M64 with respect to the R11265-
23 M64, except for the pixel size which is 6 mm instead of 2.9 mm, is the entrance window thickness. The
24 R12699-M64 has an entrance window thickness of 1.5 mm. Transmission curves of both the R11265-M64
25 and the R12699-M64 are reported in Figure 53.

26 The loss of photoelectrons due to the larger thickness with respect to the R11265-M64 has been
27 calculated. The R11265-M64 spectral response has been corrected taking into account the difference
28 between the two transmittance curves. The estimated spectral response for the R12699-M64 is reported
29 in Figure 54.

30 A small loss of efficiency in the low wavelength region is visible. The loss of photoelectrons for the
31 R12699-M64 with respect to the R11265-M64 is $\sim 3.5\%$ in the case of UV glass and $\sim 2.2\%$ for the
32 borosilicate.

D The new R12699-M64 Flat Panel MaPMT in the RICH of LHCb

E Data Sheets

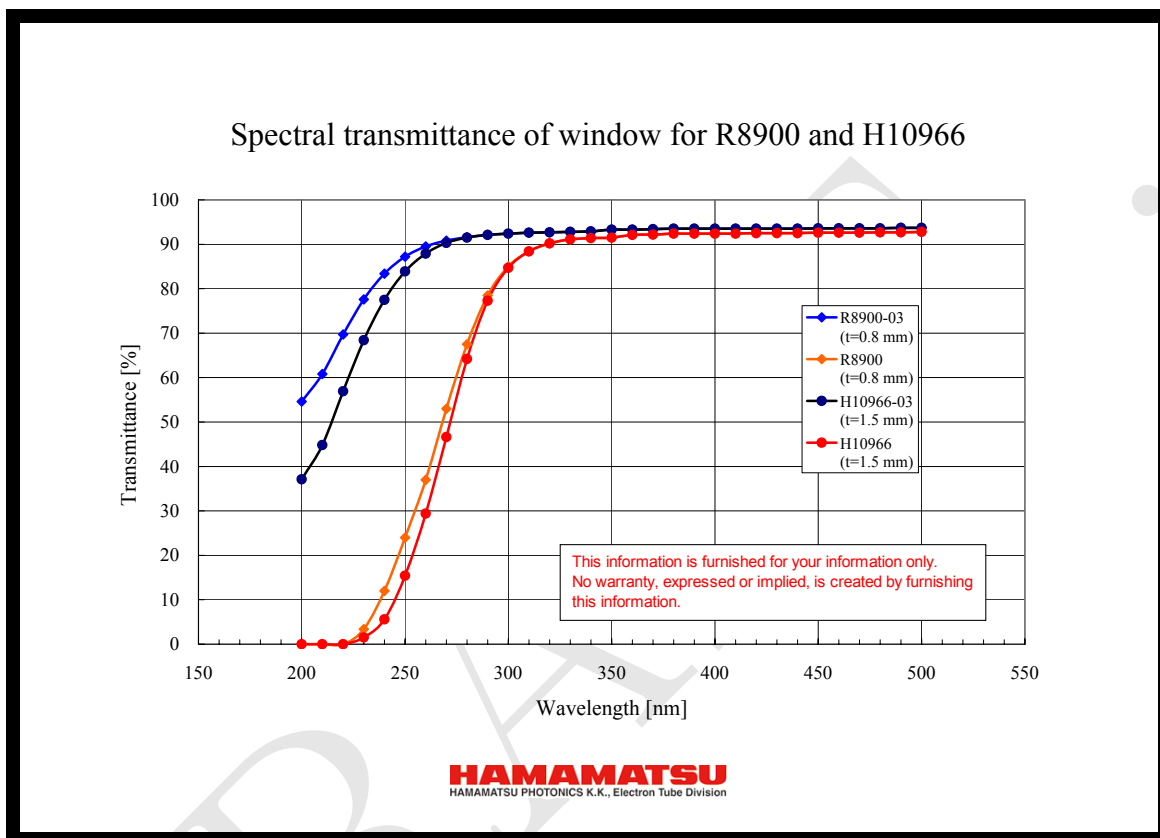


Figure 53: Spectral transmittance of the window of R8900 (equal to R11265-M64 according to Hamamatsu) and of the H10966 (equal to the R12699-M64 according to Hamamatsu) for both UV glass and borosilicate glass window. The -03 suffix indicates the UV glass curve.

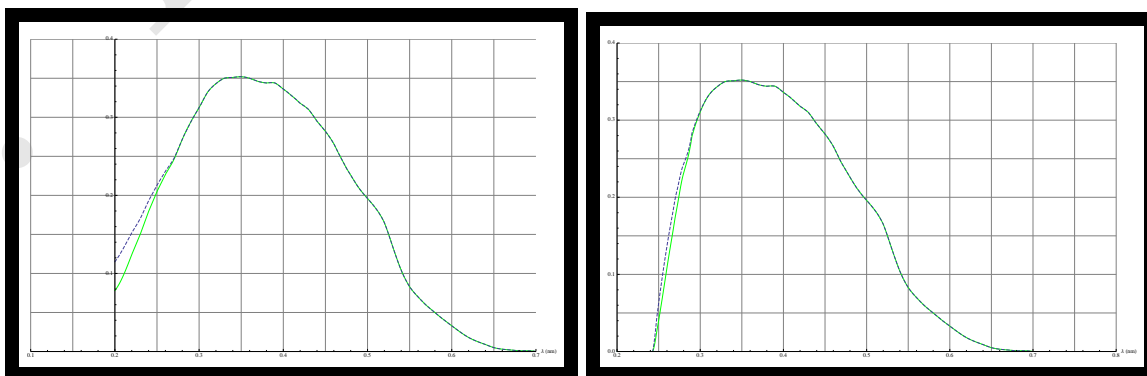


Figure 54: Spectral response of the R12699-M64 for UV glass (left) and borosilicate glass (right) entrance window (in green) compared with the spectral response of the R11265-M64 (dashed).

Tentative
Nov. 2012

R11265-103-M64

1 inch Square, 8×8 Multianode, Fast Time Response, UV window
Super Bialkali Photocathode, Metal Channel Dynode 12-Stage, Head-on Type

General

Parameter	Description	Unit
Spectral Response Range	185 to 650	nm
Window Material / Thickness	UV glass / 0.8	mm
Photocathode	Material	Super Bialkali
	Minimum Effective Area	23×23
Dynode Structure	Metal channel Dynode	-
Number of Stages	12	-
Weight	27	g
Operating Ambient Temperature	-50 to +50	deg C
Storage Temperature	-80 to +50	deg C

Maximum Ratings (Absolute Maximum Values)

Parameter	Value	Unit
Supply Voltage Between Anode and Cathode	1100	V
Average Anode Output Current in Total	0.1	mA

Characteristics at 25 deg C

Parameter	Min.	Typ.	Max.	Unit
Cathode Sensitivity	Luminous (2856K)	90	105	-
	Blue Sensitivity Index	2.5	13.5	-
Anode Sensitivity	Luminous (2856K)	-	105	-
Gain	-	1×10 ⁶	-	-
Anode Dark Current (Each anode)	-	0.4	4	nA
Time Response	Rise Time	-	0.6	-
	Transit Time	-	5.1	-
	Transit Time Spread (FWHM)	-	0.35	-
Uniformity Between Each Anode	-	1 : 3	1 : 5	-
Pulse Linearity (Each Anode)	at ±5% Deviation	-	0.2	-
	at ±5% Deviation	-	0.4	-

NOTE: Anode characteristics are measured with a voltage distribution ratio shown below :

Voltage Distribution Ratio and Supply Voltage

Electrodes	K	Dy1	Dy2	Dy3	Dy4	Dy5	Dy6	Dy7	Dy8	Dy9	Dy10	Dy11	Dy12	G.R	P
Ratio	2.3	1.2	1	1	1	1	1	1	1	1	1	1	1	0.5	

Supply Voltage : 1000 V K : Cathode Dy : Dynode G.R : Guard Ring P : Anode

DRAFT

DRAFT

1

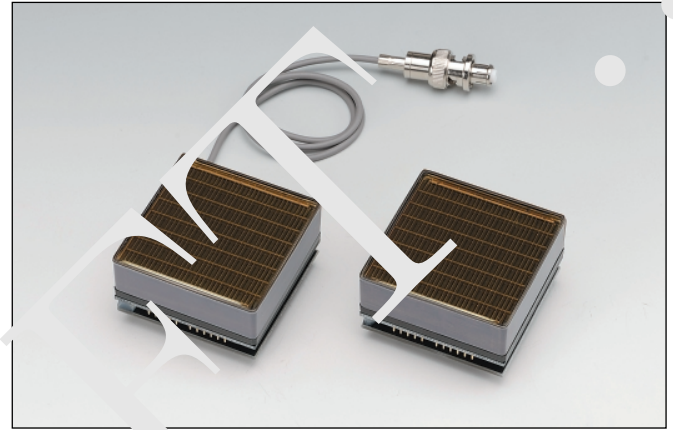
52 mm Square, Bialkali Photocathode, 10-stage 8 × 8 Multianode, Small Dead Space, Fast Time Response

FEATURES

- Large Effective Area: 48.5 mm × 48.5 mm
- Packing Density: 87 %
- 8 × 8 Multianode,
Pixel Size: 6 mm × 6 mm / Anode
- High Quantum Efficiency: 33 % Typ.
- Two Types are Available for HV Input
H12700A Series: Cable Input Type
H12700B Series: Pin Input Type

APPLICATIONS

- Academic Research
(RICH, Gamma Ray Telescope, etc.)
- Nuclear Medicine Equipment
(PET, Gamma Camera, etc.)
- 2D Radiation Imaging



Left: H12700A, Right: H12700B

Figure 1: Typical Spectral Response

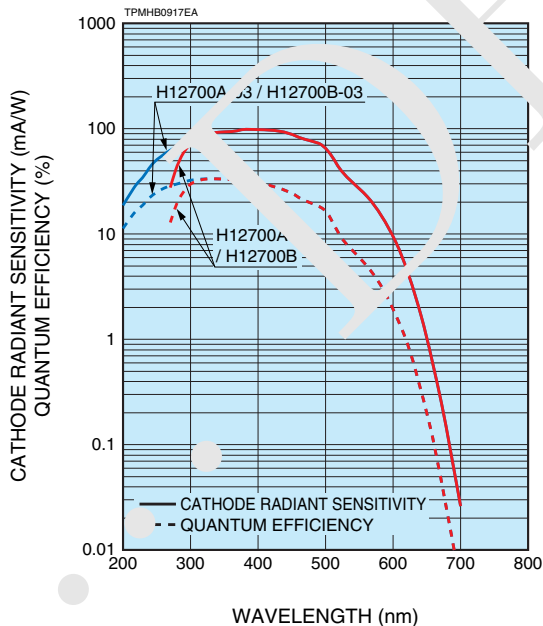
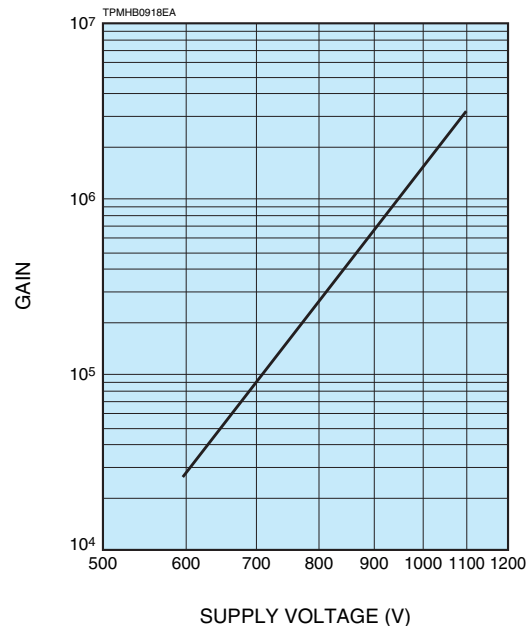


Figure 2: Typical Gain



Subject to local technical requirements and regulations, availability of products included in this promotional material may vary. Please consult with our sales office. Information furnished by HAMAMATSU is believed to be reliable. However, no responsibility is assumed for possible inaccuracies or omissions. Specifications are subject to change without notice. No patent rights are granted to any of the circuits described herein. ©2014 Hamamatsu Photonics K.K.

SPECIFICATIONS

Type No. ¹	Spectral Response		Photo-cathode Material	Window Material	Dynode Structure / Stages	Maximum Ratings			Cathode Characteristics			Anode to Cathode Supply Voltage (V)
	Range (nm)	Peak Wavelength (nm)				Supply Voltage Between Anode and Cathode (V)	Average Anode Output Current in Total (μA)	Divider Current at -1100 V (μA)	Luminous ^④		Blue Sensitivity Index (CS 5-58) Typ.	
									Min. (μA/lm)	Typ. (μA/lm)		
H12700A	300 to 650	380	BA	K	MC/10	-1100	100	225	60	75	12	-1000
H12700B	300 to 650	380	BA	K	MC/10	-1100	100	225	60	75	12	-1000
H12700A-03	185 to 650	380	BA	U	MC/10	-1100	100	225	60	75	12	-1000
H12700B-03	185 to 650	380	BA	U	MC/10	-1100	100	225	60	75	12	-1000

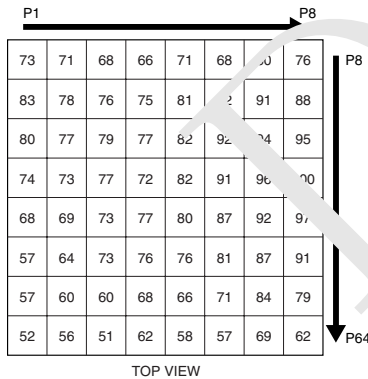
NOTE: (A) BA: Bialkali (B) K: Borosilicate glass, U: UV glass (C) MC: Metal channel
 (D) The light source is a tungsten filament lamp operated at a distribution temperature of 2856 K. Supply voltage is 150 volts between the cathode and all other electrodes connected together as anode.
 (E) The value is cathode output current when a blue filter (corning CS 5-58 polished to 1/2 stock thickness) is superposed between the light source and the tube under the same condition as Note (D).
 (F) Measured with the same light source as Note (D) and with the anode-to-cathode supply voltage and voltage distribution ratio shown in Table 1 below.
 (G) Measured with the same supply voltage and voltage distribution ratio as Note (F) after 30 minute storage in darkness.
 (H) Those are test data when a signal from a central channel (P28) of 64 anodes is used, while all photocathode are illuminated by pulsed light source.
 (I) The rise time is the time for the output pulse to rise from 10% to 90% of the peak amplitude when the whole photocathode is illuminated by a delta function light pulse.
 (K) The electron transit time is the interval between the arrival of delta function light pulse at the entrance window of the tube and the time when the anode output reaches the peak amplitude. In measurement, the whole photocathode is illuminated.
 (L) Also called transit time jitter. This is the fluctuation in electron transit time between individual pulses in the single photoelectron event, and defined as the FWHM of the frequency distribution of electron transit time.

Table 1: Voltage Distribution Ratio and Supply Voltage

Electrodes	K	Dy1	Dy2	Dy3	Dy4	Dy5	Dy6	Dy7	Dy8	Dy9	Dy10	GR	P
Distribution Ratio	2	1	1	1	1	1	1	1	1	1	1	1	0.5

Supply Voltage: -1000 V, K: Cathode, Dy: Dynode, GR: Guard Ring, P: Anode

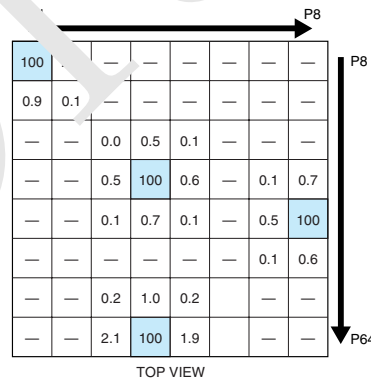
Figure 3: Anode Uniformity (Example)



SUPPLY VOLTAGE: -1000 V
 LIGHT SOURCE: TUNGSTEN LAMP with BLUE FILTER (DC LIGHT)
 SPOT ILLUMINATION (APERTURE SIZE): 6 mm square on each channel

TPMHB0919EA

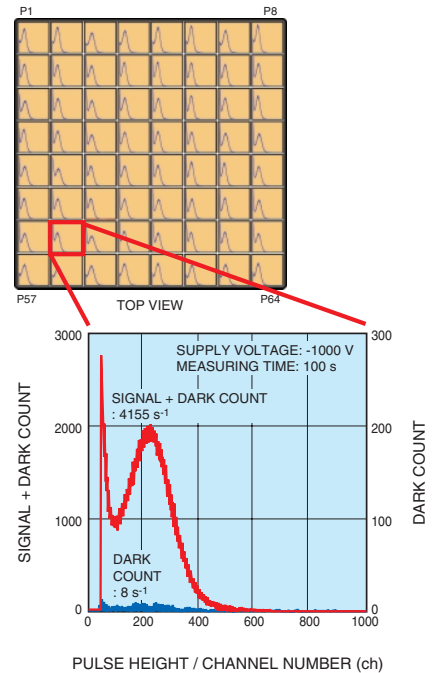
Figure 4: Anode Cross-talk (Example)



SUPPLY VOLTAGE: -1000 V
 LIGHT SOURCE: TUNGSTEN LAMP with BLUE FILTER (DC LIGHT)
 FIBER SIZE: φ1.0 mm (Kuraray: Clear Fiber NA=0.72)

TPMHB0920EA

Figure 5: Single Photon Counting (Example)



TPMHB0921EA

Anode Characteristics										Pulse Linearity per Channel [±2% Deviation] (mA)	Uniformity Between Each Anode		Type No.
Luminous [Ⓕ]		Gain [Ⓕ]	Dark Current per Channel [Ⓖ]		Dark Current in Total [Ⓖ]		Time Response [Ⓕ]						
Min. (A/lm)	Typ. (A/lm)		Typ.	Typ.	Max.	Max.	Rise Time [Ⓕ]	Transit Time [Ⓕ]	Transit Time Spread [Ⓕ]				
—	110	1.5×10^6	0.1	—	6	50	0.65	5.3	0.28	0.8	1: 2	1: 3	H12700A
—	110	1.5×10^6	0.1	—	6	50	0.65	5.3	0.28	0.8	1: 2	1: 3	H12700B
—	110	1.5×10^6	0.1	—	6	50	0.65	5.3	0.28	0.8	1: 2	1: 3	H12700A-03
—	110	1.5×10^6	0.1	—	6	50	0.65	5.3	0.28	0.8	1: 2	1: 3	H12700B-03

Figure 6: Dimensional Outlines and Basing Diagram (Unit: mm)

●HV Cable Input Type (H12700A/H12700A-03)

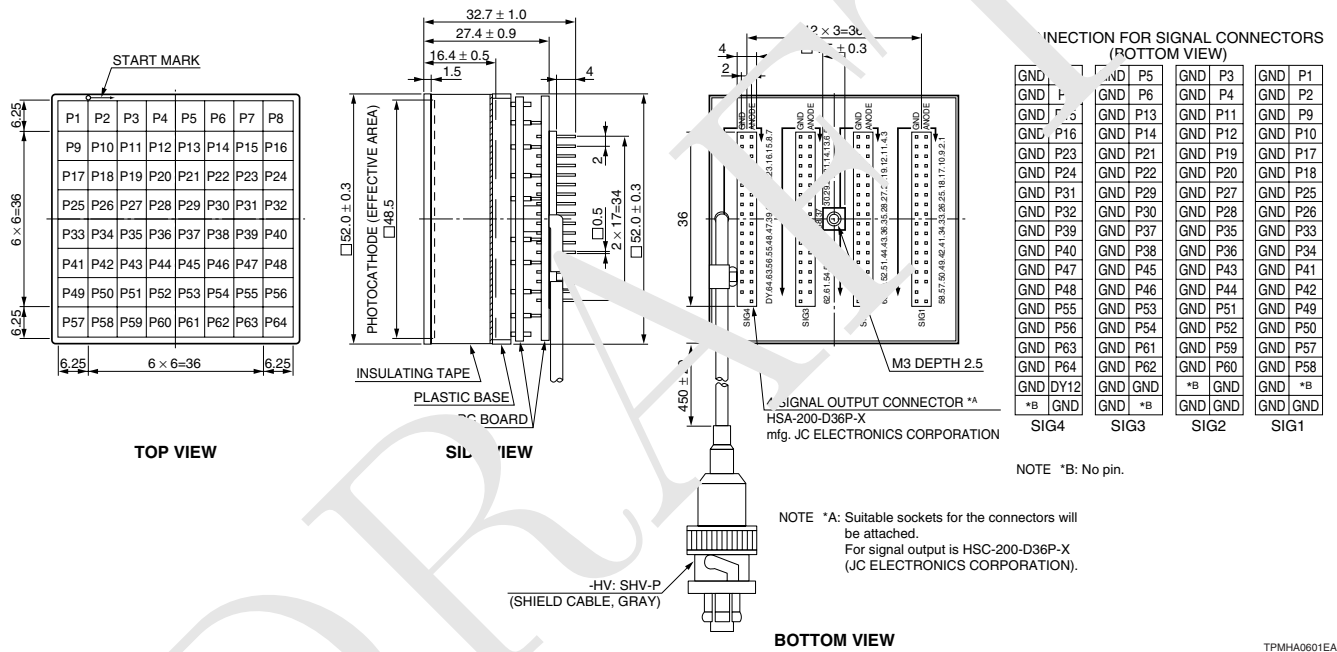
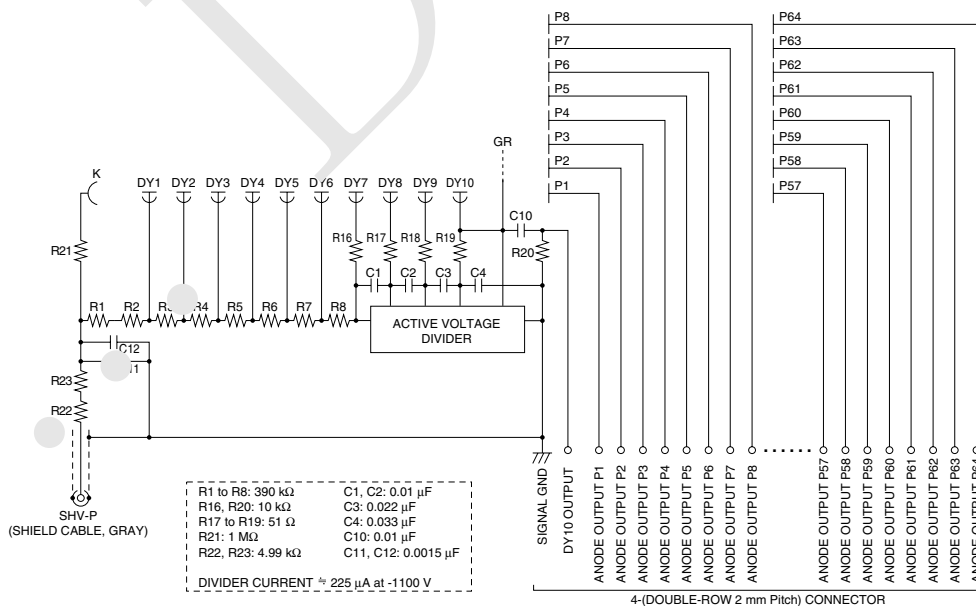


Figure 7: Internal Circuit (H12700A/H12700A-03)



F Referee's report

Report of LHCb RICH Elementary Cell Engineering Design Review

Review committee:

Eddy Jans (Nikhef - Amsterdam) and Saverio Minutoli (INFN - Genova).

The review took place on the 16th of October, 2014 at CERN. For the agenda of the meeting and its presentations see: <https://indico.cern.ch/event/344560/>

The reviewers thank the RICH group for the complete and extensive documentation presented before and during the meeting. The project is well advanced and structured, the discussions during the meeting have been very constructive. The status of the design is considered sufficiently advanced that an EDR is justified.

Comments:

1. The Elementary Cell (EC) hosts the actual detector, based on the MaPMTs R1165 and H12700, Base Board (BB), the electronic Front End Boards (FEBs) and a Back Board (BkBd).
 - a. Because of the high integration and compactness of the front end chain, particular care must be taken to prevent crosstalk between channels. The FE data transmission chain does not use zero suppression, which means that particularly in the region of high occupancy many transitions can happen simultaneously at the output of the CLARO comparators, which might lead to interferences. We suggest the RICH group to continue the EMI characterization of the full assembly at various thresholds during and beyond the test-beam campaign of 2014.
 - b. The committee has appreciated the thermal simulation that is performed. We know how complicated it is to input the simulator with realistic input data. This is especially important since the temperature has a non-negligible effect on the performance of the MaPMT and CLARO. Due to this, we suggest an additional effort in trying to improve the thermal simulation by importing the CAE model of the Base Board in the CFD environment, and then simulate the thermal effects in a more realistic manner. Thermal measurements with a mechanical mock-up consisting of a 3x3 array of cells should also be pursued, since the very limited surface contact of the six copper layers of the Base Board with the casing via the four M1.6 stainless steel screws, poses some worries.
2. The design of the Base Board for the EC-R module looks solid and compact.
 - a. The passive components of the bleeder are compatible with the system requirements. In case the Base Board is any further reduced in size the committee advises to pay special attention to the HV isolation.
 - b. Appreciable effort has been devoted to reduce the capacitance of the CLARO input lines by limiting their length. However, the committee noticed that there isn't any specification about the impedance lines matching. In order to reduce as much as possible the noise contribution due to impedance mismatch, we suggest to analyse the impedance effects at the level of CAE simulations and if necessary, modify accordingly the width of the input lines and/or the order of the stack-up of the Base Board.
3. Assuming that the FE input characteristics of the system match the required specifications, the committee suggests the RICH group to adopt the FEB of the EC-R for the EC-H module. The

benefits of using the same FEB are clear: less types of boards to handle, same maintenance, same test bench, etc.

4. The Detector Control System (DCS) has been presented at the review.
 - ¹ a. The committee agrees with the strategy to use a floating HV power supply, since this type of source helps to reduce the ground loops. We strongly recommend to design as soon as possible a detailed breakdown of the HV system distribution. This will also help to determine how many detectors will be grouped together and how many HV channels and cables the whole RICH will need.
 - b. The above recommendation also concerns the Low Voltage system.
 - c. It is proposed to monitor the temperature by two TMP102 sensors located on the Base Board, although the TMP102 is not qualified for a radiation environment. For this reason we recommend to replace these sensors with standard thermistors (PT100 – PT1000) driven and readout by the GBT SCA device, which is already foreseen in the electronic chain.
5. At the review, no Detector Safety System (DSS) was presented. The DSS should be realized by an acquisition system that works in parallel to the DCS. This architecture keeps the detector in a safe state, even if the DCS is in the Off or Standby state.
 - a. As the temperature is the parameter that mostly can damage the system, the committee suggests to devote one of the two temperature sensors of the Base Board to the DSS system.
 - b. Neither the Cooling System nor the Cooling Liquid Circulation System (LCS) was presented. The LCS must be equipped with some kind of alarm handling; if severe conditions occurs, the control system should automatically put the LCS in a safe state, which triggers the HV and LV to ramp down, thus reducing the chances on any additional harmful conditions. This issue should be addressed soon.
6. At the review, no Grounding and Shielding scheme was presented. All of us know that the ground loops and the connection of the ground planes between analog and digital paths can strongly determine the performance of the whole system. The committee recommends to organize an internal meeting on this topic, with as goal to design a scheme of the electrical connections along the detector of the (negative in particular) low voltage wires and of the cables shielding.
7. The committee agrees with the Quality Assurance strategy proposed, but suggests to check the functionality of the system at least at two temperature values. The only worry can be about the delivery of the MCPMTs, the schedule of which is tight but still compatible with the installation period. We support the plan to delegate the test of the electronics boards to external companies. It is advised to investigate whether this procedure can also be applied to the Base Board.
8. The committee appreciated the radiation damage tests performed on some parts of the system and stimulates the RICH group to continue the tests on the remaining parts according to the presented plan. We encourage the group to investigate the radiation hardness of the complete EC at different doses/fluences, well before full production starts. Especially in case any new components are going to be added to the system, like the low voltage regulator ALDO.

9. We took notice of the analysis about the need to use a Magnetic Shield (MS). In the presentation it was argued that all the EC-R and some of the EC-H boards need a MS. Since the edge of the MS passes closely by the bleeder and HV wires, particular care must be taken to the electrical isolation.
 - a. We suggest to make a comparison of the EC-R performance between the proposed mu-metal flat shield versus the Skudotech wrapped shield, which represents a unique solution for the EC-H.
 - b. The grounding strategy adopted for the MS is essential for the whole design, so we advise to include this point in the proposed meeting on Grounding and Shielding.
10. In view of the large number of components to be qualified and the need to group sixteen MaPMTs with comparable gain, it is strongly advised to start setting up a user-friendly database system in which the test results of all the components can be stored and later on retrieved.

The reviewers,

Eddy Jans and Saverio Minutoli

DRAFT